Quantentheorie zu Exzitonbildung und Photolumineszenz in Halbleitern

Dissertation

zur
Erlangung des Doktorgrades
der Naturwissenschaften
(Dr. rer. nat.)

dem Fachbereich Physik
der Philipps-Universität Marburg
vorgelegt

von
WALTER HOYER
aus Herborn

Marburg (Lahn) 2002

Vom Fachbereich Physik der Philipps-Universität Marburg
als Dissertation angenommen am 26.08.2002

Erstgutachter: Prof. Dr. S. W. Koch
Zweitgutachter: Prof. Dr. F. P. Gebhard

Tag der mündlichen Prüfung: 19.09.2002

Zusammenfassung

Die moderne Festkörperphysik hat mit der „Physik der Dreckeffekte“, wie Wolfgang Pauli sie in den zwanziger Jahren noch nannte, fast nichts mehr gemeinsam. Seit der Erfindung des Transistors im Jahre 1947 hat eine technologische Revolution stattgefunden, die fast jeden Bereich unseres täglichen Lebens beeinflusst. Diese rasante Entwicklung ist das Ergebnis gemeinsamer Anstrengung von Experimentalphysikern und theoretischen Physikern, denen es gelungen ist, neue Materialien mit zuvor nicht gekannter Präzision herzustellen, zu untersuchen und zu verstehen.

Moderne epitaktische Verfahren haben es möglich gemacht, einige der reinsten, künstlich hergestellten Materialien zu fertigen, bei denen einzelne Atomlagen oder kleinste Abweichungen von der Kristallstruktur nach Wunsch kontrolliert werden können. Dadurch hat die Entwicklung der Halbleiterphysik schon zu einer Vielzahl von Anwendungen geführt — als Beispiel seien nur die Laser in der optischen Telekommunikation oder unsere heutigen Computer in ihrem weltweiten Netzwerk genannt. Gleichzeitig eröffnet die rasante Entwicklung der Halbleiterlaser neue Möglichkeiten, ultraschnelle Phänomene auf winzigen Zeitskalen von nur wenigen Femtosekunden zu beobachten [1, 2]. Insgesamt bewegt sich die Forschung in Richtung der Physik von sehr kleinen Strukturen und äußerst kurzen Zeitskalen, in denen die Gesetze der Quantenmechanik gelten. In diesem Bereich werden klassisch unmögliche Vorgänge möglich, die beispielsweise die Grundlage für moderne Tunneldioden oder Teleportationsexperimente bilden. Die Halbleiterphysik bietet hierbei eine einzigartige Möglichkeit, um faszinierende Quantenphänomene in kontrollierter Weise zu untersuchen und um neue theoretische Konzepte unter anderem zur Beschreibung von stark wechselwirkenden Systemen zu entwickeln und zu testen.

Während der letzten Jahrzehnte hat sich die Halbleiterphysik dabei immer mehr in Richtung von quantenoptischen Anwendungen bewegt. Zum Beispiel ist die Quantennatur des Lichtes offensichtlich, wenn Halbleiterquantenpunkte wohldefinierte Photonen emittieren [3, 4] oder wenn verschränkte Zustände zwischen Licht und Materie optische Experimente in Mikroresonatoren beeinflussen [5, 6]. Weit entwickelte Theorien der Quantenelektrodynamik sind mittlerweile sehr erfolgreich in der Beschreibung der Wechselwirkung von atomaren Systemen mit einem quantisierten Lichtfeld, solange die Wechselwirkung der Atome untereinander nur eine untergeordnete Rolle spielt. Sie können vorzugsweise für verdünnte atomare Gase angewendet werden, da zur Beschreibung der Atome im allgemeinen einfache Modelle von wenigen Niveaus benutzt werden. Auf der anderen Seite liegt in Halbleitern die theoretische Herausforderung gerade in der Coulombwechselwirkung zwischen allen Ladungsträgern, sodass die Mehrzahl der Theorien den Schwerpunkt auf eine korrekte Beschreibung der fermionischen Vielteilcheneffekte gelegt hat, während die Wech-

selwirkung mit dem elektromagnetischen Feld zumeist auf klassische Felder beschränkt blieb. In diesem Zusammenhang ist das kohärente Regime klassischer Optik im Detail untersucht worden. Zur Anregung mit ultrakurzen Laserpulsen beispielsweise ist eine Vielzahl von Experimenten [7–12] und Berechnungen [13–17] durchgeführt worden. Da Elektronen und Löcher (fehlende Elektronen im Valenzband) entgegengesetzte Ladungen haben, kann die anziehende Coulombwechselwirkung zwischen ihnen zur Bildung von atomartigen, gebundenen Elektron-Loch-Paaren (Exzitonen) führen, die vielfach die physikalischen Eigenschaften von Optik und Transport dominieren [18–23].

Wenn ein klassischer Lichtpuls auf eine Halbleiterstruktur fällt, so kann dieser Puls Ladungsträger kohärent vom Grundzustand in angeregte Zustände befördern. Das Wort „kohärent“ bezieht sich hierbei auf die Tatsache, dass all diese Prozesse eine wohldefinierte Phasenbeziehung haben, die vom anregenden Puls aufgeprägt wird. Makroskopisch wird diese Phasenbeziehung in Form einer optischen Polarisation des Materials beobachtbar, die ihrerseits über die Maxwellgleichungen wieder an den Lichtpuls zurückkoppelt. Eine solche Kohärenz kann im allgemeinen jedoch nur für eine gewisse Zeit aufrecht erhalten werden, da immer auch phasenzerstörende Prozesse stattfinden. In Festkörpern sorgen vor allem die langreichweitige Coulombwechselwirkung zwischen allen Elektronen und Löchern und die Wechselwirkung zwischen Ladungsträgern und Gitterschwingungen für den Zerfall der Polarisation. Aufgrund dieses sogenannten Dephasierens der Polarisation findet die kohärente Physik typischerweise innerhalb von nur einigen Pikosekunden statt. Danach kann die Licht-Materie-Wechselwirkung nicht mehr klassisch beschrieben werden.

Im allgemeinen bleiben Elektron- und Lochdichten nach einem solchen Puls und dem nachfolgenden Zerfall der Polarisation im angeregten Zustand erhalten. In idealen Halbleitern bestimmt die spontane Rekombination als einziger Zerfallskanal die Lebensdauer der angeregten Ladungsträger. In dieser Situation muss eine Theorie unbedingt die Quantennatur des Lichtes berücksichtigen, um die fundamentalen Prozesse erklären zu können. Nur wenige Schritte sind bislang unternommen worden, das Halbleitersystem und das Lichtfeld auf voll quantisierter Ebene zu beschreiben. Aufgrund der überwältigenden numerischen Komplexität werden oft relativ starke Näherungen benutzt. So werden beispielsweise die Exzitonen als perfekte Bosonen betrachtet, wobei man die zugrunde liegende fermionische Substruktur komplett vernachlässigt [24]. Andererseits gibt es Rechnungen auf der Basis der Green-Funktionen, in denen der Freiheitsgrad des Lichtfeldes durch die Anwendung einer Beziehung zwischen Absorption und Lumineszenzspektrum [25] komplett eliminiert wird, die eigentlich nur unter thermodynamischen Gleichgewichtsbedingungen und für verschwindende Dämpfung strikt gültig ist [26].

Ein typisches Photolumineszenz-Experiment [27–30] wird häufig so ausgeführt, dass ein Halbleiterquantenfilm nichtresonant hoch im Band angeregt wird und man anschließend die Dynamik anhand zeitaufgelöster Lumineszenzspektren verfolgt. Wie in Fig. 1.1 skizziert geht man dabei davon aus, dass die Ladungsträger nach der Anregung durch Streuprozesse an die Bandkante gelangen, wo sie gebundene Exzitonen innerhalb der Bandlücke bilden können. Bis vor wenigen Jahren wurde allgemein angenommen, dass exzitonische Besetzungen nötig sind, um ein Lumineszenzsignal an der Exzitonenergie zu beobachten. Dies wurde jedoch in Frage gestellt, als theoretische Berechnungen, die *keine* gebundenen Exzitonpopulationen beinhalteten, ebenfalls exzitonische Lumineszenz vorhersagten [31]. Die

Beobachtung eines Signals an der Exzitonenergie ist folglich noch kein hinreichendes Kriterium für das Vorhandensein von gebundenen Exzitonen. In dieser Arbeit werden nun die Eigenschaften der Photolumineszenz von Halbleitern aufgrund von coulomb-korreliertem Elektron-Loch-Plasma einerseits und gebundenen Exzitonen andererseits untersucht.

Als ich begann, den Einfluss der exzitonischen Korrelationen auf Photolumineszenzspektren zu untersuchen, stellte es sich heraus, dass die Exzitonbildung selbst ein ebenso interessantes Thema darstellt. Generell ist es eine alte und immer noch offene Frage, ob und unter welchen Bedingungen sich eine signifikante Menge von inkohärenten, gebundenen Exzitonen in einem Nichtgleichgewichtssystem bilden kann, in dem das Verhältnis von gebundenen und ungebundenen Paaren stark von den charakteristischen Zeitskalen der verschiedenen Wechselwirkungsmechanismen abhängt. Es ist noch nicht einmal von vorneherein klar, wie man gebundene Exzitonen zählen soll, da ein Anzahloperator im strengen Sinne nicht existiert [32]. Natürlich möchte man dennoch die quantenstatistischen Eigenschaften der Exzitonen verstehen, Aspekte der Bose-Einstein-Kondensation [33, 34] beschreiben können und Mittel finden, um die Exzitonbildung zu manipulieren.

Die vorliegende Arbeit präsentiert daher eine mikroskopische Theorie, die in der Lage ist, die zentralen, oben genannten Fragestellungen zu beantworten. Die mikroskopische Beschreibung beinhaltet die Wechselwirkung der Ladungsträger mit dem quantisierten Lichtfeld (Photonen), mit Gitterschwingungen (Phononen) und die Wechselwirkung der Ladungsträger untereinander. Elektron- und Lochdichten, sowie mögliche Exzitonbesetzungen und Ladungsträgerkorrelationen werden konsistent im Elektron-Loch-Bild beschrieben. Dadurch können zum Beispiel Exzitonkorrelationen, Exzitonbildungsraten und Verteilungsfunktionen für unterschiedliche Gittertemperaturen und Ladungsdichten berechnet werden, ohne die zugrunde liegende fermionische Antisymmetrie zu vernachlässigen.

Nachdem in Kapitel 2 der Hamiltonoperator des wechselwirkenden Vielteilchensystems vorgestellt wird, werden in Kapitel 3 die notwendigen Gleichungen für das inkohärente Regime abgeleitet, auf das die numerischen Anwendungen dieser Arbeit beschränkt bleiben. Die Grundgleichungen, die in ihrer allgemeinen Form in Anhang A hergeleitet werden, sind allerdings sehr viel allgemeiner und mögen in Zukunft als Ausgangspunkt zur Berechnung von Vielteilchenproblemen und zur Untersuchung von quantenoptischen Eigenschaften unter verschiedensten Bedingungen genutzt werden. Das grundlegende Konzept zur Behandlung des auftretenden Hierarchieproblems ist das der Cluster-Entwicklung, die in der Quantenchemie erfolgreich angewendet wird, um elektronische Wellenfunktionen komplizierter Atome oder Moleküle näherungsweise zu berechnen. Während dort die Wellenfunktion zerlegt wird in Bestandteile, die nur unkorrelierte Elektronen, mindestens ein korreliertes Elektronenpaar, korrelierte Elektronentriplets usw. enthalten, wenden wir eine analoge Zerlegung der vollen Dichtematrix an. Da die Hierarchie, die durch die Kopplung der Ladungsträger an Photonen und Phononen entsteht, formal äquivalent ist zur Vielteilchenhierarchie der Coulombwechselwirkung, bietet die Cluster-Entwicklung eine Möglichkeit zum konsistenten Abbruch der Bewegungsgleichungen *aller* Korrelationen. Die Abbruchbedingung hat dabei eine klare physikalische Interpretation.

In Kapitel 4 wird als erste Anwendung der Gleichungen das Exzitonbildungsproblem ohne Berücksichtigung von spontaner Emission in einem eindimensionalen Modellsystem untersucht. In gewisser Weise können diese Rechnungen als Modellrechnungen für Exzi-

tonbildung in Materialien mit photonischer Bandlücke verstanden werden, in denen schon heute eine Unterdrückung der spontanen Emission um einen Faktor tausend möglich ist [35–37]. Die Exzitonbildung für verschiedene Gittertemperaturen und Dichten wird untersucht, und es ergeben sich selbst unter guten Bedingungen von Gittertemperaturen um die 10 K relative große Exzitonbildungszeiten in der Größenordnung von Hunderten von Pikosekunden. Die Studien zeigen ein interessantes Wechselspiel zwischen diagonalen Exzitonbesetzungen und nicht-diagonalen Exziton-Exziton-Korrelationen. Während die diagonalen Korrelationen häufig als Exzitonzahl interpretiert werden können, sind die nichtdiagonalen Korrelationen unabdingbar für die coulomb-assistierte Exzitonbildung unter inkohärenten Anfangssituationen.

In Kapitel 5 werden die optischen Eigenschaften untersucht, und Photolumineszenzspektren für Halbleiterstrukturen mit und ohne unterdrückte spontane Emission werden verglichen. Zusätzlich zur numerischen Lösung wird die *Elliottformel der Photolumineszenz*

$$I_{\mathrm{PL}}(\omega_{\mathbf{q}}) = -\mathrm{Im}\left[\sum_{\nu} \mathcal{A}_{\nu,\mathbf{q}} \frac{N_{\mathrm{S}}(\nu,q) + \Delta N(\nu,q)}{\hbar\omega_{\mathbf{q}} - E_{\mathrm{G}} - E_{\nu,q} + i\gamma}\right]$$

hergeleitet. Sie ist völlig analog zur klassischen Elliottformel der Absorption und zeigt die wichtigsten Aspekte der Lumineszenz von Halbleitern auf: Jedes Lumineszenzsignal wird durch die Summe der beiden Terme ΔN and N_{S} erzeugt, wobei ΔN mit echten Exzitonbesetzungen und N_{S} mit einem coulomb-korrelierten Elektron-Loch-Plasma zusammenhängt. Diese beiden Quellen für die Lumineszenz können in einem Experiment nicht unterschieden werden, sodass man allein mit Hilfe von Photolumineszenzexperimenten nicht entscheiden kann, ob gebundene Exzitonen vorliegen oder nicht, zumal jedes Spektrum einen starken Peak an der Exzitonresonanz zeigen sollte, wie man an dem Energienenner sehen kann. Das Vorhandensein eines solchen exzitonischen Peaks belegt nur, dass der Emissionsprozess selbst coulomb-korreliert ist. Tatsächlich sind sogar unter für Exzitonbildung günstigen Bedingungen die meisten Exzitonen in „dunklen“ Zuständen, da sie ihren Impuls nicht an ein Photon weitergeben können. Diese Exzitonen können erst dann zur Emission beitragen, wenn sie durch Streuung in die strahlende Zone kleiner Impulse gelangt sind. Daher ist Photolumineszenz häufig von den Plasmabeiträgen dominiert, weshalb ihre Beschreibung mit Hilfe einfacher Modellvorstellungen von Exzitonen im thermischen Gleichgewicht zum Scheitern verurteilt ist.

Eine Aufgabe der nahen Zukunft wird es sein, den vollständigen Anregungsprozess mit dem Übergang vom kohärenten zum inkohärenten Regime mikroskopisch zu untersuchen. Dazu müssen eine Vielzahl weiterer kohärenter Korrelationen berücksichtigt werden. Außerdem muss die Beschreibung der Phononen mindestens auch optische Phononen beinhalten, die eine wichtige Rolle bei der Kühlung von heißen Ladungsträgerverteilungen spielen. Solche Rechnungen können wertvollen Aufschluss darüber liefern, wie viele inkohärente Exzitonen schon während des Anregungsprozesses erzeugt werden können und inwieweit dieser Anteil von den Anregungsbedingungen abhängt. Ein weiteres Ziel ist die Benutzung derselben Methode zur Beantwortung quantenoptischer Fragestellungen. Dank der großen Breite an möglichen Wechselwirkungsprozessen sind viele interessante Resultate zu erwarten. Was die Untersuchung echter Quantenphänomene von Licht im Wechselspiel mit

Halbleiterstrukturen angeht, stehen wir erst am Beginn einer vielversprechenden, wissenschaftlichen Zukunft.

Contents

1 Introduction

The modern field of semiconductor physics has almost nothing in common with what Pauli called the "Physik der Dreckeffekte" or "dirt physics" in the 1920s. Beginning with the invention of the transistor in 1947, a technical revolution has unfolded which influences almost every aspect of our everyday life. This revolutionary development is the result of the joint effort of experimentalists and theoreticians who have learned to make, characterize, and understand new materials with unprecedented precision.

Modern epitaxial techniques have made it possible to grow some of the purest man-made materials where single atomic layers or small impurities can be added at will. Consequently, the development in semiconductor physics has already led to a vast number of applications like lasers used in optical telecommunication or our present day computers connected in a worldwide network. At the same time, the rapid development of semiconductor lasers has opened up the possibilities to investigate ultrafast phenomena on time scales of the order of femtoseconds [1,2]. These development trends have made it possible to proceed towards the physics of very small structures and very short time scales where the laws of quantum mechanics reign. This quantum regime offers intriguing possibilities to study classically impossible phenomena like tunneling, massively parallel quantum computing algorithms, and teleportation. In this respect, semiconductor physics provides a unique opportunity to investigate fascinating quantum phenomena in a controlled way and to develop new theoretical strategies to describe, e.g., the quantum mechanics of strongly interacting systems.

During the last decades, the semiconductor research has progressed towards the quantum optical regime. For example, the special quantum nature of light is apparent when semiconductor quantum dots emit well defined photons [3,4] or when light-matter entanglement influences optical experiments in microcavity structures [5,6]. Advanced theories of quantum electrodynamics are now very successful in the description of the interaction of atomic systems with a quantized light field where the interaction among the atoms plays only a minor role. These theories can mostly be applied to describe dilute and only weakly interacting atomic gases since relatively simple models like few-level systems are used to describe the material. On the other hand, semiconductor physics is usually dominated by the Coulomb interaction between the carriers such that the majority of theories has focused on the correct description of the fermionic many-body effects while the electromagnetic interaction has been limited mostly to classical fields. In this context, the coherent regime of classical optics has been investigated in detail. For excitations with ultrashort pulses, a diversity of experiments [7–12] and computations [13–17] have been performed. Since electrons and holes (missing electrons in the valence band) have opposite charges, they experience Coulomb attraction which may lead to the formation of atom-like bound electron-hole

pairs (excitons) that often dominate both optical and transport properties [18–23].

When a classical light pulse excites a semiconductor structure, this pulse can coherently lift carriers from the ground state into excited states. Here, the word "coherent" means that all these processes have a well-defined phase dependence which is enforced upon them by the phase of the exciting pulse. Macroscopically, this results in an observable optical polarization of the material which couples back to the external field via Maxwell's equations. The coherence can only be maintained over some finite time, though, because the system usually experiences phase destroying scattering processes. In solids, the long-range Coulomb interaction between all the electrons and collisions of electrons with the lattice quickly destroy all the phase relations, which can be observed as a decay of the polarization, i.e. dephasing. Due to these scattering processes, the coherent physics in typical semiconductor materials happens within at most a few tens of picoseconds. After this time, the light-matter interaction seizes to be classical.

However, electron and hole densities usually remain excited after such a pulse and the subsequent decay of the polarization. In ideal semiconductors, only spontaneous recombination determines the ultimate lifetime of the excited charge carriers. This is one case, where a full quantum theory including the quantum nature of light is important in order to understand the fundamental processes. Only few recent approaches deal with the coupled semiconductor-photon system on a fully quantized level. Due to the overwhelming numerical complexity, most of these approaches have made use of rather strong approximations. For example, excitons are treated as perfect bosons, which ignores the underlying fermionic character of electrons and holes [24]. Also a Green-functions approach has been used where the photon degree of freedom is eliminated by using a relation between absorption and luminescence spectra [25], which is strictly valid only under thermodynamic equilibrium conditions and for vanishing broadening [26].

One scenario which is often investigated in experiments [27–30], is displayed in Fig. 1.1. Here, a semiconductor quantum well is excited with an optical pulse non-resonantly high in the band. Subsequently, time-resolved photoluminescence spectra are measured in order to extract information on the formation time of excitons. Until recently, it was widely believed that excitonic populations are necessary to observe a luminescence signal at the excitonic resonance. This was questioned when theoretical computations which did *not* include bound excitons also led to photoluminescence at the excitonic resonance [31]. Thus, one has to conclude that the observation of luminescence is not sufficient evidence for the presence of bound excitons. In this thesis, the photoluminescence properties of a Coulomb-correlated electron-hole plasma and of bound excitons are investigated in detail.

When I started to study the influence of excitonic populations on photoluminescence, the exciton formation itself turned out to be an equally interesting topic. In general, it is an old but still open question whether and under which conditions a significant population of incoherent bound excitons can form in a nonequilibrium system where the ratio between bound and unbound pairs depends on the characteristic time scales of the relevant interaction processes. It is not even clear a priori how to count bound states since a rigorous exciton number operator does not exist [32]. However, one desires to understand the quantum statistical properties of these excitons, their distribution function, possible bosonic as well as Bose condensation aspects [33, 34], and find ways to manipulate the exciton formation.

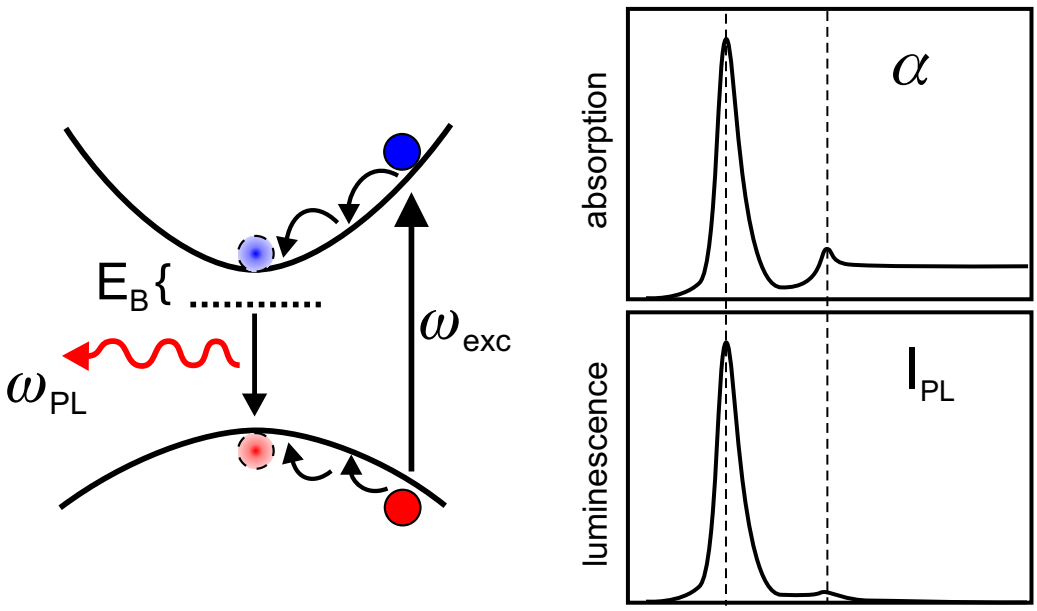

Figure 1.1: Schematic scenario of a typical photoluminescence experiment. After optical excitation energetically high in the band with the energy $\hbar\omega_{\mathrm{exc}}$, carriers equilibrate via Coulomb scattering and thermalize via phonon scattering processes and eventually may form bound excitons at an energy E_{B} below the band gap. The evolution of the carrier system is often followed indirectly by measuring time resolved luminescence and absorption spectra.

The presented thesis therefore develops and evaluates a microscopic theory which is capable of solving the central problems discussed above. The description includes photon, phonon, and Coulomb-interaction effects microscopically and describes electrons, holes, the possible exciton populations, and carrier-carrier correlations consistently in the fermionic electron-hole picture. As a result, the excitonic correlations, formation rates, distribution functions, etc. can be evaluated for different temperatures and carrier densities without neglecting the underlying fermionic anti-symmetry.

Chapter 2 outlines the many-body Hamiltonian for the interacting system. In Chapter 3, the necessary equations of motion for the incoherent scenario are derived. Only the incoherent regime is investigated in all numerical examples of this thesis. However, the equations are formulated in a more general manner in the Appendix such that they can also serve as a starting point to consistently compute, e.g., quantum-optical features of light after a coherent excitation. In Chapter 4, the full formation problem of excitons without inclusion of spontaneous emission is investigated. This can be thought of as a model for the formation of excitons inside a photonic bandgap material where a reduction of the dipole matrix element by a factor of thousand is easily possible already today [35–37]. In Chapter 5, finally, the optical properties are studied and photoluminescence spectra are compared for semiconductor heterostructures with full and reduced light-matter coupling. An adiabatic solution to compute photoluminescence spectra is derived in direct analogy to the famous Elliott formula

for absorption. This analytical result demonstrates all central elements of luminescence in semiconductor heterostructures.

2 Total Hamiltonian

The starting point of our theoretical description is the full Hamiltonian which describes the free motion of non-interacting carriers, photons, and phonons as well as the various interactions between all those quasi-particles. We introduce the Hamiltonian by summarizing the key steps in its derivation while referring to standard references in well-known details. We introduce the Bloch basis of the semiconductor and describe the Coulomb interaction between the carriers before we review the contributions of the Hamiltonian caused by light-matter and phonon-carrier interaction.

2.1 Carrier System

In semiconductor heterostructures, the microscopic properties of the fermionic carriers can be described with the field operator

$$\Psi(\mathbf{r}) = \sum_{\lambda,k_\parallel} \phi_{\lambda,k_\parallel}(\mathbf{r}) a_{\lambda,k_\parallel} \,, \tag{2.1}$$

where $a_{\lambda,k_\parallel}$ is the annihilation operator for an electron in band λ with wave vector $k_\parallel$ along the heterostructure obeying fermionic anti-commutation relations. The Bloch function of such an electron is denoted by $\phi_{\lambda,k_\parallel}$ where the band index λ may include different bands, subbands, and spins. The explicit form of the Bloch functions in envelope-function approximation [19] is given by

$$\phi_{\lambda,k_\parallel}(\mathbf{r}) = \xi_\lambda(r_\perp) \frac{\mathrm{e}^{ik_\parallel r_\parallel}}{\sqrt{\mathcal{L}^d}} w_\lambda(\mathbf{r}) \,, \tag{2.2}$$

where w_λ are the lattice periodic Bloch functions obtained from three-dimensional band structure calculations[1], ξ_λ is the normalized confinement wave function perpendicular to the heterostructure, and the plane wave part is normalized with respect to the size $\mathcal{L}^d$ of the structure. For sufficiently narrow confinement, the carrier dynamics is restricted practically completely to the lowest subband. In order to avoid explicit labels x, y and z for the directions along or perpendicular to the structure, we use the subscripts $_\parallel$ and $_\perp$. The symbol $\mathbf{r}$ denotes the full vector $(r_\parallel, r_\perp)$. For a one-dimensional quantum wire ($d = 1$), the components $r_\parallel$ and $k_\parallel$ are scalars along the wire whereas $r_\perp$ and $k_\perp$ are two-dimensional vectors.

[1] Ab-initio calculations of the bandstructure and the Bloch functions are a sophisticated field of physics in its own right.

In the remainder of this thesis, we omit the subscript $_\parallel$ for briefness; only the perpendicular components are explicitly denoted. For notational simplicity, we restrict ourselves to a two-band model with one valence and one conduction band and use the operators

$$c_k = a_{\lambda=\mathrm{c},k}\,, \tag{2.3}$$
$$v_k = a_{\lambda=\mathrm{v},k}\,. \tag{2.4}$$

The generalization to a multi-band system or the inclusion of spin is straight forward [19,38].

The Bloch functions of Eq. (2.2) are the single-particle wave functions which solve the eigenvalue equation of one electron moving in an effective lattice periodic potential U. Consequently, this choice leads to a simple diagonal structure of the single particle part of the general many-body Hamiltonian,

$$H_{\mathrm{kin}} = \int \Psi^\dagger(\mathbf{r}) \left[-\frac{\hbar^2\nabla^2}{2m_0} + U(\mathbf{r})\right] \Psi(\mathbf{r})\mathrm{d}^3r = \sum_k \left(\varepsilon_k^{\mathrm{c}} c_k^\dagger c_k + \varepsilon_k^{\mathrm{v}} v_k^\dagger v_k\right)\,. \tag{2.5}$$

In general, the eigenenergies $\varepsilon_k^{\mathrm{c/v}}$ must be obtained from precise band structure calculations. For the investigation of near-bandgap optical features, however, it is often a good approximation to assume a quadratic dispersion relation. In this case, the respective energies are given by

$$\begin{aligned} \varepsilon_k^{\mathrm{c}} &\equiv \varepsilon_k^{\mathrm{e}} + E_{\mathrm{G}} = \frac{\hbar^2k^2}{2m^{\mathrm{e}}} + E_{\mathrm{G}}\,, \\ \varepsilon_k^{\mathrm{v}} &\equiv -\varepsilon_k^{\mathrm{h}} = -\frac{\hbar^2k^2}{2m^{\mathrm{h}}}\,, \end{aligned} \tag{2.6}$$

where m^{e} and m^{h} are the effective electron and hole masses. The unrenormalized bandgap is denoted with E_{G}. Thus, the kinetic part of the Hamiltonian (2.5) can be viewed as a Hamiltonian of freely moving quasi-particles with the energies $\varepsilon_k^{\mathrm{e}}$ and $\varepsilon_k^{\mathrm{h}}$, respectively. In order to include the Coulomb interaction between the electrons in different bands beyond the effective single-particle level, we use the Hamiltonian [19,39]

$$H_{\mathrm{C}} = \frac{e^2}{8\pi\varepsilon_0} \int\int \Psi^\dagger(\mathbf{r})\Psi^\dagger(\mathbf{r}') \frac{1}{|\mathbf{r}-\mathbf{r}'|} \Psi(\mathbf{r}')\Psi(\mathbf{r})\,\mathrm{d}^3r\,\mathrm{d}^3r'\,, \tag{2.7}$$

$$= \frac{1}{2} \sum_{k,k',q\neq 0} V_q \Big(c_k^\dagger c_{k'}^\dagger c_{k'+q} c_{k-q} + v_k^\dagger v_{k'}^\dagger v_{k'+q} v_{k-q} + 2\, c_k^\dagger v_{k'}^\dagger v_{k'+q} c_{k-q}\Big)\,, \tag{2.8}$$

where V_q is the quantum-well or quantum-wire Coulomb matrix element which is derived in App. E. It is basically a Fourier transformation of the effective real space matrix element obtained from the integration over the directions perpendicular to the heterostructure. The first two terms in Eq. (2.8) lead to repulsive interaction between electrons within the same band whereas the last term gives rise to the attractive interaction between electrons and holes (missing valence band electrons) in different bands.

It is worthwhile to note that in contrast to our approach of introducing fermionic electron operators one sometimes finds treatments of light-matter interaction formulated in terms of bosonic exciton operators [40, 41], look ahead to Eq. (4.21). These exciton operators are electron-hole pair operators, describing the simultaneous generation or destruction of an electron-hole pair, i.e., the exciton creation (destruction) operator is proportional to $c^\dagger v$ ($v^\dagger c$). In lowest order, such exciton operators indeed fulfill bosonic commutation relations, but corrections containing electron-density operators exist. Even in low-density situations, nonlinearities in semiconductors can become important due to the long-range Coulomb interaction [42]. Furthermore, the first two terms in the Coulomb Hamiltonian H_C cannot directly be expressed in terms of exciton operators. Simply neglecting these terms is a dangerous and often ill controlled approximation because it includes only a subset of possible interaction processes in the nonlinear regime. Important fermionic effects like phase-space filling, screening, and dephasing are difficult to formulate with exciton operators. Also a description of the interplay between excitons and free carriers is not possible. Consequently, we perform all our computations in the basis of Bloch electrons.

2.2 Quantum Field

A standard approach for the quantization of the electromagnetic field starts from the vector potential $\mathbf{A}$ which is replaced by an operator within the canonical quantization scheme [43]. Using a complete mode basis, this operator $\mathbf{A}$ can be expressed in terms of creation and annihilation operators of photons in various modes. In the Hamiltonian we distinguish between the contribution of the free electromagnetic field and the interaction of the field with the semiconductor. In Section 2.2.1 the mode expansion and the free-field Hamiltonian are discussed. The Hamiltonian for the interaction of carriers with the quantized electromagnetic field is derived in Section 2.2.2, and the Bloch basis description of various interaction processes is outlined in Section 2.2.3.

2.2.1 Mode Expansion and Free Transverse Field

The classical vector potential for an electromagnetic field propagating in the background geometry described by a space dependent refractive index $n(\mathbf{r})$ in the absence of the active semiconductor heterostructure must obey the sourceless wave equation

$$\left[\nabla^2 - \frac{n^2(\mathbf{r})}{c^2}\frac{\partial^2}{\partial t^2}\right]\mathbf{A}_0(\mathbf{r},t) = \mathbf{0}, \tag{2.9}$$

where the Coulomb gauge ($\nabla \cdot \mathbf{A}_0 = \mathbf{0}$) has been adopted and the vacuum velocity of light is denoted by c. Any solution of Eq. (2.9) can be written as linear superposition of stationary eigenmodes of the form $\mathbf{U}_{\mathbf{q}\sigma}(\mathbf{r})\, e^{-i\omega_\mathbf{q} t}$ with polarization σ and frequency $\omega_\mathbf{q} = c|\mathbf{q}|$.

If one is interested in semiconductor structures embedded in pure substrate, the background geometry is particularly simple and can be described by a constant background refractive index $n(\mathbf{r}) = n_0$. In this case, which is the only one studied in all numerical applications in this thesis, the eigenmodes $\mathbf{U}_{\mathbf{q}\sigma}(\mathbf{r})$ are plane waves. In principle, however, it is

as well possible to describe more complex systems like, for example, a semiconductor microcavity, where $n(\mathbf{r})$ describes the quarter-wavelength layers of the Bragg mirror plus the spacer material inside the cavity. In general, the eigenmodes of any planar structure can easily be computed if the transverse extension orthogonal to the growth direction is sufficiently large. In this case, $n(\mathbf{r}) = n(r_\perp)$ is constant within each layer, changing sharply at the layer boundaries. Thus, Eq. (2.9) is valid only inside a layer; at the layer interfaces singular corrections may occur. These corrections can be handled by relating the respective solutions within adjacent layers via Maxwell's boundary conditions, i.e., by requiring that the tangential components of the transverse electric field

$$\mathbf{E}_\mathrm{T} = -\frac{\partial \mathbf{A}}{\partial t} \tag{2.10}$$

and of the magnetic field

$$\mathbf{B} = \nabla \times \mathbf{A} \tag{2.11}$$

have to be continuous at each boundary. The solution of the wave equation (2.9) for any planar design can be formulated in a compact way using the transfer-matrix technique [16, 44]. More explicitly, Eq. (2.9) can be solved by the ansatz

$$\mathbf{U}_{\mathbf{q}\sigma}(\mathbf{r}) = \mathbf{u}_{\mathbf{q}\sigma}(r_\perp)\frac{\mathrm{e}^{i q_\parallel r_\parallel}}{\sqrt{\mathcal{L}^d}} \tag{2.12}$$

where the subscript $\mathbf{q}$ labels both the wave vector with length $|\mathbf{q}| = \omega_{|\mathbf{q}|}/c$ and the parallel component $q_\parallel$ which is conserved throughout the whole structure.

The photon operators are introduced by expanding an arbitrary field operator for the vector potential in terms of the eigenmodes $\mathbf{U}_{\mathbf{q}\sigma}$. We obtain

$$\mathbf{A}(\mathbf{r},t) = \sum_{\mathbf{q},\sigma} \frac{\mathcal{E}_\mathbf{q}}{\omega_\mathbf{q}} \left[\mathbf{u}_{\mathbf{q},\sigma}(r_\perp)\, \frac{e^{i\, q_\parallel \cdot r_\parallel}}{\sqrt{\mathcal{L}^d}}\, b_{\mathbf{q},\sigma}(t) + \mathrm{h.c.} \right], \tag{2.13}$$

where the operators $b_{\mathbf{q},\sigma}$ and $b^\dagger_{\mathbf{q},\sigma}$ destroy or create a photon in mode $\mathbf{q}$ with polarization σ. The quantization procedure [43] fixes the value of the expansion coefficient

$$\mathcal{E}_\mathbf{q} = \sqrt{\frac{\hbar\omega_{|\mathbf{q}|}}{2\epsilon_0}}, \tag{2.14}$$

which is often referred to as vacuum field amplitude, and the commutation relations for the photon operators

$$[b_{\mathbf{q}\sigma}, b_{\mathbf{q}'\sigma'}] = \left[b^\dagger_{\mathbf{q}\sigma}, b^\dagger_{\mathbf{q}'\sigma'}\right] = 0; \quad \left[b_{\mathbf{q}\sigma}, b^\dagger_{\mathbf{q}'\sigma'}\right] = \delta_{\mathbf{q},\mathbf{q}'}\delta_{\sigma,\sigma'}. \tag{2.15}$$

From the energy of the transverse field, we obtain the corresponding free-field Hamiltonian

$$H_\mathrm{em} = \frac{\epsilon_0}{2}\int \mathrm{d}^3 r \;\left[n^2(r_\perp)\mathbf{E}^2_\mathrm{T}(\mathbf{r},t) + c^2\mathbf{B}^2(\mathbf{r},t)\right] = \sum_{\mathbf{q},\sigma} \hbar\omega_\mathbf{q}\left(b^\dagger_{\mathbf{q}\sigma}b_{\mathbf{q}\sigma} + \frac{1}{2}\right), \tag{2.16}$$

where Eqs. (2.10), (2.11), (2.13)–(2.15), and the normalization properties of the eigenfunctions $\mathbf{U}_{\mathbf{q}\sigma}(\mathbf{r})$ have been used [44]. This Hamiltonian formally corresponds to a Hamiltonian of a set of independent Harmonic oscillators, one for each field mode.

2.2.2 Interaction between Light Field and Carriers

The typical starting point for the description of light matter interaction is the minimal-substitution Hamiltonian containing the quantized vector potential. It is convenient to derive the dipole interaction between the semiconductor and the quantized light field before introducing the Bloch basis for carriers. Thus, we start with the general interaction Hamiltonian for a fermionic many-body system, given by

$$H = H_{\mathrm{min}} + H_{\mathrm{C}} + H_{\mathrm{em}}\,, \tag{2.17}$$

with the two contributions from Eqs. (2.7) and (2.16) and the minimal-substitution Hamiltonian obtained from Eq. (2.5) as [43–45]

$$H_{\mathrm{min}} = \int \Psi^\dagger(\mathbf{r}) \left[\frac{1}{2m_0}\Big(\mathbf{p} + e\,\mathbf{A}(\mathbf{r})\Big)^2 + U(\mathbf{r})\right] \Psi(\mathbf{r})\,\mathrm{d}^3 r\,. \tag{2.18}$$

Here, the elementary charge of an electron is given by $-e$ and $\mathbf{p} = -i\hbar\nabla$ is the momentum operator. The operators $\Psi^\dagger(\mathbf{r})$ and $\Psi(\mathbf{r})$ are electron creation and annihilation operators and obey fermionic anti-commutation relations

$$\big[\Psi(\mathbf{r}), \Psi(\mathbf{r}')\big]_+ = \big[\Psi^\dagger(\mathbf{r}), \Psi^\dagger(\mathbf{r}')\big]_+ = 0\,. \tag{2.19}$$

$$\big[\Psi(\mathbf{r}), \Psi^\dagger(\mathbf{r}')\big]_+ = \delta(\mathbf{r} - \mathbf{r}')\,. \tag{2.20}$$

As a side remark, we note that in the Coulomb gauge the longitudinal electric field is no independent variable. The longitudinal electric field of the interacting carriers is a function of the carrier density itself and thus fully described by the Coulomb Hamiltonian. Only an additional external electric field could in principle result in an additional contribution $-e\,\Phi(\mathbf{r})$ to Eq. (2.18).

The interaction Hamiltonian, Eq. (2.18), describes the interaction between charge carriers and the quantized light field by the operator product $\mathbf{p}\cdot\mathbf{A}$. At the same time, it involves a term proportional to $\mathbf{A}^2$. This term is often neglected in semiclassical computations as being weak and leading only to non-resonant contributions to the intraband dynamics. This is still true in many cases even for a quantized electromagnetic field. In principle, however, this term ensures the correct operator expression and the correct wave equation for the electric field operator [44]. Since it does not make the derivation more difficult, we keep it and rather make use of the freedom of gauge to choose a unitary operator T such that the transformed Hamiltonian $\tilde{H} = :THT^\dagger:$ has the form of a dipole interaction $\mathbf{r}\cdot\mathbf{E}$ which is linear in the electric field. The normal ordering $::$ is adopted to ensure identical results compared to Ref. [44], where this derivation is done in first quantization. For a classical electromagnetic field, the transformation is known as Göppert-Mayer transformation [43]. In second quantization, the operator

$$T = \exp\left\{\frac{i}{\hbar}\int e\,\Psi^\dagger(\mathbf{r})\Big[\mathbf{A}(\mathbf{r})\cdot\mathbf{r}\Big]\Psi(\mathbf{r})\,\mathrm{d}^3 r\right\} \tag{2.21}$$

gives the desired result.

The new Hamiltonian can be obtained directly from the transformed photon and carrier operators. These are derived most easily by using the relation [46]

$$TOT^\dagger = e^S O e^{-S} = O + [S,O] + \frac{1}{2!}[S,[S,O]] + \ldots \tag{2.22}$$

Thus, one first needs to know the commutator between the respective operator $\Psi(\mathbf{r})$, $\Psi^\dagger(\mathbf{r})$, $b_{\mathbf{q},\sigma}$, and $b^\dagger_{\mathbf{q},\sigma}$ and the operator $S = \frac{i}{\hbar}\int e\,\Psi^\dagger(\mathbf{r})\,[\mathbf{A}(\mathbf{r})\cdot\mathbf{r}]\,\Psi(\mathbf{r})\,\mathrm{d}^3r$. With the help of the anti-commutation relations, Eq. (2.20), we obtain

$$\begin{aligned}
[S,\Psi(\mathbf{r})] &= -\Big(\frac{i}{\hbar}\,e\,\mathbf{A}(\mathbf{r})\cdot\mathbf{r}\Big)\,\Psi(\mathbf{r})\,,\\
\big[S,\Psi^\dagger(\mathbf{r})\big] &= [S,\Psi(\mathbf{r})]^\dagger = \Big(\frac{i}{\hbar}\,e\,\mathbf{A}(\mathbf{r})\cdot\mathbf{r}\Big)\,\Psi^\dagger(\mathbf{r})\,,
\end{aligned} \tag{2.23}$$

whereas the operator of the vector potential obviously commutes with S such that we find

$$\widetilde{\Psi}(\mathbf{r}) = T\Psi(\mathbf{r})T^\dagger = \exp\Big(-\frac{i}{\hbar}e\,\mathbf{A}(\mathbf{r})\cdot\mathbf{r}\Big)\,\Psi(\mathbf{r})\,, \tag{2.24}$$

$$\widetilde{\Psi}^\dagger(\mathbf{r}) = \Big(\widetilde{\Psi}(\mathbf{r})\Big)^\dagger = \exp\Big(\frac{i}{\hbar}e\,\mathbf{A}(\mathbf{r})\cdot\mathbf{r}\Big)\,\Psi^\dagger(\mathbf{r})\,, \tag{2.25}$$

$$\widetilde{\mathbf{A}}(\mathbf{r}) = \mathbf{A}(\mathbf{r})\,. \tag{2.26}$$

We note that $\Psi(\mathbf{r})$ is only changed by a phase factor such that the operator of the electron density $\Psi^\dagger(\mathbf{r})\Psi(\mathbf{r})$ remains unaffected by the transformation. Such a spatially changing phase factor is known from general gauge theory. There, it is referred to as local gauge invariance [47] and the requirement of such a local gauge invariance leads in a natural way to the minimal substitution Hamiltonian.

From the Eqs. (2.24)–(2.26), one can already obtain the transformed contributions $\tilde{H}_{\mathrm{min}}$ and $\tilde{H}_{\mathrm{C}}$. Taking the derivative of $\widetilde{\Psi}(\mathbf{r})$ results in

$$\begin{aligned}
\mathbf{p}\widetilde{\Psi}(\mathbf{r}) &= \frac{\hbar}{i}\nabla\left(\exp\Big(-\frac{i}{\hbar}e\,\mathbf{A}(\mathbf{r})\cdot\mathbf{r}\Big)\,\Psi(\mathbf{r})\right)\\
&= \exp\Big(-\frac{i}{\hbar}e\,\mathbf{A}(\mathbf{r})\cdot\mathbf{r}\Big)\,\frac{\hbar}{i}\,\nabla\Psi(\mathbf{r}) - \Big(e\,\nabla(\mathbf{A}(\mathbf{r})\cdot\mathbf{r})\Big)\widetilde{\Psi}(\mathbf{r})\\
&= \exp\Big(-\frac{i}{\hbar}e\,\mathbf{A}(\mathbf{r})\cdot\mathbf{r}\Big)\,\mathbf{p}\Psi(\mathbf{r}) - e\left[\mathbf{A}(\mathbf{r}) + \mathbf{r}\cdot\frac{\partial\mathbf{A}}{\partial\mathbf{r}}\right]\widetilde{\Psi}(\mathbf{r}).
\end{aligned} \tag{2.27}$$

In the dipole approximation we assume that the electric field changes slowly compared to all important length scales of the semiconductor — particularly compared to the extension of the unit cell. In that case, the third term of Eq. (2.27) can be neglected and we recover $\tilde{H}_{\mathrm{min}} = H_{\mathrm{kin}}$, i.e., the single particle contribution from Eq. (2.5). The Coulomb Hamiltonian is completely unaffected by the transformation.

The remaining part of the Hamiltonian, Eq. (2.17), which has to be transformed according to Eq. (2.22), is the contribution H_{em} of the free electromagnetic field. First, we compute

$$[\mathbf{A}(\mathbf{r}), b_{\mathbf{q},\sigma}] = -\frac{\mathcal{E}_{\mathbf{q}}}{\omega_{\mathbf{q}}}\mathbf{u}^*_{\mathbf{q},\sigma}(r_\perp)\,\frac{e^{-i\,q_\parallel\cdot r_\parallel}}{\sqrt{\mathcal{L}^d}} = -\frac{\mathcal{E}_{\mathbf{q}}}{\omega_{\mathbf{q}}}\mathbf{U}^*_{\mathbf{q},\sigma}(\mathbf{r}) \tag{2.28}$$

which can be used to derive

$$\begin{aligned}[\mathbf{A}(\mathbf{r}), H_{\mathrm{em}}] &= \left[\mathbf{A}(\mathbf{r}), \sum_{\mathbf{q},\sigma} \hbar\omega_{\mathbf{q}} b^\dagger_{\mathbf{q},\sigma} b_{\mathbf{q},\sigma}\right] \\ &= \sum_{\mathbf{q},\sigma} \left(\hbar\mathcal{E}_{\mathbf{q}} \mathbf{U}_{\mathbf{q},\sigma}(\mathbf{r})\, b_{\mathbf{q},\sigma} - \hbar\mathcal{E}_{\mathbf{q}} \mathbf{U}^*_{\mathbf{q},\sigma}(\mathbf{r})\, b^\dagger_{\mathbf{q},\sigma}\right) , \end{aligned} \tag{2.29}$$

where we have used Eq. (2.13). The second term of Eq. (2.22) is thus given by

$$\begin{aligned} H_{\mathrm{D}} = [S, H_{\mathrm{em}}] &= \int \Psi^\dagger(\mathbf{r}) \left(e\,\mathbf{r} \cdot \frac{1}{\epsilon_0}\mathbf{D}(\mathbf{r})\right) \Psi(\mathbf{r})\, \mathrm{d}^3 r \\ &= -\int \mathbf{P}(\mathbf{r}) \cdot \frac{1}{\epsilon_0}\mathbf{D}(\mathbf{r})\, \mathrm{d}^3 r\,, \end{aligned} \tag{2.30}$$

where we have defined the operator of the electric displacement field

$$\frac{1}{\epsilon_0}\mathbf{D}(\mathbf{r}) = \sum_{\mathbf{q},\sigma} \left(i\mathcal{E}_{\mathbf{q}} \mathbf{u}_{\mathbf{q},\sigma}(r_\perp)\, \frac{e^{i\, q_\parallel \cdot r_\parallel}}{\sqrt{\mathcal{L}^d}}\, b_{\mathbf{q},\sigma}\right) + \mathrm{h.c.} \tag{2.31}$$

Here, we identify the expected dipole interaction between electronic polarization density $\mathbf{P}(\mathbf{r}) = -\Psi^\dagger(\mathbf{r})\, e\,\mathbf{r}\, \Psi(\mathbf{r})$ and the quantized field. Finally, the third term of the expansion, Eq. (2.22), results in a dipole self-energy

$$\begin{aligned} H_{\mathrm{dip}} &= :\frac{1}{2}[S,[S,H_{\mathrm{em}}]]: \\ &= :\frac{1}{2\epsilon_0}\iint \sum_{\mathbf{q},\sigma} \Psi^\dagger(\mathbf{r})\Psi(\mathbf{r}) \left[e\mathbf{r}\cdot\mathbf{U}^*_{\mathbf{q},\sigma}(\mathbf{r})\right] \left[\mathbf{U}_{\mathbf{q},\sigma}(\mathbf{r}')\cdot e\mathbf{r}'\right] \Psi^\dagger(\mathbf{r}')\Psi(\mathbf{r}')\mathrm{d}^3 r\, \mathrm{d}^3 r' : \\ &= :\frac{1}{2\epsilon_0}\iint \sum_{\mathbf{q},\sigma} \left[\mathbf{P}(\mathbf{r})\cdot\mathbf{U}^*_{\mathbf{q},\sigma}(\mathbf{r})\right] \left[\mathbf{U}_{\mathbf{q},\sigma}(\mathbf{r}')\cdot\mathbf{P}(\mathbf{r}')\right] \mathrm{d}^3 r\, \mathrm{d}^3 r' :, \end{aligned} \tag{2.32}$$

where we have used the property $[\Psi, \mathbf{D}] = [\Psi, \mathbf{A}] = 0$. All remaining terms from Eq. (2.22) vanish. In total, the Hamiltonian of the coupled carrier-light system after the transformation is given by the sum

$$\tilde{H} = H_{\mathrm{kin}} + H_{\mathrm{C}} + H_{\mathrm{em}} + H_{\mathrm{D}} + H_{\mathrm{dip}} \tag{2.33}$$

with the contributions given by Eq. (2.5), (2.7), (2.16), (2.30), and (2.32). We note that the unitary transformation removes the $\mathbf{A}^2$ term but introduces the additional two-particle interaction H_{dip}. However, this two-particle term presents no additional complications in our approach because the system already contains the two-particle Coulomb interaction.

Even though the operator of the vector potential remains formally unchanged during the transformation, its dynamics and interpretation does change, as can be seen by using the Heisenberg equation of motion

$$i\hbar\frac{\partial O}{\partial t} = [O, H]\,. \tag{2.34}$$

before and after the transformation. Before the transformation, for example, the transverse electric field is given by the expectation value of the operator

$$\mathbf{E} = -\frac{\partial}{\partial t}\mathbf{A} = \frac{i}{\hbar}\left[\mathbf{A}, H\right] = \frac{i}{\hbar}\left[\mathbf{A}, H_{\mathrm{em}}\right] = \sum_{\mathbf{q},\sigma} i\mathcal{E}_{\mathbf{q}}\mathbf{U}_{\mathbf{q},\sigma}(\mathbf{r})\, b_{\mathbf{q},\sigma} + \mathrm{h.c.}\,, \tag{2.35}$$

and thus totally expressible in terms of photon operators. After the transformation, however, we obtain

$$\begin{aligned}
\epsilon_0\tilde{\mathbf{E}}(\mathbf{r}) = -\epsilon_0\frac{\partial}{\partial t}\tilde{\mathbf{A}}(\mathbf{r}) &= \epsilon_0\frac{i}{\hbar}\left[\tilde{\mathbf{A}}(\mathbf{r}), \tilde{H}\right] = \epsilon_0\frac{i}{\hbar}\left[\mathbf{A}(\mathbf{r}), H_{\mathrm{em}} + H_{\mathrm{D}}\right] \\
&= \mathbf{D}(\mathbf{r}) - \int \sum_{\mathbf{q},\sigma} \mathbf{P}(\mathbf{r}')\cdot\mathbf{U}^*_{\mathbf{q},\sigma}(\mathbf{r}'))\,\mathbf{U}_{\mathbf{q},\sigma}(\mathbf{r})\,\mathrm{d}^3r' \\
&= \mathbf{D}(\mathbf{r}) - \frac{1}{n^2(\mathbf{r})}\mathbf{P}^{(\mathrm{T})}(\mathbf{r})\,,
\end{aligned} \tag{2.36}$$

where $\mathbf{P}^{(\mathrm{T})}$ is the transversal polarization provided by the semiconductor structure. This relation justifies the definition of the displacement field operator, Eq. (2.31), because it obviously describes only the part of the electric field which is due to the passive background material.

2.2.3 Semiconductor Bloch Basis

Before one can start to compute the equations of motion based on the Hamiltonian from Eq. (2.33), its new contributions must be expanded in terms of the Bloch basis introduced in Sec. 2.1. Starting with the dipole interaction Hamiltonian and using Eqs. (2.1) and (2.2), we obtain

$$\begin{aligned}
H_{\mathrm{D}} &= -\sum_{\substack{k,k'\\ \lambda,\lambda'}} a^\dagger_{\lambda',k'}a_{\lambda,k}\,\frac{1}{\mathcal{L}^d}\int \mathrm{d}^3r\;\xi^*_{\lambda'}(r_\perp)\,\xi_\lambda(r_\perp)\;e^{i(k-k')\cdot r_\parallel} \\
&\qquad \times\frac{1}{\epsilon_0}\mathbf{D}(\mathbf{r})\cdot\mathbf{r}\,(-e)\;w^*_{\lambda'}(\mathbf{r})\;w_\lambda(\mathbf{r}).
\end{aligned} \tag{2.37}$$

The space integral extends over the entire crystal lattice consisting of identical unit cells. Its evaluation can be simplified under the following assumptions: (i) Only small carrier momenta k near the optical band gap are important. Then $e^{i(k-k')\cdot r_\parallel}$ is slowly varying over a unit cell. (ii) The confinement wave functions $\xi_\lambda(r_\perp)$ are taken as constant within a unit cell. (iii) For optical frequencies, changes of $\mathbf{D}(\mathbf{r})$ over a unit cell are negligible. As a consequence, the space integral in Eq. (2.37) can be divided into a sum of unit-cell integrals using

$$\int \mathrm{d}^3r\, f(\mathbf{r}) = \sum_i \int \mathrm{d}^3r_0\; f(\mathbf{r}_0 + \mathbf{R}^0_i), \tag{2.38}$$

where the $\mathbf{r}_0$ integral extends over the volume Ω_0 of a unit cell, the i summation runs over the unit cells, and $\mathbf{R}^0_i$ is a Bravais lattice vector. The unit-cell integral defines the dipole matrix element

$$\mathbf{d}_{\lambda'\lambda} = \frac{1}{\Omega_0}\int \mathrm{d}^3r_0\; w^*_{\lambda'}(\mathbf{r}_0)\;(-e)\;(\mathbf{r}_0 + \mathbf{R}^0_i)\;w_\lambda(\mathbf{r}_0). \tag{2.39}$$

Since the lattice periodic Bloch functions for conduction and valence-band electrons in GaAs-like materials correspond to s and p-like atomic wave functions, respectively, in $\mathbf{d}_{\lambda'\lambda}$ the $\mathbf{R}_i^0$ term does not contribute to interband transitions with $\lambda \neq \lambda'$. Weak contributions due to intraband transitions are neglected in the following. Then $\mathbf{d}_{\lambda'\lambda}$ is independent of the unit cell.

In the limit of a large crystal, the remaining summation can be evaluated as integral which leads to

$$H_{\mathrm{D}} = -\int \mathrm{d}^3 r \; \mathbf{P}(\mathbf{r}) \cdot \frac{1}{\epsilon_0}\mathbf{D}(\mathbf{r}), \tag{2.40}$$

where the dipole density operator in the Bloch basis is

$$\mathbf{P}(\mathbf{r}) = \frac{1}{\mathcal{L}^d} \sum_{k,q} \sum_{\lambda \neq \lambda'} a^\dagger_{\lambda',k+q} \; a_{\lambda,k} \; \mathbf{d}_{\lambda'\lambda} \; e^{-i\,q\cdot r_\parallel} \; g(r_\perp). \tag{2.41}$$

The space dependence of $\mathbf{P}(\mathbf{r})$ along the semiconductor structure is described by a plane wave whereas the $r_\perp$ dependence is determined by the product of the envelope functions of the electron in the conduction and valence bands, yielding the confinement factor $g(r_\perp) = \xi_{\mathrm{c}}^*(r_\perp)\xi_{\mathrm{v}}(r_\perp) = \xi_{\mathrm{v}}^*(r_\perp)\xi_{\mathrm{c}}(r_\perp)$. Hence, the integral over the in-plane coordinates $r_\parallel$ in Eq. (2.40) defines a partial Fourier transformation of the displacement field,

$$\begin{aligned} \frac{1}{\epsilon_0}\mathbf{D}(q, r_\perp) &= \frac{1}{\mathcal{L}^d}\int \mathrm{d}r_\parallel \; \frac{1}{\epsilon_0}\mathbf{D}(\mathbf{r}) \; e^{-i\,q\cdot r_\parallel} \\ &= \frac{1}{\sqrt{\mathcal{L}^d}} \sum_{q_\perp} \; i\mathcal{E}_{\mathbf{q}} \left[\mathbf{u}_{q_\perp,q}(r_\perp) \; b_{q_\perp,q} - \mathbf{u}^*_{q_\perp,-q}(r_\perp) \; b^\dagger_{q_\perp,-q} \right], \end{aligned} \tag{2.42}$$

whereas the $r_\perp$ integral in Eq. (2.40) gives the effective displacement field at the position of the active material. Putting everything together, we obtain the final expression

$$\begin{aligned} H_{\mathrm{D}} &= -\frac{1}{\sqrt{\mathcal{L}^d}} \sum_{q_\perp,q,k} \Big[i\mathcal{E}_{\mathbf{q}} \, \bar{u}_{\mathbf{q}} \, d_{\mathbf{q}} \; c^\dagger_{k+q} v_k b_{q_\perp,q} \\ &\qquad + i\mathcal{E}_{\mathbf{q}} \, \bar{u}_{\mathbf{q}} \, d^*_{\mathbf{q}} \; v^\dagger_k c_{k-q} b_{q_\perp,q} \Big] \; + \; \mathrm{h.c.} \end{aligned} \tag{2.43}$$

The overlap integral between the confinement wave functions included in $g(r_\perp)$ and the mode function $u_{\mathbf{q}}(r_\perp)$ determines the effective interaction strength

$$\bar{u}_{\mathbf{q}} = \int \mathrm{d}r_\perp \; g(r_\perp) |\mathbf{u}_{\mathbf{q}}(r_\perp)| \tag{2.44}$$

for the photon mode $\mathbf{q}$. The vector character of the original product $\mathbf{D} \cdot \mathbf{r}$ is included in the effective dipole matrix element

$$d_{\mathbf{q}} \equiv \frac{\bar{\mathbf{u}}_{\mathbf{q}} \cdot \mathbf{d}_{\mathrm{cv}}}{\bar{u}_{\mathbf{q}}}. \tag{2.45}$$

After a similar derivation, the dipole self energy, Eq. (2.32), in Bloch representation becomes

$$\begin{aligned} H_{\mathrm{dip}} &= \frac{\bar{g}}{2\epsilon_0 n^2 \mathcal{L}^d} \sum_{k,k',q} \Big[d_{\mathbf{q}} d^*_{\mathbf{q}} c^\dagger_{k+q} v^\dagger_{k'} c_{k'+q} v_k \\ &\qquad + d_{\mathbf{q}} d_{\mathbf{q}} c^\dagger_{k+q} c^\dagger_{k'-q} v_{k'} v_k \Big] \; + \; \mathrm{h.c.} \end{aligned} \tag{2.46}$$

where we have defined an effective matrix element for the dipole-dipole interaction,

$$\begin{aligned}\bar{g} &= n^2 \int\int \mathrm{d}r_\perp \mathrm{d}r'_\perp \; g(r_\perp) g(r'_\perp) \sum_{q_\perp} u^*_{\mathbf{q}}(r'_\perp) u_{\mathbf{q}}(r_\perp) \\ &= n^2 \int\int \mathrm{d}r_\perp \mathrm{d}r'_\perp \; g(r_\perp) g(r'_\perp) \frac{\delta(r_\perp - r'_\perp)}{n^2(r_\perp)} = \int g(r_\perp) g(r_\perp) \mathrm{d}r_\perp, \end{aligned} \tag{2.47}$$

by using a property of the mode functions [44]. In principle, the dipole self-energy, Eq. (2.46), ensures the consistent coupling of the semiconductor polarization to the total electric field. In practice, however, it often leads only to an energetic shift of the optical spectra. Since the difference between the displacement field $\mathbf{D}/\epsilon_0$ and the total electric field $\mathbf{E}$ according to Eq. (2.36) is given by $\mathbf{P}^{(T)}/n^2$, this shift is particularly small for GaAs-like materials with a relatively large background refractive index of $n \approx 3.6$. For that reason, we have not included the dipole self-energy in the numerical calculations in this thesis.

2.3 Phonon Interaction

In every semiconductor, the coupling of carriers to lattice vibrations provides a mechanism of energy transfer such that the energy within the carrier-photon system alone does not have to be conserved. Instead, the coupling to lattice vibrations can lead to cooling of a hot carrier system or contribute to dephasing of coherent quantities. Corresponding to the three independent modes of sound waves in a solid, three branches of acoustic phonons always exist in a three-dimensional semiconductor [48]. In lattices with more than one atom within a unit cell, additional optical phonon branches are present.

The dispersion relation for optical and acoustic phonons is very distinct. While the energies of acoustic phonons in the long wavelength limit increase linearly with the wave vector, the optical phonon energy is practically constant. In GaAs it amounts to 36 meV, corresponding to a temperature of 400 K. For the temperatures, which we study in this thesis, the dominant coupling between lattice and carriers is thus provided by the acoustic phonons. After presenting a short derivation for the quantization of the lattice vibrations in Sec. 2.3.1, we treat the interaction between the carrier system and the longitudinal acoustic phonons due to deformation potential coupling in Sec. 2.3.2. In principle, also piezoelectric effects may occur in GaAs. Compared to II-VI materials such as CdS or ZnO, however, they are relatively weak in GaAs-like materials [49]. In particular at low temperatures, these effects are smaller than those from the deformation potential coupling by two orders of magnitude [50].

2.3.1 Lattice Vibrations

Typically, the dynamics of the electronic system inside a semiconductor is much faster than that of all the lattice ions. Therefore, in the investigations of the lattice itself, one typically assumes that the electrons quickly adjust themselves to every constellation of the ionic cores such that one can treat the lattice dynamics independent from the electronic subsystem. This approach is commonly known as the Born-Oppenheimer approximation [51].

For simplicity, we first consider a linear chain of N lattice ions. In first-quantized form, their Hamiltonian is given by

$$H = \sum_i \frac{P_i^2}{2M} + \frac{1}{2}\sum_{i,j} \frac{M\Omega_{i,j}^2}{2}(\Delta R_i - \Delta R_j)^2 \tag{2.48}$$

where M is the mass of a single lattice ion and ΔR_j is the deviation of the jth lattice ion from its equilibrium position R_j^0. A harmonic potential is assumed between all the ions and the coupling strength between ion i and j is given by $\Omega_{i,j}$ (for a textbook discussion see e.g. Ref. [48, 52]). Such a harmonic approximation is valid for small deviations from the equilibrium positions. The extra factor of $1/2$ in front of the potential accounts for double counting every pair of ions in the unrestricted sum. Since Eq. (2.48) includes only harmonic forces, we can apply the canonical quantization procedure by introducing the new dimensionless operators [52]

$$D_p = \frac{1}{\sqrt{N}}\sum_j e^{-i\,R_j^0\cdot p}\frac{1}{\sqrt{2}}\left(\sqrt{\frac{1}{\hbar\Omega_p M}}P_j - i\sqrt{\frac{\Omega_p M}{\hbar}}\Delta R_j\right)\,, \tag{2.49}$$

corresponding to a collective excitation of the N lattice ions. Such a collective excitation is referred to as phonon. The frequency Ω_p determines the phonon dispersion relation and is given by

$$|\Omega_p|^2 = \frac{1}{2}\sum_j \Omega_{0,j}^2 |1 - e^{i\,R_j^0\cdot p}|^2\,, \tag{2.50}$$

where we have assumed that $\Omega_{i,j}$ only depends on the relative position of the ions. Consequently, $\Omega_{0,j}$ denotes the coupling strength between one atom at the origin and one at a position R_j^0. The operators D_p and their Hermitian conjugates fulfill Bose commutation relations

$$[D_p, D_{p'}^\dagger] = \delta_{p,p'} \tag{2.51}$$

$$[D_p^\dagger, D_{p'}^\dagger] = [D_p, D_{p'}] = 0 \tag{2.52}$$

and can be used to expand ΔR_j and P_j. This gives a diagonal Hamiltonian

$$H = \sum_p \hbar\Omega_p\left(D_p^\dagger D_p + \frac{1}{2}\right) \tag{2.53}$$

formally equivalent to a set of harmonic oscillators. As in the photon problem, every phonon eigenmode can be viewed as an independent oscillator. In the long wavelength limit, the dispersion relation, Eq. (2.50), is approximately linear,

$$\Omega_p = c_\mathrm{A}|p|\,. \tag{2.54}$$

Due to this linear dependence, these phonons are referred to as acoustic phonons and c_A is called the phonon velocity of sound.

The generalization to a three dimensional lattice is straight forward. In that case, one obtains three phonon branches corresponding to different excitation directions of the lattice ions. In a lattice with cubic symmetry, these modes can be divided into two transversal modes, where the displacement of the lattice ions is perpendicular to the wave vector of the phonon, and one longitudinal mode with the displacement along the wave vector. In this case, Eq. (2.53) must be generalized to

$$H_{\mathrm{phon}} = \sum_{\mathbf{p},\sigma} \hbar\Omega_{\mathbf{p},\sigma} \left(D^{\dagger}_{\mathbf{p},\sigma} D_{\mathbf{p},\sigma} + \frac{1}{2} \right) , \tag{2.55}$$

where $\mathbf{p}$ has become a vector and the summation over the different phonon branches σ has been included.

2.3.2 Electron-Phonon Interaction

In this Section, the electron-phonon interaction is investigated. Fundamentally, the interaction mechanism is due to the fact that the electrons do not move in a perfect periodic potential anymore. Instead, the deviations of the ionic cores from their equilibrium position is taken into account such that the effective one-particle Hamiltonian of an electron in the lattice potential is given by

$$H = -\frac{\hbar^2}{2m_{\mathrm{e}}}\nabla^2 + \sum_j U(\mathbf{r} - \mathbf{R}_j) , \tag{2.56}$$

where $\mathbf{R}_j$ is the actual position of the atom number j, not its equilibrium position. For the case of small deviations from the equilibrium positions, one can expand the lattice potential and gets

$$U(\mathbf{r} - \mathbf{R}_j) = U(\mathbf{r} - \mathbf{R}_j^0) - \nabla U(\mathbf{r} - \mathbf{R}_j^0) \cdot \Delta\mathbf{R}_j + O\left((\Delta\mathbf{R}_j)^2\right) . \tag{2.57}$$

The first contribution is the potential of the perfectly periodic lattice and leads to the band structure of the crystal which has been taken into account already in Eq. (2.5). The second part provides the interaction between electrons and phonons. Here the vector $\Delta\mathbf{R}_j$ denotes the deviation of atom j from its equilibrium position and can be expressed via

$$\Delta\mathbf{R}_j = \frac{i}{\sqrt{N}} \sum_{\mathbf{p},\sigma} \sqrt{\frac{\hbar}{2\,M\,\Omega_p}} \left(D_{\mathbf{p},\sigma} - D^{\dagger}_{-\mathbf{p},\sigma} \right)) e^{i\,\mathbf{R}_j^0 \cdot \mathbf{p}} \mathbf{e}_{\mathbf{p},\sigma} \tag{2.58}$$

where σ labels the three phonon branches and we have used the generalization of Eq. (2.49). The unit vector $\mathbf{e}_{\mathbf{p},\sigma}$ defines the polarization direction. At long wavelengths, it points along the direction of $\mathbf{p}$ for the longitudinal mode and perpendicular to $\mathbf{p}$ for the two transversal modes [49].

If we use this expansion and express the interaction Hamiltonian in second quantized form using the Bloch basis, we have to evaluate matrix elements

$$\langle k', \lambda' | H_{\mathrm{int}} | k, \lambda \rangle \equiv \int \phi^*_{\lambda',k'}(\mathbf{r}) H_{\mathrm{int}} \phi^*_{\lambda,k}(\mathbf{r}) \mathrm{d}^3 r$$

$$= \frac{-i}{\mathcal{L}^d} \int |\xi_0(r_\perp)|^2 e^{-i(k'-k)r_\parallel} \sum_j \nabla U(\mathbf{r} - \mathbf{R}_j^0) \cdot \left(\sum_{\mathbf{p},\sigma} \sqrt{\frac{\hbar}{2N\Omega_p M}} e^{i\mathbf{R}_j^0 \cdot \mathbf{p}} \mathbf{e}_{\mathbf{p},\sigma} \right) w_{\lambda'}^*(\mathbf{r}) w_\lambda(\mathbf{r}) \mathrm{d}^3 r. \tag{2.59}$$

Separating the integrals over fast oscillating Bloch functions and slowly varying envelope, changing the quasi-continuous summation over lattice vectors into an integration, and expressing the gradient ∇_r via a gradient ∇_R, we obtain after an additional partial integration over R

$$\begin{aligned} \langle k', \lambda' | H_{\mathrm{int}} | k, \lambda \rangle &= \delta_{\lambda,\lambda'} \frac{-i}{\mathcal{L}^d} \int |\xi_0(r_\perp)|^2 e^{-i(k'-k)r_\parallel} \\ &\qquad \left(\sum_{\mathbf{p}} \sqrt{\frac{\hbar}{2N\Omega_p M}} U_p e^{i\,\mathbf{p}\cdot\mathbf{r}}\, i|\mathbf{p}| \right) \mathrm{d}^3 r \\ &= \delta_{\lambda,\lambda'} \sum_{\mathbf{p}} f_R(p_\perp) \delta_{k', k+p_\parallel} \sqrt{\frac{\hbar |U_p|^2 |\mathbf{p}|}{2 c_{\mathrm{LA}} N M}}. \end{aligned} \tag{2.60}$$

In this final equation, c_{LA} is the velocity of sound of the longitudinal acoustic phonons and U_p is the Fourier transformation

$$U_p = \frac{1}{\Omega_0} \int \mathrm{e}^{-i\,\mathbf{p}\cdot\mathbf{r}} U(\mathbf{r}) \mathrm{d}^3 r, \tag{2.61}$$

where Ω_0 is the volume of the unit cell. In the long wavelength limit, we can use the p-independent deformation constant D instead of U_p and get the matrix element for electron phonon interaction

$$|C_{\mathbf{p}}|^2 = \frac{\hbar |D|^2 |\mathbf{p}|}{2 c_{\mathrm{LA}} N M} = \frac{\hbar |D|^2 |\mathbf{p}|}{2 V c_{\mathrm{LA}} \rho} \tag{2.62}$$

with the mass density ρ of the semiconductor material under consideration. The form factor $f_R(p_\perp)$ is a consequence of the confinement of the electrons perpendicular to the direction of the semiconductor. We choose parabolic confinement as described in App. D and obtain

$$f_R(p_\perp) = \iint |\xi_0(r_\perp)|^2 e^{i\,p_\perp \cdot r_\perp}\, \mathrm{d}^2 r_\perp = e^{-\frac{\mathbf{p}^2}{2}}. \tag{2.63}$$

for a one-dimensional quantum wire characterized by the parameter R.

The starting point for calculating the dynamics due to carrier-phonon interaction is thus the Hamiltonian in the form

$$\begin{aligned} H_{\mathrm{P}} &= \sum_{p,p_\perp,\lambda,k} G_{p,p_\perp} D_{p,p_\perp}^\dagger a_{\lambda,k}^\dagger a_{\lambda,k+p} + \text{ h.c.} \\ &= \sum_{p,p_\perp,\lambda,k} G_{p,p_\perp} \left(D_{p,p_\perp}^\dagger + D_{-p,p_\perp} \right) a_{\lambda,k}^\dagger a_{\lambda,k+p} \\ &= \sum_{p,\lambda,k} \mathcal{G}_p^\dagger a_{\lambda,k}^\dagger a_{\lambda,k+p} \end{aligned} \tag{2.64}$$

where $G_{\mathbf{p}} = C_{\mathbf{p}}\, f_R(p_\perp)$ is the full matrix element including the form factor and

$$\mathcal{G}_p^\dagger = \sum_{p_\perp} G_{p,p_\perp} \left(D_{p,p_\perp}^\dagger + D_{-p,p_\perp} \right) \tag{2.65}$$

is an effective phonon operator where the summation perpendicular to the heterostructure has already been performed.

2.4 Total Hamiltonian

In this Chapter, we have derived all necessary contributions to the total Hamiltonian including the non-interacting Bloch electrons, photons, and phonons as well as the Coulomb interaction between carriers, the light-matter interaction in form of the dipole interaction, and the coupling to lattice vibrations via the deformation potential. In summary, the starting point of all further investigations is the total Hamiltonian of Eq. (2.5), (2.8), (2.16), (2.43), (2.46), (2.55), and (2.64),

$$H_{\mathrm{tot}} = H_{\mathrm{kin}} + H_{\mathrm{em}} + H_{\mathrm{phon}} + H_{\mathrm{C}} + H_{\mathrm{D}} + H_{\mathrm{dip}} + H_{\mathrm{P}}\,, \tag{2.66}$$

where all four interaction parts of the total Hamiltonian lead to non-trivial coupling to higher order correlations.

3 Explicit Equations for Incoherent Regime

At the ground state of a direct-gap semiconductor, all electrons are in the fully filled valence band while the conduction band is completely empty. However, an optical excitation, which is nearly resonant with the band-gap energy, can lift carriers from the valence to the conduction band. Such an excitation creates coherent polarization, carrier densities, and coherent as well as incoherent correlations in the system. When the excitation is weak enough, the polarization and the corresponding probe-absorption spectrum can show excitonic resonances which locate energetically below the fundamental band-gap energy due to the attractive Coulomb interaction between electrons and holes. The resulting excitonic features are often related to the so-called coherent excitons. After the optical excitation, polarization and other coherences decay away in a picosecond time scale due to: i) excitation-induced dephasing resulting from the carrier-carrier Coulomb scattering [16, 53], ii) phonon scattering [19, 54, 55], and iii) the finite radiative lifetime [12, 13, 56] in confined semiconductor structures. In a typical situation, carrier densities and incoherent correlations remain in the system and continue their many-body dynamics for several nanoseconds because their life time is limited only by slow radiative and non-radiative recombination processes.

When the coherent excitation dephases, the corresponding energy can be transferred into carrier densities, incoherent exciton correlations, and carrier-carrier correlations. In order to determine unambiguously how the ratio of these different contributions evolves, one has to describe them on the same microscopic level. So far, only approximative solutions have been obtained. Several authors have investigated relaxation and decay dynamics of excitons with a direct bosonic approximation for the exciton [57,58] or with implicit bosonic approximations resulting from the treatment up to third order in the exciting pulse [41, 59]. Since these approaches do not involve fermionic carrier densities, they cannot resolve how much of the excitation is transferred directly into carrier densities.[1] Nevertheless, it has been shown that a significant amount of incoherent excitons can be created if, firstly, the excitation is resonant with the exciton energy and if, secondly, phonon scattering is the dominant mechanism [41, 59].

In this thesis, we present and utilize a microscopic theory where fermionic carriers, incoherent exciton populations, carrier-carrier correlations, as well as phonon and photon-

[1] In bosonic models, excitonic contributions are typically separated into bound and continuum excitons. In this description, one cannot determine the plasma carrier density since the continuum excitons determined from the two-particle reduced density matrix are not trivially related to the carrier densities given by the one-particle reduced density matrix.

assisted correlations are treated at the same level. Our preliminary computations verify that a resonant excitation produces a considerable amount of incoherent excitons after the coherences decay when the generated carrier density and the consequent excitation-induced dephasing are low enough. The situation changes drastically when the system is excited clearly above the lowest exciton resonance but below the lowest longitudinal optical phonon resonance. Since this excitation configuration creates coherences mainly to the continuum, the created polarization and the other coherences decay fast. Especially, the excitation-induced dephasing of continuum coherences is strongly increased compared to the decay of resonantly excited excitonic polarization even for ultra low carrier densities. As a result, the transfer of coherences into incoherent quantities is dominated by excitation-induced dephasing which takes place on a nearly sub-picosecond time scale. Our preliminary computations, which exclude optical phonons but include the radiative decay and the dominant excitation-induced dephasing at the second-Born level [16], show that the off-resonant excitation leads to vanishingly small exciton populations. Even a bosonic analysis with only phonon-scattering [41] shows a significant reduction of generated exciton populations. In principle, if the off-resonant excitation becomes resonant with the LO-phonon energy, the amount of generated excitons can increase due to phonon-assisted processes. However, the excitation-induced dephasing is typically dominant also in these cases such that the relative effect of the phonon channel is reduced compared to an analysis where the excitation-induced dephasing is omitted. Thus, a typical off-resonant excitation leads to truly incoherent and uncorrelated initial conditions where carrier densities are present while the incoherent correlations are negligible. A similar situation can be realized with a current injection of carriers since this process does not induce coherences.

In all numerical investigations in this thesis, we therefore restrict ourselves to the genuinely incoherent regime, where we start with vanishing correlations and finite carrier densities and view the evolution of the system developing from that initial condition. As discussed above, such a situation follows, e.g., from off-resonant optical excitation or current injection. Without any additional assumptions about the nature of excitons or of correlated carrier pairs, we follow the formation of correlations out of the initial incoherent electron-hole plasma.

3.1 Hierarchy Problem

Starting from the total Hamiltonian derived in Chapter 2, one can compute the equations of motion for all relevant expectation values of interest. In general, the time evolution of an operator O is described by the Heisenberg equation (2.34).

The simplest examples of incoherent one-particle expectation values are the electron and hole densities

$$f_k^{\mathrm{e}} = \langle c_k^\dagger c_k \rangle, \quad f_k^{\mathrm{h}} = \langle v_{-k} v_{-k}^\dagger \rangle \,. \tag{3.1}$$

These expectation values are called two-point quantities since they contain two electronic operators. However, the dynamics of f_k^λ does not yield a closed set of equations if one simply computes the equation of motion with Hamiltonian Eq. (2.66). For example, the

commutator with the Coulomb Hamiltonian leads to the operator equation

$$\left[i\hbar\frac{\partial}{\partial t}a_{\lambda,k}\right]_{H_\mathrm{C}} = \sum_{\nu,k',q} V_q\, a^\dagger_{\nu,k'} a_{\nu,k'+q} a_{\lambda,k-q} \tag{3.2}$$

such that two-point quantities are coupled to four-point quantities due to the many-body interaction. In general, N-point quantities are coupled to (N+2)-point quantities via the Coulomb interaction leading to the well-known hierarchy problem of many-body physics [19, 60].

In the same way, also the coupling to the quantized phonon- or photon fields leads to an equation of the form

$$\left[i\hbar\frac{\partial}{\partial t}a_{\lambda,k}\right]_{H_\mathrm{D/P}} = \sum_{q,q_\perp} \left(M^\lambda_{q,q_\perp}\, b^\dagger_{q,q_\perp}\, a_{\bar\lambda,k+q} + (M^\lambda_{q,q_\perp})^*\, b_{-q,q_\perp}\, a_{\bar\lambda,k+q}\right) \tag{3.3}$$

where $M_{q,q_\perp}$ is the respective coupling matrix element and $\bar\lambda$ is either equal to λ for phonon interaction or equal to $c\,(v)$ for $\lambda = v\,(c)$ in the case of the dipole interaction. In both cases, pure carrier operators are coupled to mixed carrier-boson operators which leads to a similar hierarchy problem as the Coulomb interaction. Only in the semiclassical limit when the electric field can be treated classically, the expectation value over mixed operators can be factorized such that the only hierarchy is due to Coulomb interaction.

The hierarchy problem induced by the coupling to a boson field is formally identical to the traditional Coulomb hierarchy. For example, the operator equation of motion for a photon operator is given by

$$\left[i\hbar\frac{\partial}{\partial t}b_{q,q_\perp}\right]_{H_\mathrm{em}+H_\mathrm{D}} = \hbar\omega_{q,q_\perp}\, b_{q,q_\perp} + i\mathcal{E}_{q,q_\perp}\bar u^*_{q,q_\perp} d^*_{q,q_\perp} \sum_{\nu,k} a^\dagger_{\nu,k} a_{\bar\nu,k+q}\,, \tag{3.4}$$

which can be formally solved and gives

$$b_{q,q_\perp}(t) = b_{q,q_\perp}(0) + i\mathcal{E}_\mathbf{q}\bar u^*_\mathbf{q} d^*_\mathbf{q} \sum_{\nu,k} \int_0^t a^\dagger_{\nu,k}(t') a_{\bar\nu,k+q}(t')\, \mathrm{e}^{-i\omega_\mathbf{q}(t-t')}\mathrm{d}t'\,. \tag{3.5}$$

This shows that a photon operator is formally equivalent to a product of two electronic operators. With every photon absorption or emission process, an electron changes its state. The same is true for phonons. Therefore, both Eqs. (3.2) and (3.3) can be viewed as leading to an equivalent infinite series of equations. This infinite series of equations of motion has to be closed by a suitable truncation. Due to the formal equivalence, our truncation procedure cannot only be applied to carrier correlations but also to any mixed correlations between operators of different species. Schematically, the problem can be presented as

$$i\hbar\frac{\partial}{\partial t}O_N = T[O_N] + V[O_{N+1}], \tag{3.6}$$

where O denotes a generic N-particle ($2N$-point) operator. The coupling to operator combinations of the same level, i.e. to operator combinations containing the same number of

Fermi operators, is described by a functional T, while the specific form of the functional V determines the coupling to higher order operator combinations via the different interactions.

The hierarchy problem seems to have a simple form; nevertheless, it is basically responsible for all the complications in many-body and semiconductor quantum-optical investigations. In fact, current theoretical and numerical approaches can solve the hierarchy problem exactly only in very limited cases [61]. Thus, much of the current research effort is devoted to develop consistent approximation schemes to deal with this hierarchy problem. Many-body techniques, such as non-equilibrium Green functions are available [39,60], but become rather tedious once one wants to deal with quantum-optical problems at the same level of sophistication as the Coulomb problem. Hence, we use a method known from quantum chemistry, where the truncation problem has successfully been approached with the so-called cluster expansion [62–64]. Here, the electronic wave functions are divided into classes where electrons in an atom or molecule are: i) independent single particles (singlets), ii) coupled in pairs (doublets) iii) coupled in triplets, and iv) coupled in higher order clusters. The N-particle wave function is constructed from a suitable amount of coupled clusters including the correct antisymmetry of fermions. In other words, an approximative solution can be found by limiting the wave function to a certain level of coupled clusters. Typically, the cluster expansion method leads to rapidly converging results such that clusters up to doublets or triplets describe the system properties sufficiently accurately; beyond this, computer resources are usually exceeded.

3.2 Classification of Correlations

In semiconductors, the number of particles largely exceeds the electron number in atoms or molecules such that a direct solution of the wave function is not convenient. Thus, we rather utilize a density-matrix approach and evaluate the relevant expectation values from the corresponding Heisenberg equations of motion. In general, the system properties can be evaluated from $2N$-point expectation values

$$\langle\{N\}^\dagger\{N\}\rangle \equiv \langle a^\dagger_{\lambda_1,k_1}\dots a^\dagger_{\lambda_N,k_N}a_{\nu_N,p_N}\dots a_{\nu_1,p_1}\rangle, \tag{3.7}$$

which also determine the reduced-density matrix in the Bloch basis. If the system contains exactly $\mathcal{N}$ particles, $\langle\{\mathcal{N}\}^\dagger\{\mathcal{N}\}\rangle$ fully describes the system properties. In this case, $2N$-point expectation values exist for all $N \leq \mathcal{N}$.

To truncate the hierarchy problem, one has to find a consistent way of approximating $\langle\{N\}^\dagger\{N\}\rangle$. Perhaps the simplest scheme is provided by the Hartree-Fock approximation which implicitly assumes that the many-body system is described by a so-called Slater determinant of $\mathcal{N}$ independent single-particle wave functions. In this case, $2N$-point expectation values can simply be expressed in terms of two-point expectation values via

$$\langle\{N\}^\dagger\{N\}\rangle_{\mathrm{S}} = \langle\{N\}^\dagger\{N\}\rangle_{\mathrm{HF}} = \sum_\sigma (-1)^\sigma \prod_{i=1}^{N}\langle a^\dagger_{\mathbf{k}_i}a_{\mathbf{p}_{\sigma[i]}}\rangle \tag{3.8}$$

where we have included the band index in $\mathbf{k} = (\lambda, k)$ for notational simplicity. The antisymmetry of the approximated $2N$-point expectation value is guaranteed by the permutation

σ acting on the coordinate group $\{\mathbf{p}_1 \dots \mathbf{p}_N\}$ such that even and odd permutations lead to $(-1)^\sigma = +1$ or -1, respectively. Since $\langle\{N\}^\dagger\{N\}\rangle_\mathrm{S}$ consists of single particle expectation values, it can describe accurately only uncorrelated situations where each carrier behaves effectively like a single particle influenced by the average field of all other particles. On that level of approximation, it is sufficient to know the single-particle expectation values of the system. All higher order correlations can then be calculated via Eq. (3.8) and do not contain additional information.

The Hartree-Fock approximation, in which the full density matrix is represented by singlets, represents only the first step of the general cluster expansion. The next step to improve the level of approximation is to include also doublets. In this case, the full density matrix can describe uncorrelated carriers and an arbitrary amount of correlated pairs. Again, it is sufficient to compute all two-point and four-point quantities because higher order expectation values can be obtained from those. In general, the classification scheme can be extended to any arbitrary order [65]. By assuming that we formally know all quantities from $\langle\{1\}^\dagger|\{1\}\rangle$ up to $\langle\{N\}^\dagger|\{N\}\rangle$, the true N-point correlations are defined via a recursion relation,

$$\langle\{2\}^\dagger|\{2\}\rangle = \langle\{2\}^\dagger|\{2\}\rangle_\mathrm{S} + \Delta\langle\{2\}^\dagger|\{2\}\rangle, \tag{3.9}$$

$$\begin{aligned}\langle\{3\}^\dagger|\{3\}\rangle &= \langle\{3\}^\dagger|\{3\}\rangle_\mathrm{S} + \langle\{1\}^\dagger|\{1\}\rangle\,\Delta\langle\{2\}^\dagger|\{2\}\rangle \\ &\quad + \Delta\langle\{3\}^\dagger|\{3\}\rangle,\end{aligned} \tag{3.10}$$

$$\begin{aligned}\langle\{N\}^\dagger|\{N\}\rangle &= \langle\{N\}^\dagger|\{N\}\rangle_\mathrm{S} \\ &\quad + \langle\{N-2\}^\dagger|\{N-2\}\rangle_\mathrm{S}\,\Delta\langle\{2\}^\dagger|\{2\}\rangle \\ &\quad + \langle\{N-4\}^\dagger|\{N-4\}\rangle_\mathrm{S}\,\Delta\langle\{2\}^\dagger|\{2\}\rangle\,\Delta\langle\{2\}^\dagger|\{2\}\rangle + \dots \\ &\quad + \langle\{N-3\}^\dagger|\{N-3\}\rangle_\mathrm{S}\,\Delta\langle\{3\}^\dagger|\{3\}\rangle \\ &\quad + \langle\{N-5\}^\dagger|\{N-5\}\rangle_\mathrm{S}\,\Delta\langle\{3\}^\dagger|\{3\}\rangle\,\Delta\langle\{2\}^\dagger|\{2\}\rangle + \dots \\ &\quad + \Delta\langle\{N\}^\dagger|\{N\}\rangle.\end{aligned} \tag{3.11}$$

Here, each term denotes a sum over all possibilities to reorganize the N coordinates among singlets, doublets and so on. The sign of a specific term is determined by the permutation of coordinates with respect to the original $(\mathbf{k}_1 \dots \mathbf{k}_N)$ and $(\mathbf{p}_1 \dots \mathbf{p}_N)$; an even (odd) permutation leads to a positive (negative) sign. This way all cluster groups in Eq. (3.11) are fully antisymmetric. Additionally, the proper definition of this recursion relation ensures that the quantities $\Delta\langle\{N\}^\dagger|\{N\}\rangle$ contain the purely correlated part of the N-particle cluster. The consistency of the approach implies that (i) approximations done in an $2N$-point expectation value are inherited by all lower order quantities and (ii) the knowledge of all expectation values up to the desired level of approximation suffices to construct all higher order reduced density matrices in the same approximation. Thus, the cluster expansion clearly identifies singlet, doublet, triplet, etc. states in $\langle\{N\}^\dagger|\{N\}\rangle$ in direct analogy to the cluster expansion for atomic or molecular wave functions [63,64]. More explicitly, Eq. (3.11) allows the identification $\langle\{N\}^\dagger|\{N\}\rangle = \langle\{N\}^\dagger|\{N\}\rangle_\mathrm{S} + \langle\{N\}^\dagger|\{N\}\rangle_\mathrm{D} + \dots$, in terms of

$$\langle\{N\}^\dagger|\{N\}\rangle_\mathrm{S} = \langle\{N\}^\dagger|\{N\}\rangle_\mathrm{HF}, \tag{3.12}$$

$$\begin{aligned}\langle\{N\}^\dagger|\{N\}\rangle_\mathrm{D} &= \langle\{N-2\}^\dagger|\{N-2\}\rangle_\mathrm{S}\,\Delta\langle\{2\}^\dagger|\{2\}\rangle \\ &\quad + \langle\{N-4\}^\dagger|\{N-4\}\rangle_\mathrm{S}\,\Delta\langle\{2\}^\dagger|\{2\}\rangle\,\Delta\langle\{2\}^\dagger|\{2\}\rangle + \dots \\ &= \Delta\langle\{2\}^\dagger|\{2\}\rangle\,\langle\{N-2\}^\dagger|\{N-2\}\rangle_\mathrm{SD},\end{aligned} \tag{3.13}$$

where $\langle\{N\}^\dagger|\{N\}\rangle_{\mathrm{S}}$ contains only single-particle expectation values whereas the doublet contribution $\langle\{N\}^\dagger|\{N\}\rangle_{\mathrm{D}}$ includes all expectation values with one or more pairs $\Delta\langle\{2\}^\dagger|\{2\}\rangle$ combined with the required combination of singlets $\langle\{1\}^\dagger|\{1\}\rangle$.

Even with the current supercomputers, the numerical solutions are practically limited to the doublet level for realistic semiconductor systems. In this case, one has to know the factorization scheme for four-point quantities the explicit form of which is

$$\begin{aligned}\langle a^\dagger_{\mathbf{k}_1} a^\dagger_{\mathbf{k}_2} a_{\mathbf{k}_3} a_{\mathbf{k}_4}\rangle &= \langle a^\dagger_{\mathbf{k}_1} a^\dagger_{\mathbf{k}_2} a_{\mathbf{k}_3} a_{\mathbf{k}_4}\rangle_{\mathrm{S}} + \Delta\langle a^\dagger_{\mathbf{k}_1} a^\dagger_{\mathbf{k}_2} a_{\mathbf{k}_3} a_{\mathbf{k}_4}\rangle \\ &= \Big[\langle a^\dagger_{\mathbf{k}_1} a_{\mathbf{k}_4}\rangle\langle a^\dagger_{\mathbf{k}_2} a_{\mathbf{k}_3}\rangle - \langle a^\dagger_{\mathbf{k}_1} a_{\mathbf{k}_3}\rangle\langle a^\dagger_{\mathbf{k}_2} a_{\mathbf{k}_4}\rangle\Big] + \Delta\langle a^\dagger_{\mathbf{k}_1} a^\dagger_{\mathbf{k}_2} a_{\mathbf{k}_3} a_{\mathbf{k}_4}\rangle. \end{aligned} \tag{3.14}$$

The four-point quantities in Eq. (3.14) are coupled to six-point terms which also have to be factorized according to the classification. Their explicit form is given by

$$\begin{aligned}\langle a^\dagger_{\mathbf{k}_1} a^\dagger_{\mathbf{k}_2} a^\dagger_{\mathbf{k}_3} a_{\mathbf{k}_4} a_{\mathbf{k}_5} a_{\mathbf{k}_6}\rangle &= \langle a^\dagger_{\mathbf{k}_1} a^\dagger_{\mathbf{k}_2} a^\dagger_{\mathbf{k}_3} a_{\mathbf{k}_4} a_{\mathbf{k}_5} a_{\mathbf{k}_6}\rangle_{\mathrm{S}} \\ &+ \langle a^\dagger_{\mathbf{k}_1} a_{\mathbf{k}_6}\rangle\Delta\langle a^\dagger_{\mathbf{k}_2} a^\dagger_{\mathbf{k}_3} a_{\mathbf{k}_4} a_{\mathbf{k}_5}\rangle - \langle a^\dagger_{\mathbf{k}_1} a_{\mathbf{k}_5}\rangle\Delta\langle a^\dagger_{\mathbf{k}_2} a^\dagger_{\mathbf{k}_3} a_{\mathbf{k}_4} a_{\mathbf{k}_6}\rangle \\ &+ \langle a^\dagger_{\mathbf{k}_1} a_{\mathbf{k}_4}\rangle\Delta\langle a^\dagger_{\mathbf{k}_2} a^\dagger_{\mathbf{k}_3} a_{\mathbf{k}_5} a_{\mathbf{k}_6}\rangle - \langle a^\dagger_{\mathbf{k}_2} a_{\mathbf{k}_6}\rangle\Delta\langle a^\dagger_{\mathbf{k}_1} a^\dagger_{\mathbf{k}_3} a_{\mathbf{k}_4} a_{\mathbf{k}_5}\rangle \\ &+ \langle a^\dagger_{\mathbf{k}_2} a_{\mathbf{k}_5}\rangle\Delta\langle a^\dagger_{\mathbf{k}_1} a^\dagger_{\mathbf{k}_3} a_{\mathbf{k}_4} a_{\mathbf{k}_6}\rangle - \langle a^\dagger_{\mathbf{k}_2} a_{\mathbf{k}_4}\rangle\Delta\langle a^\dagger_{\mathbf{k}_1} a^\dagger_{\mathbf{k}_3} a_{\mathbf{k}_5} a_{\mathbf{k}_6}\rangle \\ &+ \langle a^\dagger_{\mathbf{k}_3} a_{\mathbf{k}_6}\rangle\Delta\langle a^\dagger_{\mathbf{k}_1} a^\dagger_{\mathbf{k}_2} a_{\mathbf{k}_4} a_{\mathbf{k}_5}\rangle - \langle a^\dagger_{\mathbf{k}_3} a_{\mathbf{k}_5}\rangle\Delta\langle a^\dagger_{\mathbf{k}_1} a^\dagger_{\mathbf{k}_2} a_{\mathbf{k}_4} a_{\mathbf{k}_6}\rangle \\ &+ \langle a^\dagger_{\mathbf{k}_3} a_{\mathbf{k}_4}\rangle\Delta\langle a^\dagger_{\mathbf{k}_1} a^\dagger_{\mathbf{k}_2} a_{\mathbf{k}_5} a_{\mathbf{k}_6}\rangle + \Delta\langle a^\dagger_{\mathbf{k}_1} a^\dagger_{\mathbf{k}_2} a^\dagger_{\mathbf{k}_3} a_{\mathbf{k}_4} a_{\mathbf{k}_5} a_{\mathbf{k}_6}\rangle \end{aligned} \tag{3.15}$$

with

$$\begin{aligned}\langle a^\dagger_{\mathbf{k}_1} a^\dagger_{\mathbf{k}_2} a^\dagger_{\mathbf{k}_3} a_{\mathbf{k}_4} a_{\mathbf{k}_5} a_{\mathbf{k}_6}\rangle_{\mathrm{S}} = \\ &\langle a^\dagger_{\mathbf{k}_1} a_{\mathbf{k}_6}\rangle\langle a^\dagger_{\mathbf{k}_2} a_{\mathbf{k}_5}\rangle\langle a^\dagger_{\mathbf{k}_3} a_{\mathbf{k}_4}\rangle - \langle a^\dagger_{\mathbf{k}_1} a_{\mathbf{k}_6}\rangle\langle a^\dagger_{\mathbf{k}_2} a_{\mathbf{k}_4}\rangle\langle a^\dagger_{\mathbf{k}_3} a_{\mathbf{k}_5}\rangle \\ &+ \langle a^\dagger_{\mathbf{k}_1} a_{\mathbf{k}_5}\rangle\langle a^\dagger_{\mathbf{k}_2} a_{\mathbf{k}_4}\rangle\langle a^\dagger_{\mathbf{k}_3} a_{\mathbf{k}_6}\rangle - \langle a^\dagger_{\mathbf{k}_1} a_{\mathbf{k}_5}\rangle\langle a^\dagger_{\mathbf{k}_2} a_{\mathbf{k}_6}\rangle\langle a^\dagger_{\mathbf{k}_3} a_{\mathbf{k}_4}\rangle \\ &+ \langle a^\dagger_{\mathbf{k}_1} a_{\mathbf{k}_4}\rangle\langle a^\dagger_{\mathbf{k}_2} a_{\mathbf{k}_6}\rangle\langle a^\dagger_{\mathbf{k}_3} a_{\mathbf{k}_5}\rangle - \langle a^\dagger_{\mathbf{k}_1} a_{\mathbf{k}_4}\rangle\langle a^\dagger_{\mathbf{k}_2} a_{\mathbf{k}_5}\rangle\langle a^\dagger_{\mathbf{k}_3} a_{\mathbf{k}_6}\rangle. \end{aligned} \tag{3.16}$$

If one wants to perform calculations including all correlations up to the two-particle level, one has to set up the equations of motion for all terms up to the four-point level

$$\begin{aligned} i\hbar\frac{\partial}{\partial t}\langle a^\dagger_{\mathbf{k}_1} a_{\mathbf{p}_1}\rangle &= T_1\left[\langle a^\dagger_{\mathbf{k}_1} a_{\mathbf{p}_1}\rangle\right] + V_1\left[\langle a^\dagger_{\mathbf{k}_1} a^\dagger_{\alpha_2} a_{\beta_2} a_{\mathbf{p}_1}\rangle\right] \\ &= T_1\left[\langle a^\dagger_{\mathbf{k}_1} a_{\mathbf{p}_1}\rangle\right] + V_1\left[\langle a^\dagger_{\mathbf{k}_1} a^\dagger_{\alpha_2} a_{\beta_2} a_{\mathbf{p}_1}\rangle_{\mathrm{S}}\right] \\ &\quad + V_1\left[\Delta\langle a^\dagger_{\mathbf{k}1} a^\dagger_{\alpha_2} a_{\beta_2} a_{\mathbf{p}_1}\rangle\right], \end{aligned} \tag{3.17}$$

$$\begin{aligned} i\hbar\frac{\partial}{\partial t}\Delta\langle a^\dagger_{\mathbf{k}_1} a^\dagger_{\mathbf{k}_2} a_{\mathbf{p}_2} a_{\mathbf{p}_1}\rangle &= T_2\left[\Delta\langle a^\dagger_{\mathbf{k}_1} a^\dagger_{\mathbf{k}_2} a_{\mathbf{p}_2} a_{\mathbf{p}_1}\rangle\right] \\ &\quad + V_2\left[\langle a^\dagger_{\mathbf{k}_1} a^\dagger_{\mathbf{k}_2} a^\dagger_{\alpha_3} a_{\beta_3} a_{\mathbf{p}_2} a_{\mathbf{p}_1}\rangle_{\mathrm{SD}}\right], \end{aligned} \tag{3.18}$$

where the six-point term on the right-hand side is kept at the singlet-doublet approximation and the triplet contributions are neglected.

Since we investigate exciton formation, we need to determine at least the correlations between two particles. Therefore, we define the exciton and carrier-carrier correlations

$$c_{\mathrm{X}}^{q,k',k} = \Delta\langle c_k^\dagger v_{k'}^\dagger c_{k'+q} v_{k-q}\rangle\,, \tag{3.19}$$
$$c_{\mathrm{e}}^{q,k',k} = \Delta\langle c_k^\dagger c_{k'}^\dagger c_{k'+q} c_{k-q}\rangle\,, \tag{3.20}$$
$$c_{\mathrm{h}}^{q,k',k} = \Delta\langle v_k^\dagger v_{k'}^\dagger v_{k'+q} v_{k-q}\rangle\,, \tag{3.21}$$

which are the only existing incoherent four-particle correlations.

The advantage of the factorization is its direct physical interpretation. By subtracting the single-particle contribution from the full expectation value, the resulting correlated part really describes the true two-particle correlations. All higher order correlations can be interpreted in the same spirit. In this thesis, we treat all terms up to the four-point level exactly, factorize the emerging six-point correlations into all products of two-point and four-point correlations and only neglect the true six-point correlations beyond the correlated pair level. Physically, we thus allow the presence of uncorrelated particles and any number of correlated pairs. This scheme includes all terms which are present in the so called $\chi^{(3)}$-limit based on the Dynamics-Controlled Truncation Scheme [66,67] and has the additional advantage of being applicable also in the long time limit where a classification according to powers in the field strength of an exciting laser pulse becomes questionable. Furthermore, it can be used to describe the dynamics for arbitrarily strong pulses. In general, the cluster expansion cut at the $2n$-point level contains all equations of the $\chi^{(2n-1)}$ expansion as a subset.

The cluster expansion can also be used directly to classify and truncate quantum-optical correlations or carrier-phonon correlations using the formal equivalence between a boson operator and a pair of fermion operators established in Eq. (3.5). The corresponding results are summarized in the following where we denote the generic photon or phonon operator by O_i which can either be a creation or an annihilation operator. For a sequence $O_1 O_2 \ldots O_N$, the operators O_i are assumed to be normally ordered.

In the case of photons, $\langle O\rangle$ represents the coherent, classical part of the electric field. In the further derivations, we also need the following singlet contributions

$$\langle a_{\mathbf{k}}^\dagger O a_{\mathbf{p}}\rangle_{\mathrm{S}} = \langle a_{\mathbf{k}}^\dagger a_{\mathbf{p}}\rangle\langle O\rangle, \tag{3.22}$$
$$\langle O_1 O_2\rangle_{\mathrm{S}} = \langle O_1\rangle\langle O_2\rangle, \tag{3.23}$$
$$\langle a_{\mathbf{k}_1}^\dagger a_{\mathbf{k}_2}^\dagger O a_{\mathbf{p}_2} a_{\mathbf{p}_1}\rangle_{\mathrm{S}} = \langle a_{\mathbf{k}_1}^\dagger a_{\mathbf{p}_1}\rangle\langle a_{\mathbf{k}_2}^\dagger a_{\mathbf{p}_2}\rangle\langle O\rangle - \langle a_{\mathbf{k}_1}^\dagger a_{\mathbf{p}_2}\rangle\langle a_{\mathbf{k}_2}^\dagger a_{\mathbf{p}_1}\rangle\langle O\rangle, \tag{3.24}$$
$$\langle a_{\mathbf{k}}^\dagger O_1 O_2 a_{\mathbf{p}}\rangle_{\mathrm{S}} = \langle a_{\mathbf{k}}^\dagger a_{\mathbf{p}}\rangle\langle O_2\rangle\langle O_1\rangle, \tag{3.25}$$
$$\langle O_1 O_2 O_3\rangle_{\mathrm{S}} = \langle O_1\rangle\langle O_2\rangle\langle O_3\rangle. \tag{3.26}$$

Equations (3.22)–(3.26) show that the singlet contributions of photon operators correspond to the classical (coherent) part where the electric field can be treated as a complex valued number, not as an operator. According to the cluster expansion, the correlated doublets are found from

$$\Delta\langle a_{\mathbf{k}}^\dagger O a_{\mathbf{p}}\rangle = \langle a_{\mathbf{k}}^\dagger O a_{\mathbf{p}}\rangle - \langle a_{\mathbf{k}}^\dagger O a_{\mathbf{p}}\rangle_{\mathrm{S}}, \tag{3.27}$$
$$\Delta\langle O_1 O_2\rangle = \langle O_1 O_2\rangle - \langle O_1 O_2\rangle_{\mathrm{S}}, \tag{3.28}$$

where the classical part is subtracted from the full expectation value. Such terms include correlations between carriers and photons or between two photons and lead to quantum-optical effects resulting, e.g., in squeezing and entanglement [5,6,44].

The actual truncation has to be performed for the six-point expectation values while Eq. (3.27)–(3.28) serve as an identification of quantum-optical features. At the consistent singlet-doublet level, the truncation of the hierarchy follows from

$$\begin{aligned}
\langle a^\dagger_{\mathbf{k}_1} a^\dagger_{\mathbf{k}_2} O a_{\mathbf{p}_2} a_{\mathbf{p}_1}\rangle_{\mathrm{SD}} &= \langle a^\dagger_{\mathbf{k}_1} a^\dagger_{\mathbf{k}_2} O a_{\mathbf{p}_2} a_{\mathbf{p}_1}\rangle_{\mathrm{S}} + \langle O\rangle \Delta\langle a^\dagger_{\mathbf{k}_1} a^\dagger_{\mathbf{k}_2} a_{\mathbf{p}_2} a_{\mathbf{p}_1}\rangle \\
&\quad + \langle a^\dagger_{\mathbf{k}_1} a_{\mathbf{p}_1}\rangle \Delta\langle a^\dagger_{\mathbf{k}_2} O a_{\mathbf{p}_2}\rangle - \langle a^\dagger_{\mathbf{k}_1} a_{\mathbf{p}_2}\rangle \Delta\langle a^\dagger_{\mathbf{k}_2} O a_{\mathbf{p}_1}\rangle \\
&\quad - \langle a^\dagger_{\mathbf{k}_2} a_{\mathbf{p}_1}\rangle \Delta\langle a^\dagger_{\mathbf{k}_1} O a_{\mathbf{p}_2}\rangle + \langle a^\dagger_{\mathbf{k}_2} a_{\mathbf{p}_2}\rangle \Delta\langle a^\dagger_{\mathbf{k}_1} O a_{\mathbf{p}_1}\rangle, \qquad (3.29) \\
\langle a^\dagger_{\mathbf{k}} O_1 O_2 a_{\mathbf{p}}\rangle_{\mathrm{SD}} &= \langle a^\dagger_{\mathbf{k}} O_1 O_2 a_{\mathbf{p}}\rangle_{\mathrm{S}} + \langle a^\dagger_{\mathbf{k}} a_{\mathbf{p}}\rangle \Delta\langle O_1 O_2\rangle \\
&\quad + \langle O_2\rangle \Delta\langle a^\dagger_{\mathbf{k}} O_1 a_{\mathbf{p}}\rangle + \langle O_1\rangle \Delta\langle a^\dagger_{\mathbf{k}} O_2 a_{\mathbf{p}}\rangle, \qquad (3.30) \\
\langle O_1 O_2 O_3\rangle_{\mathrm{SD}} &= \langle O_1 O_2 O_3\rangle_{\mathrm{S}} + \langle O_3\rangle \Delta\langle O_1 O_2\rangle \\
&\quad + \langle O_2\rangle \Delta\langle O_1 O_3\rangle + \langle O_1\rangle \Delta\langle O_2 O_3\rangle. \qquad (3.31)
\end{aligned}$$

The singlet-doublet truncation (3.29)–(3.31) leads to a closed set of consistent equations which include the dominant quantum-optical correlations.

3.3 Coulomb Interaction

Since the total Hamiltonian (2.66) consists of different contributions and Eq. (2.34) is linear, one can examine these different parts one by one. We begin by presenting the Heisenberg equations of motion for the excitonic correlations, Eq. (3.19), using only the free kinetic part H_{kin} and the Coulomb part H_{C} of the full Hamiltonian (2.66). The general derivation using the cluster expansion up to the four-point level is performed in App. A. Here, we use this derivation to obtain the equations under incoherent conditions. For the exciton correlations, one obtains

$$\begin{aligned}
\left[i\hbar\frac{\partial}{\partial t} c^{q,k',k}_{\mathrm{X}}\right]_{H_{\mathrm{kin}}+H_{\mathrm{C}}} &= \left(\tilde{\epsilon}^{\mathrm{e}}_{k'+q} + \tilde{\epsilon}^{\mathrm{h}}_{k'} - \tilde{\epsilon}^{\mathrm{h}}_{k-q} - \tilde{\epsilon}^{\mathrm{e}}_{k}\right) c^{q,k',k}_{\mathrm{X}} \\
&\quad + V_{k-k'-q}\left[\left(1-f^{\mathrm{e}}_{k}\right)\left(1-f^{\mathrm{h}}_{k-q}\right) f^{\mathrm{e}}_{k'+q} f^{\mathrm{h}}_{k'} - f^{\mathrm{e}}_{k} f^{\mathrm{h}}_{k-q}\left(1-f^{\mathrm{e}}_{k'+q}\right)\left(1-f^{\mathrm{h}}_{k'}\right)\right] \\
&\quad + V_{k-k'-q}\left[\left(f^{\mathrm{h}}_{k-q} - f^{\mathrm{h}}_{k'}\right)\sum_{l} c^{q+k'-l,l,k}_{\mathrm{e+X}} + \left(f^{\mathrm{e}}_{k} - f^{\mathrm{e}}_{k'+q}\right)\sum_{l} c^{q-k+l,k',l}_{\mathrm{h+X}}\right] \\
&\quad + \left[1 - f^{\mathrm{e}}_{k} - f^{\mathrm{h}}_{k-q}\right]\sum_{l} V_{l-k}\, c^{q,k',l}_{\mathrm{X}} - \left[1 - f^{\mathrm{e}}_{k'+q} - f^{\mathrm{h}}_{k'}\right]\sum_{l} V_{l-k'}\, c^{q,l,k}_{\mathrm{X}} \\
&\quad + \left[f^{\mathrm{h}}_{k-q} - f^{\mathrm{e}}_{k'+q}\right]\sum_{l} V_{l-q}\, c^{l,k',k}_{\mathrm{X}} + \left[f^{\mathrm{e}}_{k} - f^{\mathrm{h}}_{k'}\right]\sum_{l} V_{l-q}\, c^{l,q+k'-l,k-q+l}_{\mathrm{X}} \\
&\quad + \left[f^{\mathrm{e}}_{k'+q} - f^{\mathrm{e}}_{k}\right]\sum_{l} V_{l-k}\, c^{q-k+l,k',l}_{\mathrm{X}} + \left[f^{\mathrm{h}}_{k'} - f^{\mathrm{h}}_{k-q}\right]\sum_{l} V_{l-k'}\, c^{q+k'-l,l,k}_{\mathrm{X}}, \qquad (3.32)
\end{aligned}$$

which is coupled both to carrier densities and to electron and hole correlations $c^{q,k',k}_{\mathrm{e(h)}}$. The dynamics of these correlations is described by similar equations

$$\begin{aligned}
\left[i\hbar\frac{\partial}{\partial t}c^{q,k',k}_{\mathrm{e}}\right]_{H_{\mathrm{kin}}+H_{\mathrm{C}}} &= \left(\tilde{\epsilon}^{\mathrm{e}}_{k-q}+\tilde{\epsilon}^{\mathrm{e}}_{k'+q}-\tilde{\epsilon}^{\mathrm{e}}_{k'}-\tilde{\epsilon}^{\mathrm{e}}_{k}\right)c^{q,k',k}_{\mathrm{e}}\\
&+V_{k-k'-q}\left[f^{\mathrm{e}}_{k-q}f^{\mathrm{e}}_{k'+q}\left(1-f^{\mathrm{e}}_{k}\right)\left(1-f^{\mathrm{e}}_{k'}\right)-f^{\mathrm{e}}_{k}f^{\mathrm{e}}_{k'}\left(1-f^{\mathrm{e}}_{k-q}\right)\left(1-f^{\mathrm{e}}_{k'+q}\right)\right]\\
&-V_{q}\left[f^{\mathrm{e}}_{k-q}f^{\mathrm{e}}_{k'+q}\left(1-f^{\mathrm{e}}_{k}\right)\left(1-f^{\mathrm{e}}_{k'}\right)-f^{\mathrm{e}}_{k}f^{\mathrm{e}}_{k'}\left(1-f^{\mathrm{e}}_{k-q}\right)\left(1-f^{\mathrm{e}}_{k'+q}\right)\right]\\
&+V_{q}\left[\left(f^{\mathrm{e}}_{k'+q}-f^{\mathrm{e}}_{k'}\right)\sum_{l}c^{k-q-l,l,k}_{\mathrm{e+X}}-\left(f^{\mathrm{e}}_{k}-f^{\mathrm{e}}_{k-q}\right)\sum_{l}c^{q+k'-l,l,k'}_{\mathrm{e+X}}\right]\\
&-V_{k-k'-q}\left[\left(f^{\mathrm{e}}_{k'+q}-f^{\mathrm{e}}_{k}\right)\sum_{l}c^{k-q-l,l,k'}_{\mathrm{e+X}}-\left(f^{\mathrm{e}}_{k'}-f^{\mathrm{e}}_{k-q}\right)\sum_{l}c^{q+k'-l,l,k}_{\mathrm{e+X}}\right]\\
&+\left[1-f^{\mathrm{e}}_{k-q}-f^{\mathrm{e}}_{k'+q}\right]\sum_{l}V_{l-q}\,c^{l,k',k}_{\mathrm{e}}-\left[1-f^{\mathrm{e}}_{k}-f^{\mathrm{e}}_{k'}\right]\sum_{l}V_{l-q}\,c^{l,q+k'-l,k-q+l}_{\mathrm{e}}\\
&-\left[f^{\mathrm{e}}_{k}-f^{\mathrm{e}}_{k-q}\right]\sum_{l}V_{l-k}\,c^{q,k',l}_{\mathrm{e}}+\left[f^{\mathrm{e}}_{k'+q}-f^{\mathrm{e}}_{k}\right]\sum_{l}V_{l-k}\,c^{q-k+l,k',l}_{\mathrm{e}}\\
&+\left[f^{\mathrm{e}}_{k'+q}-f^{\mathrm{e}}_{k'}\right]\sum_{l}V_{l-k'}\,c^{q,l,k}_{\mathrm{e}}-\left[f^{\mathrm{e}}_{k'}-f^{\mathrm{e}}_{k-q}\right]\sum_{l}V_{l-k'}\,c^{q+k'-l,l,k}_{\mathrm{e}},
\end{aligned}\tag{3.33}$$

$$\begin{aligned}
\left[i\hbar\frac{\partial}{\partial t}c^{q,k',k}_{\mathrm{h}}\right]_{H_{\mathrm{kin}}+H_{\mathrm{C}}} &= \left(-\tilde{\epsilon}^{\mathrm{h}}_{k-q}-\tilde{\epsilon}^{\mathrm{h}}_{k'+q}+\tilde{\epsilon}^{\mathrm{h}}_{k'}+\tilde{\epsilon}^{\mathrm{h}}_{k}\right)c^{q,k',k}_{\mathrm{h}}\\
&+V_{k-k'-q}\left[\left(1-f^{\mathrm{h}}_{k-q}\right)\left(1-f^{\mathrm{h}}_{k'+q}\right)f^{\mathrm{h}}_{k}f^{\mathrm{h}}_{k'}-\left(1-f^{\mathrm{h}}_{k}\right)\left(1-f^{\mathrm{h}}_{k'}\right)f^{\mathrm{h}}_{k-q}f^{\mathrm{h}}_{k'+q}\right]\\
&-V_{q}\left[\left(1-f^{\mathrm{h}}_{k-q}\right)\left(1-f^{\mathrm{h}}_{k'+q}\right)f^{\mathrm{h}}_{k}f^{\mathrm{h}}_{k'}-\left(1-f^{\mathrm{h}}_{k}\right)\left(1-f^{\mathrm{h}}_{k'}\right)f^{\mathrm{h}}_{k-q}f^{\mathrm{h}}_{k'+q}\right]\\
&+V_{q}\left[\left(f^{\mathrm{h}}_{k'}-f^{\mathrm{h}}_{k'+q}\right)\sum_{l}c^{q-k+l,k,l}_{\mathrm{h+X}}-\left(f^{\mathrm{h}}_{k-q}-f^{\mathrm{h}}_{k}\right)\sum_{l}c^{l-q-k',k',l}_{\mathrm{h+X}}\right]\\
&+V_{k-k'-q}\left[\left(f^{\mathrm{h}}_{k'+q}-f^{\mathrm{h}}_{k}\right)\sum_{l}c^{q-k+l,k',l}_{\mathrm{h+X}}-\left(f^{\mathrm{h}}_{k'}-f^{\mathrm{h}}_{k-q}\right)\sum_{l}c^{l-q-k',k,l}_{\mathrm{e+X}}\right]\\
&-\left[1-f^{\mathrm{h}}_{k-q}-f^{\mathrm{h}}_{k'+q}\right]\sum_{l}V_{l-q}\,c^{l,k',k}_{\mathrm{h}}+\left[1-f^{\mathrm{h}}_{k}-f^{\mathrm{h}}_{k'}\right]\sum_{l}V_{l-q}\,c^{l,q+k'-l,k-q+l}_{\mathrm{h}}\\
&+\left[f^{\mathrm{h}}_{k}-f^{\mathrm{h}}_{k-q}\right]\sum_{l}V_{l-k}\,c^{q,k',l}_{\mathrm{h}}-\left[f^{\mathrm{h}}_{k'+q}-f^{\mathrm{h}}_{k}\right]\sum_{l}V_{l-k}\,c^{q-k+l,k',l}_{\mathrm{h}}\\
&-\left[f^{\mathrm{h}}_{k'+q}-f^{\mathrm{h}}_{k'}\right]\sum_{l}V_{l-k'}\,c^{q,l,k}_{\mathrm{h}}+\left[f^{\mathrm{h}}_{k'}-f^{\mathrm{h}}_{k-q}\right]\sum_{l}V_{l-k'}\,c^{q+k'-l,l,k}_{\mathrm{h}}.
\end{aligned}\tag{3.34}$$

In Eqs. (3.32)–(3.34), we have introduced the abbreviation $c^{q,k',k}_{\mathrm{e(h)+X}}=c^{q,k',k}_{\mathrm{e(h)}}+c^{q,k',k}_{\mathrm{X}}$. The interpretation of these equations is straightforward: The first line of Eq. (3.32), for example, gives the kinetic evolution of the four-point operator with the renormalized energies

$$\tilde{\epsilon}^{\mathrm{e(h)}}=\epsilon^{\mathrm{e(h)}}-\sum_{k'}V_{k-k'}f^{\mathrm{e(h)}}_{k'}\,.\tag{3.35}$$

The second line of Eq. (3.32) contains the factorized source term which leads to the creation of excitonic correlations as soon as electrons and holes are present. This source is altered by the direct influence of the correlations in the third line. The remaining six Coulomb sums describe the different possibilities how two out of four particles can interact via Coulomb interaction. These sums lead to the possibility to form bound excitons. The major contributions originate from the first two of the six sums which are multiplied by a phase space filling factor instead of a density difference and are thus appreciable even for low densities. All other sums vanish for low density but become important when the density is increased. They are a consequence of the indistinguishability of electrons and holes and correspond to Coulomb interaction between carriers formally "belonging" to two different excitons. Equations investigating exciton formation in the $\chi^{(2)}$-limit [41] do not contain these additional f-dependent contributions.

For low densities, it is often a good approximation to neglect all but the two dominant sums. These two terms formally describe the Coulomb interaction within one exciton. Whenever the restriction to these two "main sums" and to the factorized source is possible, Eq. (3.32) becomes diagonal in the center-of-mass momentum q. Consequently, the numerical evaluation is much easier and the resulting set of equations can be computed also for two-dimensional quantum-well structures. This is also the starting point of an adiabatic solution in Sec. 4.3. Yet, we want to point out that the source term as a product of carrier densities is dominantly fermionic and cannot be obtained by starting with a bosonic exciton model.

The Eqs. (3.33) and (3.34) of the carrier-carrier correlation functions can be interpreted analogously. They contain factorized source terms which lead to the formation of correlations as soon as excited carriers are present in the semiconductor. This source is modified by a purely correlated contribution in line 4 and 5 of Eq. (3.33) and (3.34). The Coulomb resonances are introduced by all the other sums describing the various interactions between the electrons within the correlated pairs.

In order to obtain a closed set of equations for the incoherent dynamics of the pure carrier system, one finally has to derive the equation of motion for electron and hole densities. They are given by

$$\left[\frac{\partial}{\partial t} f_k^{\mathrm{e}}\right]_{H_{\mathrm{kin}}+H_{\mathrm{C}}} = \frac{2}{\hbar}\mathrm{Im}\left[\sum_{k',q} V_q\, c_{\mathrm{e}}^{q,k',k} - \sum_{k',q} V_{k-q-k'}\, c_{\mathrm{X}}^{q,k',k}\right] \tag{3.36}$$

$$\left[\frac{\partial}{\partial t} f_k^{\mathrm{h}}\right]_{H_{\mathrm{kin}}+H_{\mathrm{C}}} = \frac{2}{\hbar}\mathrm{Im}\left[-\sum_{k',q} V_q\, c_{\mathrm{h}}^{q,k',k} + \sum_{k',q} V_{k-q-k'}\, c_{\mathrm{X}}^{-q,k,k'}\right] \tag{3.37}$$

and describe effects of the correlations back onto the carrier densities. Since all incoherent four-point correlations are treated exactly, this approach includes the microscopic carrier-carrier scattering beyond the second-Born approach [16].

3.4 Phonon Interaction

When electrons and holes are under the influence of Coulomb interaction, excitonic correlations can build up, i.e., the carriers of opposite charge are attracted towards each other. Due to the energy conservation, they are forced to accelerate and thus increase their kinetic energy in order to compensate the decrease in Coulomb energy. In principle, Eqs. (3.32)–(3.37) provide a closed set of equations which describes exactly this scenario, starting from a number of totally uncorrelated charge carriers. Nevertheless, a real semiconductor offers a larger variety of possible processes: Whenever a third particle takes over the kinetic excess energy of a Coulomb correlated electron-hole pair, a bound exciton can form. In a many-body system, in principle every carrier can play this role and compensate the energy gained by formation. Processes of that kind, however, would inevitably lead to a heating of the remaining carrier system such that further formation would get more and more improbable. A more prominent formation channel is therefore provided by phonons since the excess energy can be directed out of the many-body system and into the phonon reservoir. Since the phonon system is typically unperturbed by the carrier dynamics, we solve the phonon operator dependent dynamics using the steady-state Markov approximation with the assumption of thermal occupation of the different phonon states.

The general starting point is the phonon-interaction Hamiltonian (2.64). It couples carrier densities and the different exciton and carrier correlations to phonon-assisted correlations which are solved in Markov approximation as discussed in App. B. In the strict singlet-doublet approximation, the carrier-phonon dynamics is fully determined by the phonon-assisted carrier densities. The resulting density and correlation dynamics follow from

$$\left[\frac{\partial}{\partial t} f^{\mathrm{e}}_k\right]_{H_{\mathrm{P}}} = \frac{2}{\hbar}\sum_p \mathrm{Im}\left[\Pi^{\mathrm{e}}_{k,p}\right] , \tag{3.38}$$

$$\left[\frac{\partial}{\partial t} f^{\mathrm{h}}_k\right]_{H_{\mathrm{P}}} = -\frac{2}{\hbar}\sum_p \mathrm{Im}\left[\Pi^{\mathrm{h}}_{k,p}\right] , \tag{3.39}$$

$$\left[i\hbar\frac{\partial}{\partial t} c^{q,k',k}_{\mathrm{X}}\right]_{H_{\mathrm{P}},\mathrm{SD}} = \Pi^{\mathrm{e}}_{k,k-q-k'}\left(f^{\mathrm{h}}_{k'} - f^{\mathrm{h}}_{k-q}\right) - \Pi^{\mathrm{h}}_{k',k'+q-k}\left(f^{\mathrm{e}}_{k} - f^{\mathrm{e}}_{k'+q}\right) , \tag{3.40}$$

$$\left[i\hbar\frac{\partial}{\partial t} c^{q,k',k}_{\mathrm{e}}\right]_{H_{\mathrm{P}},\mathrm{SD}} = \Pi^{\mathrm{e}}_{k,k-q-k'}\left(f^{\mathrm{e}}_{k-q} - f^{\mathrm{e}}_{k'}\right) + \Pi^{\mathrm{e}}_{k',k'+q-k}\left(f^{\mathrm{e}}_{k'+q} - f^{\mathrm{e}}_{k}\right) + \Pi^{\mathrm{e}}_{k',-q}\left(f^{\mathrm{e}}_{k} - f^{\mathrm{e}}_{k-q}\right) + \Pi^{\mathrm{e}}_{k,q}\left(f^{\mathrm{e}}_{k'} - f^{\mathrm{e}}_{k'+q}\right) , \tag{3.41}$$

$$\left[i\hbar\frac{\partial}{\partial t} c^{q,k',k}_{\mathrm{h}}\right]_{H_{\mathrm{P}},\mathrm{SD}} = \Pi^{\mathrm{h}}_{k,k-q-k'}\left(f^{\mathrm{h}}_{k'} - f^{\mathrm{h}}_{k-q}\right) + \Pi^{\mathrm{h}}_{k',k'+q-k}\left(f^{\mathrm{h}}_{k} - f^{\mathrm{h}}_{k'+q}\right) + \Pi^{\mathrm{h}}_{k',-q}\left(f^{\mathrm{h}}_{k-q} - f^{\mathrm{h}}_{k}\right) + \Pi^{\mathrm{h}}_{k,q}\left(f^{\mathrm{h}}_{k'+q} - f^{\mathrm{h}}_{k'}\right) , \tag{3.42}$$

where we have defined the terms

$$\Pi^{\mathrm{e}}_{k,p} = i\sum_{p_\perp} |G_{p,p_\perp}|^2 f^{\mathrm{e}}_{k-p}(1 - f^{\mathrm{e}}_{k})\Big\{ N^{\mathrm{PH}}_{p,p_\perp} g(\varepsilon^{\mathrm{e}}_{k} - \varepsilon^{\mathrm{e}}_{k-p} - \hbar\Omega_{p,p_\perp})$$

$$
\begin{aligned}
&\qquad\qquad +(N^{\mathrm{PH}}_{p,p_\perp}+1)g(\varepsilon^{\mathrm{e}}_k-\varepsilon^{\mathrm{e}}_{k-p}+\hbar\Omega_{p,p_\perp})\Big\}\\
&-i\sum_{p_\perp}|G_{p,p_\perp}|^2 f^{\mathrm{e}}_k(1-f^{\mathrm{e}}_{k-p})\Big\{N^{\mathrm{PH}}_{p,p_\perp}g(\varepsilon^{\mathrm{e}}_k-\varepsilon^{\mathrm{e}}_{k-p}+\hbar\Omega_{p,p_\perp})\\
&\qquad\qquad +(N^{\mathrm{PH}}_{p,p_\perp}+1)g(\varepsilon^{\mathrm{e}}_k-\varepsilon^{\mathrm{e}}_{k-p}-\hbar\Omega_{p,p_\perp})\Big\}\\
&+i\sum_{l,p_\perp}|G_{p,p_\perp}|^2 c^{p,l,k}_{\mathrm{e}}\\
&\qquad\Big\{g(\varepsilon^{\mathrm{e}}_{l+p}-\varepsilon^{\mathrm{e}}_l+\hbar\Omega_{p,p_\perp})-g(\varepsilon^{\mathrm{e}}_{l+p}-\varepsilon^{\mathrm{e}}_l-\hbar\Omega_{p,p_\perp})\Big\}\\
&-i\sum_{l,p_\perp}|G_{p,p_\perp}|^2 c^{k-p-l,l,k}_{\mathrm{X}}\\
&\qquad\Big\{g(\varepsilon^{\mathrm{h}}_l-\varepsilon^{\mathrm{h}}_{l+p}+\hbar\Omega_{p,p_\perp})-g(\varepsilon^{\mathrm{h}}_l-\varepsilon^{\mathrm{h}}_{l+p}-\hbar\Omega_{p,p_\perp})\Big\},
\end{aligned}
\tag{3.43}
$$

$$
\begin{aligned}
\Pi^{\mathrm{h}}_{k,p} \;=\;& i\sum_{p_\perp}|G_{p,p_\perp}|^2 f^{\mathrm{h}}_k(1-f^{\mathrm{h}}_{k-p})\Big\{N^{\mathrm{PH}}_{p,p_\perp}g(\varepsilon^{\mathrm{h}}_{k-p}-\varepsilon^{\mathrm{h}}_k-\hbar\Omega_{p,p_\perp})\\
&\qquad\qquad +(N^{\mathrm{PH}}_{p,p_\perp}+1)g(\varepsilon^{\mathrm{h}}_{k-p}-\varepsilon^{\mathrm{h}}_k+\hbar\Omega_{p,p_\perp})\Big\}\\
&-i\sum_{p_\perp}|G_{p,p_\perp}|^2 f^{\mathrm{h}}_{k-p}(1-f^{\mathrm{h}}_k)\Big\{N^{\mathrm{PH}}_{p,p_\perp}g(\varepsilon^{\mathrm{h}}_{k-p}-\varepsilon^{\mathrm{h}}_k+\hbar\Omega_{p,p_\perp})\\
&\qquad\qquad +(N^{\mathrm{PH}}_{p,p_\perp}+1)g(\varepsilon^{\mathrm{h}}_{k-p}-\varepsilon^{\mathrm{h}}_k-\hbar\Omega_{p,p_\perp})\Big\}\\
&+i\sum_{l,p_\perp}|G_{p,p_\perp}|^2 c^{p,l,k}_{\mathrm{h}}\\
&\qquad\Big\{g(\varepsilon^{\mathrm{h}}_l-\varepsilon^{\mathrm{h}}_{l+p}+\hbar\Omega_{p,p_\perp})-g(\varepsilon^{\mathrm{h}}_l-\varepsilon^{\mathrm{h}}_{l+p}-\hbar\Omega_{p,p_\perp})\Big\}\\
&-i\sum_{l,p_\perp}|G_{p,p_\perp}|^2 c^{l+p-k,k,l}_{\mathrm{X}}\\
&\qquad\Big\{g(\varepsilon^{\mathrm{e}}_{l+p}-\varepsilon^{\mathrm{e}}_l+\hbar\Omega_{p,p_\perp})-g(\varepsilon^{\mathrm{e}}_{l+p}-\varepsilon^{\mathrm{e}}_l-\hbar\Omega_{p,p_\perp})\Big\},
\end{aligned}
\tag{3.44}
$$

with $g(\varepsilon)=\pi\delta(\varepsilon)+iP(\frac{1}{\varepsilon})$. After being inserted into Eqs. (3.38) and (3.39), the first four lines of Eqs. (3.43) and (3.44) have a straight forward interpretation as scattering rates. They are the typical scattering equations with a balance between scattering into (lines one and two) and scattering out of (lines three and four) electron state k. In both cases, phonon absorption and emission processes are possible. Since emission can happen even without any phonons present, the respective terms are proportional to $N^{\mathrm{PH}}_{p,p_\perp}+1$. The g-function ensures energy conservation. The last two lines are due to phonon coupling to higher order correlations.

Since both the carrier and correlation dynamics is determined by similar Π-terms in Eqs. (3.38)–(3.42), the corresponding phonon effects in the singlet-doublet limit result from the cooling of the carrier plasma. The actual exciton formation dynamics follows from the genuine six-point, i.e. triplet, correlations. However, it is numerically impossible to treat all equations up to the consistent six-point level and we are forced to use an approximative solution. We expect that the major contribution of the six-point correlations can be evaluated at a level similar to the second-Born level used successfully to describe microscopic

Coulomb and phonon scattering [16, 19, 68, 69]. The inclusion of the phonon-assisted four-point operators on this level already allows scattering of excitons with a third body but no higher-order correlations between phonons and correlated pairs. As discussed in App.B, the resulting triplet contribution is given by

$$\begin{aligned}
\left[i\hbar\frac{\partial}{\partial t}c_{\mathrm{X}}^{q,k',k}\right]_{H_{\mathrm{P}},\mathrm{T}} &= \sum_{p}\left(\tilde{\gamma}_{k-q,p}^{\mathrm{h}}+\tilde{\gamma}_{k'+q,p}^{\mathrm{e}}-(\tilde{\gamma}_{k',p}^{\mathrm{h}})^{*}-(\tilde{\gamma}_{k,p}^{\mathrm{e}})^{*}\right)c_{\mathrm{X}}^{q,k',k}\\
&\quad-\sum_{p}\left(\gamma_{k,k-p}^{\mathrm{e}}-(\gamma_{k-q,k-p}^{\mathrm{h}})^{*}\right)c_{\mathrm{X}}^{q,k',p}\\
&\quad-\sum_{p}\left(\gamma_{k',k'-p}^{\mathrm{h}}-(\gamma_{k'+q,k'-p}^{\mathrm{e}})^{*}\right)c_{\mathrm{X}}^{q,p,k}\\
&\quad-\sum_{p}\left((\gamma_{k-q,p-q}^{\mathrm{h}})^{*}+(\gamma_{k'+q,q-p}^{\mathrm{e}})^{*}\right)c_{\mathrm{X}}^{p,k',k}\\
&\quad+\sum_{p}\left(\gamma_{k',p-q}^{\mathrm{h}}+\gamma_{k,q-p}^{\mathrm{e}}\right)(c_{\mathrm{X}}^{p,k-q,k'+q})^{*}\\
&\quad-\sum_{p}\left(\gamma_{k',p-q}^{\mathrm{h}}-(\gamma_{k-q,p-q}^{\mathrm{h}})^{*}\right)c_{\mathrm{X}}^{p,k'+q-p,k}\\
&\quad-\sum_{p}\left(\gamma_{k,q-p}^{\mathrm{e}}-(\gamma_{k'+q,q-p}^{\mathrm{e}})^{*}\right)c_{\mathrm{X}}^{p,k',k-q+p},
\end{aligned}\tag{3.45}$$

where γ and $\tilde{\gamma}$ are defined according to

$$\begin{aligned}
\gamma_{k,p}^{\mathrm{e}} &= (-i)\sum_{p_\perp}|G_{p,p_\perp}|^2\left[(N_{p,p_\perp}^{\mathrm{PH}}+1-f_k^{\mathrm{e}})\,g(\varepsilon_k^{\mathrm{e}}-\varepsilon_{k-p}^{\mathrm{e}}+\hbar\Omega_{p,p_\perp})\right.\\
&\qquad\left.+(N_{p,p_\perp}^{\mathrm{PH}}+f_k^{\mathrm{e}})\,g(\varepsilon_k^{\mathrm{e}}-\varepsilon_{k-p}^{\mathrm{e}}-\hbar\Omega_{p,p_\perp})\right], &(3.46)\\
\gamma_{k,p}^{\mathrm{h}} &= (-i)\sum_{p_\perp}|G_{p,p_\perp}|^2\left[(N_{p,p_\perp}^{\mathrm{PH}}+f_k^{\mathrm{h}})\,g(\varepsilon_{k-p}^{\mathrm{h}}-\varepsilon_k^{\mathrm{h}}+\hbar\Omega_{p,p_\perp})\right.\\
&\qquad\left.+(N_{p,p_\perp}^{\mathrm{PH}}+1-f_k^{\mathrm{h}})\,g(\varepsilon_{k-p}^{\mathrm{h}}-\varepsilon_k^{\mathrm{h}}-\hbar\Omega_{p,p_\perp})\right], &(3.47)\\
\tilde{\gamma}_{k,p}^{\mathrm{e}} &= (-i)\sum_{p_\perp}|G_{p,p_\perp}|^2\left[(N_{p,p_\perp}^{\mathrm{PH}}+f_{k-p}^{\mathrm{e}})\,g(\varepsilon_k^{\mathrm{e}}-\varepsilon_{k-p}^{\mathrm{e}}+\hbar\Omega_{p,p_\perp})\right.\\
&\qquad\left.+(N_{p,p_\perp}^{\mathrm{PH}}+1-f_{k-p}^{\mathrm{e}})\,g(\varepsilon_k^{\mathrm{e}}-\varepsilon_{k-p}^{\mathrm{e}}-\hbar\Omega_{p,p_\perp})\right], &(3.48)\\
\gamma_{k,p}^{\mathrm{h}} &= (-i)\sum_{p_\perp}|G_{p,p_\perp}|^2\left[(N_{p,p_\perp}^{\mathrm{PH}}+1-f_{k-p}^{\mathrm{h}})\,g(\varepsilon_{k-p}^{\mathrm{h}}-\varepsilon_k^{\mathrm{h}}+\hbar\Omega_{p,p_\perp})\right.\\
&\qquad\left.+(N_{p,p_\perp}^{\mathrm{PH}}+f_{k-p}^{\mathrm{h}})\,g(\varepsilon_{k-p}^{\mathrm{h}}-\varepsilon_k^{\mathrm{h}}-\hbar\Omega_{p,p_\perp})\right]. &(3.49)
\end{aligned}$$

The electron and hole correlations obey similar phonon dynamics

$$\begin{aligned}
\left[i\hbar\frac{\partial}{\partial t}c_{\mathrm{e}}^{q,k',k}\right]_{H_{\mathrm{P}},\mathrm{T}} &= \sum_{p}\left(\tilde{\gamma}_{k-q,p}^{\mathrm{e}}+\tilde{\gamma}_{k'+q,p}^{\mathrm{e}}-(\tilde{\gamma}_{k',p}^{\mathrm{e}})^{*}-(\tilde{\gamma}_{k,p}^{\mathrm{e}})^{*}\right)c_{\mathrm{e}}^{q,k',k}\\
&\quad-\sum_{p}\left(\gamma_{k,k-p}^{\mathrm{e}}-(\gamma_{k-q,k-p}^{\mathrm{e}})^{*}\right)c_{\mathrm{e}}^{q,k',p}
\end{aligned}$$

$$
\begin{aligned}
&- \sum_p \left(\gamma^{\mathrm{e}}_{k',k'-p} - \left(\gamma^{\mathrm{e}}_{k'+q,k'-p}\right)^* \right) c_{\mathrm{e}}^{q,p,k} \\
&- \sum_p \left(\left(\gamma^{\mathrm{e}}_{k-q,p-q}\right)^* + \left(\gamma^{\mathrm{e}}_{k'+q,q-p}\right)^* \right) c_{\mathrm{e}}^{p,k',k} \\
&+ \sum_p \left(\gamma^{\mathrm{e}}_{k',p-q} + \gamma^{\mathrm{e}}_{k,q-p} \right) \left(c_{\mathrm{e}}^{p,k-q,k'+q}\right)^* \\
&- \sum_p \left(\gamma^{\mathrm{e}}_{k',p-q} - \left(\gamma^{\mathrm{e}}_{k-q,p-q}\right)^* \right) c_{\mathrm{e}}^{p,k'+q-p,k} \\
&- \sum_p \left(\gamma^{\mathrm{e}}_{k,q-p} - \left(\gamma^{\mathrm{e}}_{k'+q,q-p}\right)^* \right) c_{\mathrm{e}}^{p,k',k-q+p}
\end{aligned} \tag{3.50}
$$

and

$$
\begin{aligned}
\left[i\hbar \frac{\partial}{\partial t} c_{\mathrm{h}}^{q,k',k} \right]_{H_{\mathrm{P}},\mathrm{T}} \;=\; & \sum_p \left(\tilde{\gamma}^{\mathrm{h}}_{k-q,p} + \tilde{\gamma}^{\mathrm{h}}_{k'+q,p} - \left(\tilde{\gamma}^{\mathrm{h}}_{k',p}\right)^* - \left(\tilde{\gamma}^{\mathrm{h}}_{k,p}\right)^* \right) c_{\mathrm{h}}^{q,k',k} \\
&- \sum_p \left(\gamma^{\mathrm{h}}_{k,k-p} - \left(\gamma^{\mathrm{h}}_{k-q,k-p}\right)^* \right) c_{\mathrm{h}}^{q,k',p} \\
&- \sum_p \left(\gamma^{\mathrm{h}}_{k',k'-p} - \left(\gamma^{\mathrm{h}}_{k'+q,k'-p}\right)^* \right) c_{\mathrm{h}}^{q,p,k} \\
&- \sum_p \left(\left(\gamma^{\mathrm{h}}_{k-q,p-q}\right)^* + \left(\gamma^{\mathrm{h}}_{k'+q,q-p}\right)^* \right) c_{\mathrm{h}}^{p,k',k} \\
&+ \sum_p \left(\gamma^{\mathrm{h}}_{k',p-q} + \gamma^{\mathrm{h}}_{k,q-p} \right) \left(c_{\mathrm{h}}^{p,k-q,k'+q}\right)^* \\
&- \sum_p \left(\gamma^{\mathrm{h}}_{k',p-q} - \left(\gamma^{\mathrm{h}}_{k-q,p-q}\right)^* \right) c_{\mathrm{h}}^{p,k'+q-p,k} \\
&- \sum_p \left(\gamma^{\mathrm{h}}_{k,q-p} - \left(\gamma^{\mathrm{h}}_{k'+q,q-p}\right)^* \right) c_{\mathrm{h}}^{p,k',k-q+p} \,.
\end{aligned} \tag{3.51}
$$

These six-point phonon scattering contributions lead to a microscopic dephasing of correlations. One easily verifies the conservation law

$$
\left[\frac{\partial}{\partial t} \sum_{k,k',q} c_\lambda^{q,k',k} \right]_{H_{\mathrm{P}}} = 0 \tag{3.52}
$$

for the complex valued correlations $c_\lambda^{q,k',k}$. Hence, the phonon scattering has a diffusive character. This property allows formation as well as equilibration of correlations. In Sec. 4.6, this conservation law will get a physical interpretation. For short time scales where exciton formation does not yet play a dominant role, one may introduce a phenomenological dephasing constant $\left[\frac{\partial}{\partial t} c_\lambda^{q,k',k}\right]^{\mathrm{deph}}_{H_{\mathrm{P}},\mathrm{T}} = -\gamma\, c_\lambda^{q,k',k}$. We want to point out, though, that such a simple constant dephasing cannot be justified from the microscopic equations. In this thesis, we therefore use it only in order to derive a quasi-analytical result in Sec. 4.4.

The set of equations (3.32)–(3.37) together with the phonon contributions (3.38)–(3.51) provides a closed system of coupled differential equations which can be solved under different initial conditions in order to study exciton formation for different carrier densities and lattice temperatures.

3.5 Coupling to the Quantized Light Field

The dominant consequence of the quantum nature of light for the incoherent regime investigated in this thesis is the possibility of radiative decay of excited carriers via spontaneous emission of a photon. This emission is possible due to the broken translational symmetry perpendicular to the heterostructure [70–73]. Even without non-radiative decay channels, the coupling to the vacuum fluctuations of light leads to an intrinsic life time of excited carriers, see e.g. [12] and references therein. In Chapter 5, we compute photoluminescence spectra and investigate the influence of the radiative decay on both carrier distributions and excitonic correlations.

In general, the computation of time resolved photoluminescence spectra is a subtle affair since the detection scheme itself must be included in the analysis [44, 74]. A certain energy resolution requires a corresponding integration time of the detector. Consequently, early time spectra might exhibit transient narrowing of a sharp resonance which does not reflect the material properties but rather the finite detection time [75]. However, when we restrict ourselves to the stationary photoluminescence spectrum for an ideal detector with infinite energy resolution, the spectrum is given by the rate of emitted photons [44, 59]

$$I_{\mathrm{PL}}(\omega_q) = \frac{\partial}{\partial t}\Delta\langle b^\dagger_{\mathbf{q}} b_{\mathbf{q}}\rangle \,, \tag{3.53}$$

where the full three-dimensional wave number determines both energy and propagation direction of the photons. Under incoherent conditions with vanishing classical electric field, the correlated part $\Delta\langle b^\dagger_{\mathbf{q}} b_{\mathbf{q}}\rangle$ provides the only contribution to the photon number. The photoluminescence spectrum (3.53) can be directly obtained from the light-matter interaction Hamiltonian (2.43) as

$$\frac{\partial}{\partial t}\Delta\langle b^\dagger_{\mathbf{q}} b_{\mathbf{q}}\rangle = \frac{2}{\hbar}\mathrm{Re}\left[\sum_k \mathcal{E}_{\mathbf{q}}\bar{u}^*_{\mathbf{q}} d^*_{\mathbf{q}}\Delta\langle b^\dagger_{q,q_\perp} v^\dagger_k c_{k+q}\rangle\right] , \tag{3.54}$$

where we have used the rotating-wave approximation to neglect non-resonant contributions with a time dependent phase rotating with twice the optical frequency. According to Eq. (3.54), the spontaneous emission is driven by photon-assisted processes with probability amplitudes $\Delta\langle b^\dagger_{q,q_\perp} v^\dagger_k c_{k+q}\rangle$ where a photon is emitted under simultaneous transition of a conduction-band electron into the valence band [31,44]. The same photon-assisted transition amplitudes occur in the equation of motion of the carrier densities

$$\left[\frac{\partial}{\partial t} f^{\mathrm{e}}_k\right]_{H_{\mathrm{D}}} = \frac{2}{\hbar}\mathrm{Re}\left[\sum_{q,q_\perp} \mathcal{E}_{\mathbf{q}}\bar{u}^*_{\mathbf{q}} d^*_{\mathbf{q}}\Delta\langle b^\dagger_{q,q_\perp} v^\dagger_{k-q} c_k\rangle\right] , \tag{3.55}$$

$$\left[\frac{\partial}{\partial t} f_k^{\mathrm{h}}\right]_{H_{\mathrm{D}}} = \frac{2}{\hbar}\mathrm{Re}\left[\sum_{q,q_\perp} \mathcal{E}_{\mathbf{q}} \bar{u}_{\mathbf{q}}^* d_{\mathbf{q}}^* \Delta\langle b_{q,q_\perp}^\dagger v_k^\dagger c_{k+q}\rangle\right]. \tag{3.56}$$

In fact, we note that the change of the number of carriers due to recombination $\frac{\partial}{\partial t}\sum_k f_k^{\mathrm{e/h}}$ is equal to the number of emitted photons $\frac{\partial}{\partial t}\sum_{\mathbf{q}} \Delta\langle b_{\mathbf{q}}^\dagger b_{\mathbf{q}}\rangle$.

Due to the translational symmetry of the semiconductor heterostructure, the momentum along the structure has to be conserved, i.e., the photon momentum $\hbar q$ along the heterostructure is compensated by a small momentum change in the carrier transition $v_{k-q}^\dagger c_k$. The component $q_\perp$ perpendicular to the semiconductor structure is not restricted. Equation (3.55) directly shows that spontaneous emission depletes carriers with various momenta. Only the center-of-mass momentum of the recombining electron-hole pair is restricted by momentum conservation. This conservation of the center-of-mass momentum has direct consequences for the excitonic correlations and their coupling to the quantized light field. In order to see how they are influenced by spontaneous emission, we set up the equation of motion for c_{X} and get

$$\begin{aligned}\left[i\hbar\frac{\partial}{\partial t} c_{\mathrm{X}}^{q,k',k}\right]_{H_{\mathrm{D}}} &= -i(1 - f_{k'+q}^{\mathrm{e}} - f_{k'}^{\mathrm{h}}) \sum_{q_\perp} d_{\mathbf{q}} \mathcal{E}_{\mathbf{q}} \bar{u}_{\mathbf{q}} \Delta\langle b_{q,q_\perp}^\dagger v_{k-q}^\dagger c_k\rangle^* \\ &\quad - i(1 - f_k^{\mathrm{e}} - f_{k-q}^{\mathrm{h}}) \sum_{q_\perp} d_{\mathbf{q}}^* \mathcal{E}_{\mathbf{q}} \bar{u}_{\mathbf{q}}^* \Delta\langle b_{q,q_\perp}^\dagger v_{k'}^\dagger c_{k'+q}\rangle,\end{aligned} \tag{3.57}$$

which shows that only exciton correlations with a center-of-mass momentum $\hbar q$ smaller than the photon momentum can be depleted by spontaneous emission because the wave number component q along the heterostructure is the same for both exciton correlation and photon.

In order to compute photoluminescence spectra and to include the effects of spontaneous emission into our analysis, we finally have to solve the dynamics for the photon-assisted polarizations. Computing the Heisenberg equation of motion for the carrier-photon subsystem, we obtain the semiconductor luminescence equations [31, 44]

$$\begin{aligned}i\hbar\frac{\partial}{\partial t}\Delta\langle b_{q,q_\perp}^\dagger v_k^\dagger c_{k+q}\rangle &= \left(\tilde{\varepsilon}_{k+q}^{\mathrm{e}} + \tilde{\varepsilon}_k^{\mathrm{h}} + E_{\mathrm{G}} - \hbar\omega_{q,q_\perp}\right)\Delta\langle b_{q,q_\perp}^\dagger v_k^\dagger c_{k+q}\rangle \\ &\quad -(1 - f_{k+q}^{\mathrm{e}} - f_k^{\mathrm{h}})\Omega_{\mathrm{ST}}(k,\mathbf{q}) + \Omega_{\mathrm{SE}}(k,\mathbf{q})\end{aligned} \tag{3.58}$$

with the renormalized energies, Eq. (3.35). Here, Ω_{ST} is a generalized photon-assisted Rabi frequency [44]

$$\Omega_{\mathrm{ST}}(k,\mathbf{q}) = id_{\mathbf{q}} \sum_{q'_\perp} \mathcal{E}_{q,q'_\perp} \bar{u}_{q,q'_\perp} \Delta\langle b_{q,q_\perp}^\dagger b_{q,q'_\perp}\rangle + \sum_{k'} V_{k-k'} \Delta\langle b_{q,q_\perp}^\dagger v_{k'}^\dagger c_{k'+q}\rangle. \tag{3.59}$$

In addition, we have defined the source term

$$\Omega_{\mathrm{SE}}(k,\mathbf{q}) = i\mathcal{E}_{\mathbf{q}} \bar{u}_{\mathbf{q}} d_{\mathbf{q}} \left(f_{k+q}^{\mathrm{e}} f_k^{\mathrm{h}} + \sum_{k'} c_{\mathrm{X}}^{q,k,k'}\right) \tag{3.60}$$

in Eq. (3.58) which initializes the build-up of photon assisted polarizations as soon as excited carriers are present in the system.

This Section concludes the presentation of equations used throughout the remainder of this thesis. In the following Chapter, we study exciton formation without the influence of spontaneous emission. Such a suppression of spontaneous emission can for example be obtained if semiconductor structures are placed inside a photonic band-gap material [35, 36]. In Chapter 5 we include the full dipole coupling of our system to the quantized light field. There, we investigate both the influence of correlations on the photoluminescence spectra and the influence of spontaneous recombination on the dynamics of carriers and correlations.

4 Exciton Formation

The exciton formation equations derived in Chapter 3 are generally valid for any dimensionality of the system. But since the correlations $c^{q,k',k}_{\mathrm{X/e/h}}$ depend on three different indices, the computational memory required to store them is proportional to N^{3d} for numerical grids with N points in d dimensions. In two dimensions, one can make use of the polar symmetry and reduce the exponent by one. For each index combination, several d-dimensional Coulomb sums have to be evaluated such that the computational complexity increases with N^4 in one dimension and N^7 in two dimensions. Even with the modern super computers, the *full* inclusion of the four-point correlations is thus numerically feasible only in a one-dimensional model system. It is important to understand the main physical effects in such a model system before one can proceed. With this extra insight, it is possible to use well-controlled approximations in higher dimensions which still include the full fermionic character of excitons.

We investigate such a one-dimensional model system and choose parameters close to the standard GaAs parameters used for quantum wells. The effective width of our quantum wire was chosen such that the exciton binding energy lies roughly 11 meV below the unrenormalized bandgap which is also obtained in typical 8 nm quantum wells. The reduced mass is taken identical to the GaAs effective exciton mass, but the ratio between electron and hole mass is adjusted to 3 instead of the typical ratio of around 7 in order to have slightly narrower hole distributions. This improves the numerics because a smaller maximum value of our k-grid can be used. Still, effects due to different masses should be seen. Since a microscopic description of screening of the Coulomb interaction would require the additional computation of six-point correlations and is thus beyond the current numerical possibilities, we always use a statically screened Coulomb potential introduced by hand. This screened potential is evaluated with the help of the Lindhard formula [19]. We solve all the coupled equations discussed above using a standard fourth order Runge-Kutta scheme.

4.1 Direct Evidence of Exciton Formation

The formation of any significant amount of bound excitons can be directly observed via the electron-hole pair-correlation function [76]

$$g^{\mathrm{eh}}(r) \equiv \langle \Psi^\dagger_{\mathrm{e}}(r) \Psi^\dagger_{\mathrm{h}}(0) \Psi_{\mathrm{h}}(0) \Psi_{\mathrm{e}}(r) \rangle, \tag{4.1}$$

which measures the conditional probability to find an electron at position r while the hole is located at $r = 0$. To distinguish coherent from incoherent and plasma from true excitonic

aspects, we separate the correlation function into its singlet part and the genuinely correlated four-point contribution. In the Bloch basis, the pair-correlation function can thus be expressed as

$$g^{\mathrm{eh}}(r) = \frac{1}{\mathcal{L}^2} \sum_{k,k',p,p'} e^{-i(k-k')r} \langle c_k^\dagger c_{k'} v_p v_{p'}^\dagger \rangle = g_{\mathrm{S}}^{\mathrm{eh}}(r) + \Delta g^{\mathrm{eh}}(r,t) \tag{4.2}$$

with the singlet contribution

$$g_{\mathrm{S}}^{\mathrm{eh}}(r) = n^{\mathrm{e}}\, n^{\mathrm{h}} + \left| \frac{1}{\mathcal{L}} \sum_k e^{ikr} P_k \right|^2 = n^{\mathrm{e}}\, n^{\mathrm{h}} + |P(r,t)|^2 \tag{4.3}$$

and the correlated part

$$\Delta g^{\mathrm{eh}}(r) = \frac{1}{\mathcal{L}^2} \sum_{k,k',q} e^{-i(k-k'-q)r}\; c_{\mathrm{X}}^{q,k',k}\,. \tag{4.4}$$

In Eq. (4.3), the coherent microscopic interband-transition amplitudes

$$P_k = \langle v_k^\dagger c_k \rangle \tag{4.5}$$

between conduction and valence band electrons, which determine the macroscopic polarization of the semiconductor, have been introduced [19]. Furthermore, we have used Eq. (3.1) and (3.19).

After a coherent excitation with a classical field, the term proportional to the polarization is clearly dominant [77]. As soon as this polarization dephases, however, the factorized contribution becomes constant and the only r-dependence is provided by the correlated part $\Delta g^{\mathrm{eh}}(r)$. This quantity provides an intuitive measure of when and how fast exciton formation and ionization takes place under particular carrier excitation conditions. Since $\Delta g^{\mathrm{eh}}(r)$ is a true two-particle correlation, it is absolutely necessary to solve the carrier-photon-phonon dynamics up to a level of correlations including four field operators.

First, we analyze the result of a computation for a lattice temperature of $T = 10\,\mathrm{K}$. In principle, the full excitation process is a complicated interplay between the electric field, the excited carriers and the different phonons [19, 60, 78]. Not only the many-body interaction provides a significant challenge [16, 17], but also the carrier-phonon interaction including coherent phonons exhibits interesting features on short time scales [79, 80]. For excitations energetically more than one optical phonon energy above the bandgap, the optical phonons also provide the dominant cooling mechanism [54, 69]. In combination with the microscopic Coulomb scattering, they lead to equilibration of the carrier distributions towards the lattice temperature at a time scale on the order of several picoseconds. For optical excitations below the optical phonon energy or after the fast cooling of the carriers by the optical phonons, eventually all carriers are at energies sufficiently low such that they cannot emit further optical phonons. From that point on, further cooling is provided by acoustic phonons. This is where our computation starts. The carrier distributions are initially set to Fermi-Dirac distributions of the lattice temperature while the correlations are set to zero. As discussed in the beginning of Chapter 3, these initial conditions can be thought of as model conditions obtained after non-resonant optical excitation.

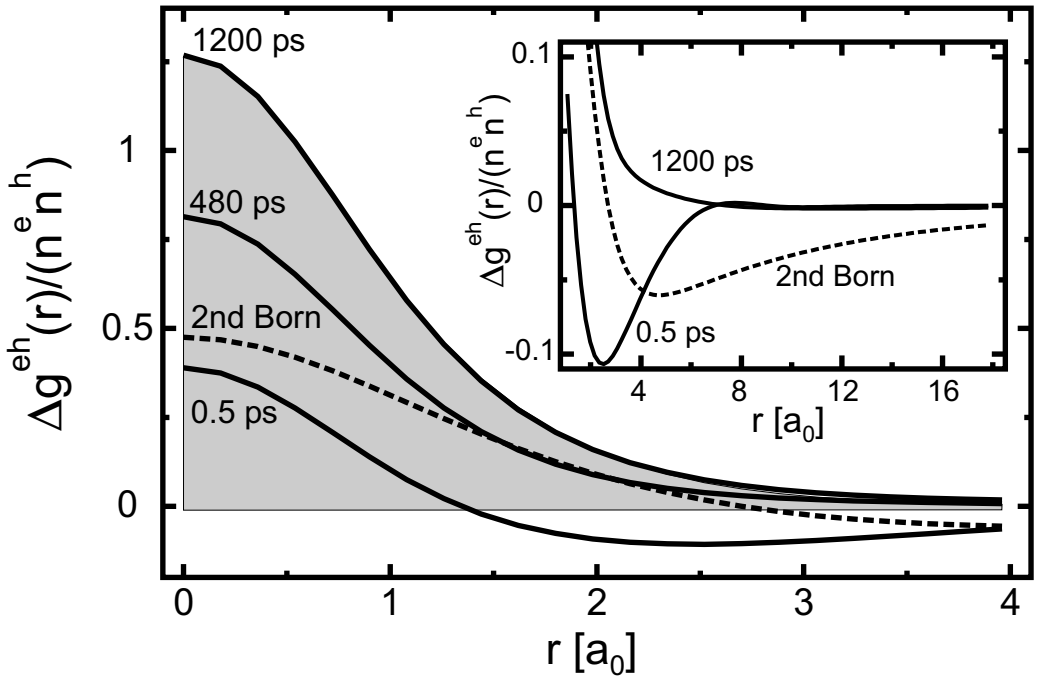

Figure 4.1: Pair-correlation function $\Delta g^{\mathrm{eh}}(r)/(n^{\mathrm{e}}n^{\mathrm{h}})$ normalized to the constant Hartree-Fock value for a lattice temperature of $T = 10\,\mathrm{K}$ and a carrier density of $n = 2 \times 10^4\,\mathrm{cm}^{-1}$ at different times. For comparison, the wave function of the lowest bound exciton is given as a shaded area. The dashed line is the corresponding result of a second-Born computation. The inset shows a magnification of the tails of the same curves.

First, we concentrate on the genuine formation scenario for cases, when effects due to spontaneous emission can be neglected, e.g., for semiconductors placed inside photonic bandgap materials which can reduce the coupling to vacuum fluctuations by several orders of magnitude [35, 36]. The important influence of spontaneous emission in general is investigated in Chapter 5. After the start of the computation, the system evolves according to all the equations derived in the previous Chapter, and we follow the dynamics up to 1.2 ns. More specifically, we compute the pair-correlation function at different times. As the spatial dependence of the pair-correlation function, Eq. (4.2), under incoherent conditions is fully given by its correlated part, we compute $\Delta g^{\mathrm{eh}}(r)/(n^{\mathrm{e}}n^{\mathrm{h}})$ which has been normalized to its two-point contribution $n^{\mathrm{e}}n^{\mathrm{h}}$.

Figure 4.1 shows the result as a function of electron-hole distance r given in multiples of the 3d Bohr radius $a_0 \approx 12.4\,\mathrm{nm}$ for a low carrier density of $n^{\mathrm{e/h}} = 2 \times 10^4\,\mathrm{cm}^{-1}$. Immediately after the beginning of the computation, the carriers react to the Coulomb attraction and the probability of finding electrons and holes close to each other increases. However, the correlated Δg^{eh} has clearly negative parts. At certain distances, the total pair correlation $g^{\mathrm{eh}}(r)$ is therefore below its factorized value. One can interpret this behavior as a fast rearrangement of the electron-hole plasma where the probability to find electrons in the close vicinity of holes is increased at the expense of the probability at around 2 to 4 a_0. Thus, the

early time dynamics does not show real formation of excitons out of the plasma. Nevertheless, after 480 ps, the pair correlation assumes the shape of an exciton wave function, which is given as a shaded area, and grows almost linearly in time. Already here, we see that the pair-correlation function offers an excellent possibility to investigate whether incoherent excitons have been formed.

This interpretation is supported by the second Born result which is shown for comparison as a dashed line. There we computed the pair-correlation function from exciton correlations as given by the second-Born result in Markov approximation [44]. More precisely, we allowed the presence of pair correlations but we did not include any of the Coulomb or phonon sums of Eq. (3.32) and (3.45); instead we included only the source term and the kinetic part of the equation. Therefore, no excitonic resonances are included in the correlation equations and bound states are not present in this specific computation. The resulting pair-correlation function of a redistributed plasma has similar characteristics as what we see at early times in the full computation. In particular, Δg^{eh} drops to negative values before it approaches zero at large distances. Since no excitonic resonances are included in the second-Born computation, the resulting shape of the pair correlation has to be interpreted as a rearrangement within the plasma. As a detail, we also note that the negative part is by far more extended than in the full computation.

4.2 Phonon Induced Energy Transfer in Exciton Formation

Since a bound exciton at rest has a lower energy than free electron-hole pairs, we study the energy transfer during the exciton formation in the many-body system. For carriers alone, the system energy is

$$\begin{aligned}\langle H_{\mathrm{kin}}\rangle + \langle H_{\mathrm{C}}\rangle &= \sum_{\lambda,k} \varepsilon^{\lambda}_{k} \langle a^{\dagger}_{\lambda,k} a_{\lambda,k}\rangle + \frac{1}{2} \sum_{\substack{\lambda,\lambda' \\ k,k',q\neq 0}} V_q \, \langle a^{\dagger}_{\lambda,k} a^{\dagger}_{\lambda',k'} a_{\lambda',k'+q} a_{\lambda,k-q}\rangle \\ &= \langle H^{\mathrm{e}}_{\mathrm{kin}}\rangle + \langle H^{\mathrm{h}}_{\mathrm{kin}}\rangle + \langle H^{\mathrm{e}}_{\mathrm{C}}\rangle_{\mathrm{S}} + \langle H^{\mathrm{h}}_{\mathrm{C}}\rangle_{\mathrm{S}} \\ &\qquad + \Delta\langle H^{\mathrm{e}}_{\mathrm{C}}\rangle + \Delta\langle H^{\mathrm{h}}_{\mathrm{C}}\rangle + \Delta\langle H^{\mathrm{eh}}_{\mathrm{C}}\rangle \end{aligned} \tag{4.6}$$

with the kinetic energies

$$\langle H^{\lambda}_{\mathrm{kin}}\rangle = \sum_{k} \varepsilon^{\lambda}_{k} f^{\lambda}_{k} , \tag{4.7}$$

the singlet (factorized) parts to the Coulomb energy

$$\langle H^{\lambda}_{\mathrm{C}}\rangle_{\mathrm{S}} = -\frac{1}{2} \sum_{k,k'\neq k} V_{k-k'} \, f^{\lambda}_{k'} f^{\lambda}_{k} , \tag{4.8}$$

and the correlated contributions

$$\Delta\langle H^{\lambda}_{\mathrm{C}}\rangle = \frac{1}{2} \sum_{k,k',q\neq 0} V_q \, c^{q,k',k}_{\lambda} , \tag{4.9}$$

$$\Delta\langle H_{\mathrm{C}}^{\mathrm{eh}}\rangle \;=\; -\sum_{k,k',q\neq 0} V_q\, c_{\mathrm{X}}^{k-q-k',k',k}\,. \tag{4.10}$$

Using Eqs. (3.32)–(3.37), one can verify

$$\left[\frac{\partial}{\partial t}\langle H_{\mathrm{kin}}\rangle + \langle H_{\mathrm{C}}\rangle\right]_{H_{\mathrm{kin}}+H_{\mathrm{C}}} = 0\,, \tag{4.11}$$

which shows that the energy is conserved within the isolated carrier system. As a result, exciton formation is not efficient for a plain carrier system. When also phonons and photons are included, one finds

$$\frac{\partial}{\partial t}\langle H_{\mathrm{tot}}\rangle = \frac{\partial}{\partial t}\left[\langle H_{\mathrm{kin}}\rangle + \langle H_{\mathrm{C}}\rangle + \langle H_{\mathrm{phon}}\rangle + \langle H_{\mathrm{P}}\rangle + \langle H_{\mathrm{em}}\rangle + \langle H_{\mathrm{D}}\rangle\right] = 0\,. \tag{4.12}$$

This shows that the truncation via the cluster expansion scheme fully conserves the total energy of the system. When the phonons are included, the plain carrier system can cool down because the energy gained via exciton formation is transferred to lattice vibrations. When the phonons are treated as a reservoir, the phonon bath acts as a sink and the energy flux directed to the phonon system is absorbed by the reservoir. Thus, the bath approximation leads to the correct behavior of the carrier energy. However, if one replaces the microscopic phonon scattering by a constant dephasing rate γ, one obtains

$$\frac{\partial}{\partial t}\Big(\langle H_{\mathrm{kin}}\rangle + \langle H_{\mathrm{C}}\rangle\Big) = -\gamma\,\Delta\langle H_{\mathrm{C}}\rangle > 0 \tag{4.13}$$

which implies an unphysical heating of the system. As a result, exciton formation studies require a microscopic description of phonon scattering.

The properties of the carrier energy are studied in Fig. 4.2 by using either constant dephasing or microscopic phonon scattering. With constant γ, the attractive Coulomb energy very quickly reaches its steady-state value such that actual formation is not observed. Even a small constant γ of approximately $50\,\mu$eV leads to a fast linear heating of the carrier distributions, i.e., to a fast increase of the total energy. With the microscopic phonon scattering and a lattice temperature of 10 K, true formation of excitons is possible as indicated by the continuous decrease of the Coulomb energy; at the same time, the total energy of the carrier system is now decreasing since part of the energy is directed to the phonon bath. This verifies that exciton formation results from six-point phonon correlations leading to scattering of excitons with phonons and carriers. Figure 4.2 offers a second possibility to monitor the exciton formation; namely, a steady decrease of the attractive Coulomb energy indicates that formation is in progress. The slope of this decrease of energy can in principle be used as a measure of how fast the exciton formation takes place.

Figure 4.2 is obtained by computing the dynamics upto 40 ps with a phonon matrix-element enhanced by a factor of 30; this corresponds to $30 \times 40\,\mathrm{ps} = 1.2\,\mathrm{ns}$ of formation dynamics. The method will be justified in Sec. 4.3 where the microscopic nature of formation is studied in detail. Since also Fig. 4.1 and all following figures have been obtained in the same manner, we must ensure that this enhancement factor only influences the results in a predictable way. In Fig. 4.3, we thus show a comparison for three enhancement factors of

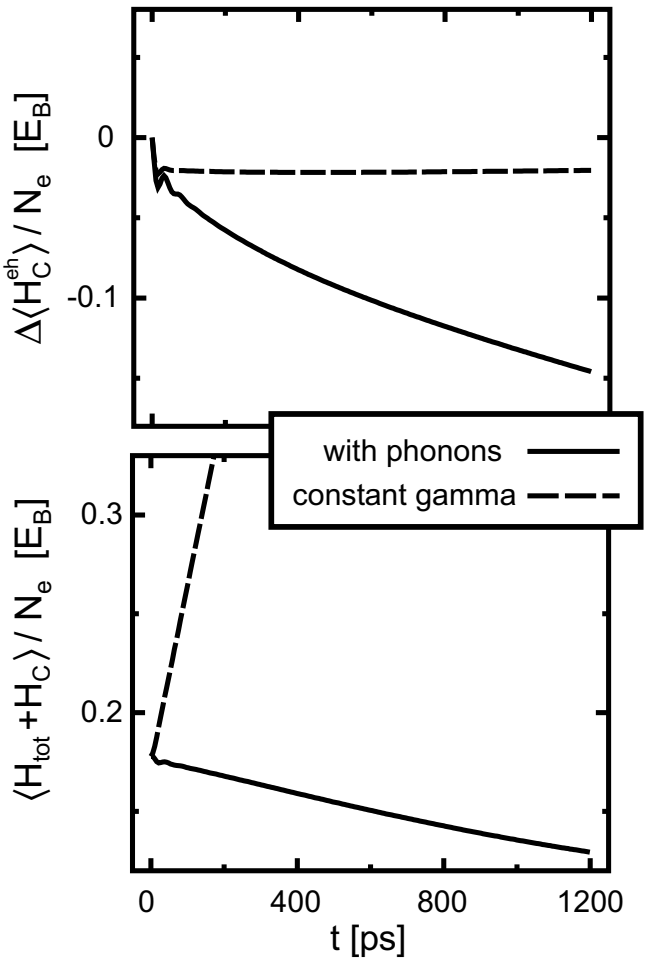

Figure 4.2: Attractive Coulomb energy (a) and total energy (b) per particle comparing a computation with constant dephasing approximation (dashed line) with the full result including microscopic phonon scattering (solid line) for the same parameters as in Fig. 4.1. Energies are given in multiples of the 3D exciton binding energy $E_{\mathrm{B}} = 4.2\,\mathrm{meV}$.

10, 15, and 30. After rescaling the time axis with the respective factor, the behavior of the correlated Coulomb energy is indeed independent of the enhancement factor. In particular, the rate of change is very similar for all three cases.

4.3 Formation of Specific Excitons

In the equation for excitonic correlations Eq. (3.32), two of the six Coulomb sums are especially important: The sums multiplied by the phase space filling factor $1 - f^{\mathrm{e}} - f^{\mathrm{h}}$ provide a large contribution for all densities. Therefore, one can expect that the restriction to these two main sums is a very good approximation to the full result.

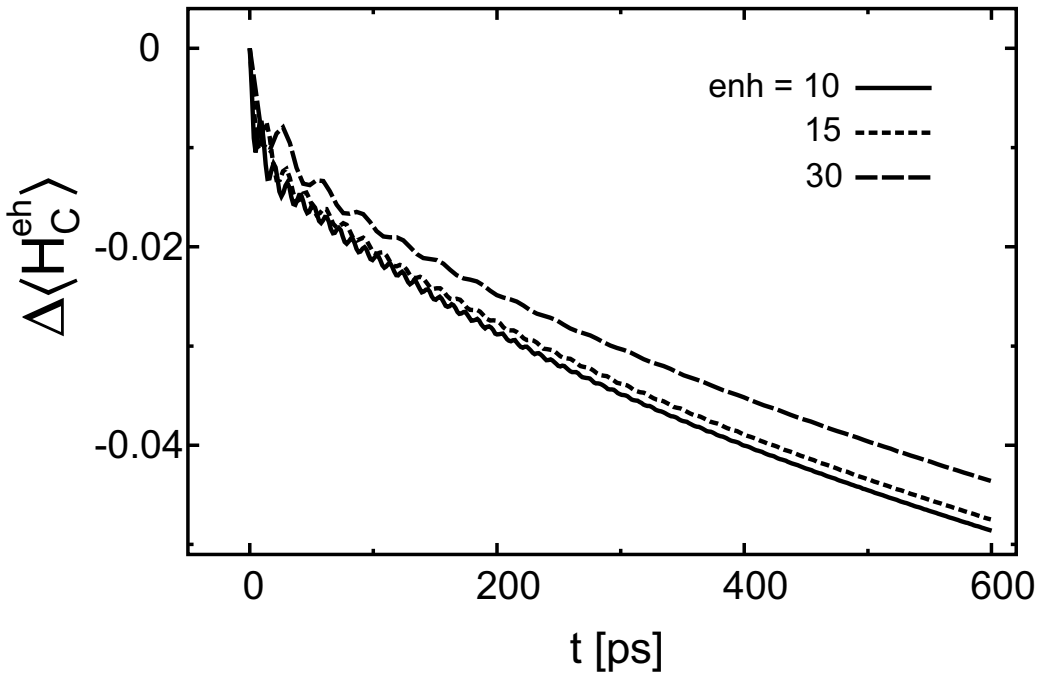

Figure 4.3: Correlated Coulomb energy $\Delta\langle H_{\mathrm{C}}\rangle$ per particle for three different computations with different enhancement factors. For each curve, the time axis has been rescaled with the respective enhancement factor. The carrier density is $n = 1 \times 10^4\,\mathrm{cm}^{-1}$ and the lattice temperature is $T = 10\,\mathrm{K}$.

The corresponding "main sum approximation" of Eq. (3.32) is

$$\begin{aligned} i\hbar\frac{\partial}{\partial t}c_{\mathrm{X}}^{q,k',k} &= \left(\tilde{\varepsilon}_{k'+q}^{\mathrm{e}} - \tilde{\varepsilon}_{k-q}^{\mathrm{h}} - \tilde{\varepsilon}_{k}^{\mathrm{e}} + \tilde{\varepsilon}_{k'}^{\mathrm{h}}\right) c_{\mathrm{X}}^{q,k',k} \\ &\quad + V_{k-k'-q}\left[(1-f_k^{\mathrm{e}})(1-f_{k-q}^{\mathrm{h}})f_{k'+q}^{\mathrm{e}}f_{k'}^{\mathrm{h}} - f_k^{\mathrm{e}}f_{k-q}^{\mathrm{h}}(1-f_{k'+q}^{\mathrm{e}})(1-f_{k'}^{\mathrm{h}})\right] \\ &\quad + [1-f_k^{\mathrm{e}}-f_{k-q}^{\mathrm{h}}]\sum_l V_{l-k}\,c_{\mathrm{X}}^{q,k',l} - [1-f_{k'+q}^{\mathrm{e}}-f_{k'}^{\mathrm{h}}]\sum_l V_{l-k'}\,c_{\mathrm{X}}^{q,l,k}\,. \end{aligned} \tag{4.14}$$

With this restriction, the excitonic correlations are not coupled to carrier-carrier correlations anymore and one obtains a closed subsystem of equations for each center-of-mass momentum q. We also know that the carrier distributions typically vary slowly such that one can try to find an adiabatic solution for Eq. (4.14). This approximative solution gives very much insight of how the formation actually takes place.

In order to solve Eq. (4.14) analytically, we use a generalized exciton basis, which is introduced in App. C. There it is shown, that the exciton functions fulfill the equations

$$\bar{\varepsilon}_{k,q}\phi_{\nu,q}^{\mathrm{r}}(k) - \bar{f}_{k,q}\sum_{k'} V_{k'-k}\phi_{\nu,q}^{\mathrm{r}}(k') = \varepsilon_{\nu,q}\phi_{\nu,q}^{\mathrm{r}}(k)\,, \tag{4.15}$$

$$\left(\phi_{\nu,q}^{\mathrm{l}}(k)\right)^*\bar{\varepsilon}_{k,q} - \sum_{k'}\left(\phi_{\nu,q}^{\mathrm{l}}(k')\right)^* V_{k'-k}\bar{f}_{k',q} = \left(\phi_{\nu,q}^{\mathrm{l}}(k)\right)^*\varepsilon_{\nu,q}\,, \tag{4.16}$$

where the abbreviations

$$\bar{\varepsilon}_{k,q} = \tilde{\varepsilon}^{\mathrm{e}}_{k+q^{\mathrm{e}}} + \tilde{\varepsilon}^{\mathrm{h}}_{k-q^{\mathrm{h}}} - \frac{\hbar^2 q^2}{2(m^{\mathrm{e}}+m^{\mathrm{h}})}\,, \tag{4.17}$$

$$\bar{f}_{k,q} = 1 - f^{\mathrm{e}}_{k+q^{\mathrm{e}}} - f^{\mathrm{h}}_{k-q^{\mathrm{h}}}\,, \tag{4.18}$$

$$q^{\mathrm{e(h)}} = \frac{m_{\mathrm{e(h)}}}{m_{\mathrm{e}}+m_{\mathrm{h}}}\,q\,, \tag{4.19}$$

have been introduced. In Eq. (4.17), the center-of-mass kinetic energy has been subtracted such that $\varepsilon_{\nu,q}$ is the exciton energy of the relative motion only. The total exciton energy will be labelled by

$$E_{\nu,q} = \varepsilon_{\nu,q} + \frac{\hbar^2 q^2}{2(m^{\mathrm{e}}+m^{\mathrm{h}})}. \tag{4.20}$$

The main difference to the usual Wannier basis is that for non-zero densities the phase-space filling factor and a screened Coulomb potential enter the effective Hamiltonian. Therefore, the eigenvalue problem Eq. (4.15) is not Hermitian anymore such that one obtains left and right handed eigenfunctions $\phi^{\mathrm{l/r}}_{\nu,q}$. Furthermore, the center-of-mass momentum q enters the equation via the phase-space filling factor such that the relative motion of an exciton depends on its center-of-mass momentum. The faster it moves, the less it is effected by phase-space filling.

By means of the generalized Wannier functions, one can introduce exciton creation and annihilation operators

$$\begin{aligned} X^\dagger_{\nu,q} &= \sum_k \phi^{\mathrm{l}}_{\nu,q}(k)\; c^\dagger_{k+q^{\mathrm{e}}} v_{k-q^{\mathrm{h}}}\,, \\ X_{\nu,q} &= \sum_k \left(\phi^{\mathrm{l}}_{\nu,q}(k)\right)^*\, v^\dagger_{k-q^{\mathrm{h}}} c_{k+q^{\mathrm{e}}}\,, \end{aligned} \tag{4.21}$$

with the inverse relations

$$\begin{aligned} c^\dagger_{k+q^{\mathrm{e}}} v_{k-q^{\mathrm{h}}} &= \sum_\nu \left(\phi^{\mathrm{r}}_{\nu,q}(k)\right)^* X^\dagger_{\nu,q}\,, \\ v^\dagger_{k-q^{\mathrm{h}}} c_{k+q^{\mathrm{e}}} &= \sum_\nu \phi^{\mathrm{r}}_{\nu,q}(k)\; X_{\nu,q}\,. \end{aligned} \tag{4.22}$$

Here, the orthogonality relation

$$\sum_k \left(\phi^{\mathrm{l}}_{\nu,q}(k)\right)^* \phi^{\mathrm{r}}_{\nu',q}(k) = \delta_{\nu,\nu'} \tag{4.23}$$

between left and right-handed exciton function has been used. Equations (4.21) and (4.22) can directly be applied to the correlations in order to transform them according to

$$c^{q,k'-q^{\mathrm{h}},k+q^{\mathrm{e}}}_{\mathrm{X}} = \sum_{\nu,\nu'} \left(\phi^{\mathrm{r}}_{\nu,q}(k)\right)^* \phi^{\mathrm{r}}_{\nu',q}(k')\,\Delta\langle X^\dagger_{\nu,q} X_{\nu',q}\rangle, \tag{4.24}$$

$$\Delta\langle X^\dagger_{\nu,q} X_{\nu',q}\rangle = \sum_{k,k'} \phi^{\mathrm{l}}_{\nu,q}(k)\left(\phi^{\mathrm{l}}_{\nu',q}(k')\right)^*\; c^{q,k'-q^{\mathrm{h}},k+q^{\mathrm{e}}}_{\mathrm{X}}. \tag{4.25}$$

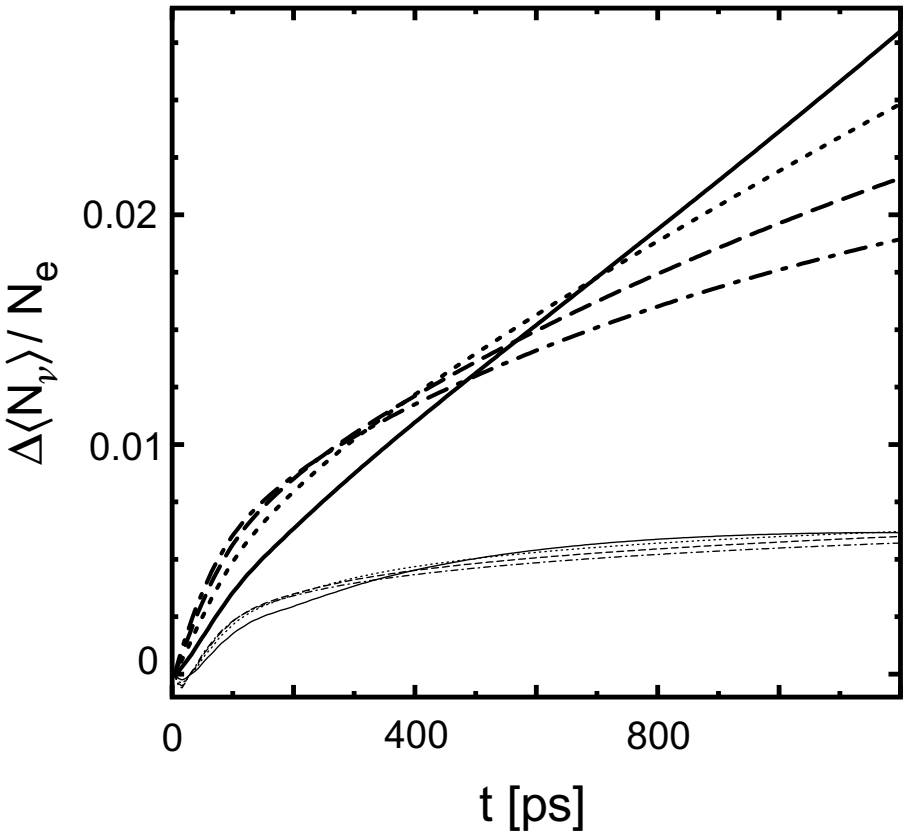

Figure 4.4: Formation dynamics of q-integrated population correlations, Eq. (4.26), out of an electron-hole plasma with $n = 2 \times 10^4\,\mathrm{cm}^{-1}$ at $T = 60\,\mathrm{K}$. The lattice temperature was 10 K (solid line), 20 K (dotted line), 30 K (dashed line), and 40 K (dash-dotted line), respectively. Thick lines indicate $\Delta\langle N_{1\mathrm{s}}\rangle$ whereas thin lines refer to $\Delta\langle N_{2\mathrm{p}}\rangle$.

This expansion cannot only be used to solve Eq. (4.14) analytically but also to compute expectation values in the exciton basis from our numerical computations performed in the k-basis.

In general, $\phi^{\mathrm{l(r)}}_{\nu,q}$ is implicitly time dependent due to the temporal evolution of the carrier densities $f^{\mathrm{e(h)}}_k$. Nevertheless, one can compute the exciton wave functions with the *momentary* carrier distributions at any time during the calculation and use Eq. (4.25) in order to compute the excitonic correlations. That way, one can study the formation of specific excitons as shown in Fig. 4.4. There, we have computed the dynamics for different lattice temperatures, always starting with initial electron and hole distributions at a temperature of $T = 60\,\mathrm{K}$. With the help of Eq. (4.25), we compute the q integrated exciton population correlations

$$\Delta\langle N_\nu\rangle = \sum_q \Delta\langle N_{\nu,q}\rangle = \sum_q \Delta\langle X^\dagger_{\nu,q} X_{\nu,q}\rangle \tag{4.26}$$

normalized to the total number of electrons in the system. These populations as a func-

tion of time are shown for the two lowest bound excitons denoted 1s and 2p, respectively[1]. Figure 4.4 clearly demonstrates how the formation rate of 1s excitons quickly drops for elevated lattice temperatures. For temperatures above 40 K, we do not expect any significant formation. The time evolution of the second exciton does not show good formation under all these conditions. Also a larger sweep through parameter space confirms that only below 40 K good formation conditions can be expected for the 1s exciton [81].

In order to continue our analytical derivation, we note that in the incoherent regime f^{e} and f^{h} typically change slowly such that the exciton wave functions $\phi_{\nu,q}$ can be assumed to be quasi stationary. With the help of this adiabatic approximation, Eq. (4.14) can be written as

$$\begin{aligned} i\hbar\frac{\partial}{\partial t}\Delta\langle X^\dagger_{\nu,q}X_{\nu',q}\rangle &= (E_{\nu',q}-E_{\nu,q})\Delta\langle X^\dagger_{\nu,q}X_{\nu',q}\rangle \\ &\quad+\sum_{k,k'}\phi^{\mathrm{l}}_{\nu,q}(k)\left(\phi^{\mathrm{l}}_{\nu',q}(k')\right)^* S_q(k,k') \end{aligned} \tag{4.27}$$

with the factorized (singlet) source term

$$\begin{aligned} S_q(k,k') &= V_{k-k'}\left[(1-f^{\mathrm{e}}_{k+q^{\mathrm{e}}}-f^{\mathrm{h}}_{k-q^{\mathrm{h}}})f^{\mathrm{e}}_{k'+q^{\mathrm{e}}}f^{\mathrm{h}}_{k'-q^{\mathrm{h}}}\right. \\ &\quad\left.-(1-f^{\mathrm{e}}_{k'+q^{\mathrm{e}}}-f^{\mathrm{h}}_{k'-q^{\mathrm{h}}})f^{\mathrm{e}}_{k+q^{\mathrm{e}}}f^{\mathrm{h}}_{k-q^{\mathrm{h}}}\right]. \end{aligned} \tag{4.28}$$

The properties of the left-handed exciton basis, Eq. (4.16), can be used to simplify the last term in Eq. (4.27) according to

$$\sum_{k,k'}\phi^{\mathrm{l}}_{\nu,q}(k)\left(\phi^{\mathrm{l}}_{\nu',q}(k')\right)^* S_q(k,k') = (E_{\nu',q}-E_{\nu,q})\langle X^\dagger_{\nu,q}X_{\nu',q}\rangle_{\mathrm{S}}\,, \tag{4.29}$$

where the factorized plasma part of the two-particle correlation is given by

$$\langle X^\dagger_{\nu,q}X_{\nu',q}\rangle_{\mathrm{S}} = \sum_k \phi^{\mathrm{l}}_{\nu,q}(k)\left(\phi^{\mathrm{l}}_{\nu',q}(k)\right)^* f^{\mathrm{e}}_{k+q^{\mathrm{e}}}f^{\mathrm{h}}_{k-q^{\mathrm{h}}}\,. \tag{4.30}$$

In the exciton basis, the full equation is therefore

$$\begin{aligned} i\hbar\frac{\partial}{\partial t}\Delta\langle X^\dagger_{\nu,q}X_{\nu',q}\rangle &= (E_{\nu',q}-E_{\nu,q})\Delta\langle X^\dagger_{\nu,q}X_{\nu',q}\rangle + (E_{\nu',q}-E_{\nu,q})\langle X^\dagger_{\nu,q}X_{\nu',q}\rangle_{\mathrm{S}} \\ &\quad+i\hbar\left[\frac{\partial}{\partial t}\Delta\langle X^\dagger_{\nu,q}X_{\nu',q}\rangle\right]_{\mathrm{T-scatt}} \end{aligned} \tag{4.31}$$

where we have included scattering contributions from six-point correlations.

The simple form of Eq. (4.31) reveals how the exciton formation proceeds. If one starts the calculations assuming initially vanishing correlations, they start to build up because the source term $\langle X^\dagger_{\nu,q}X_{\nu',q}\rangle_{\mathrm{S}}$ is non-vanishing as soon as carriers are excited in the system. However, that source term does not create diagonal correlations such that excitonic populations

[1] In a one-dimensional model system, all exciton wave functions have a defined parity and are either even or odd functions. In analogy to the common nomenclature, the bound states are labelld 1s, 2p, 3s, and so forth.

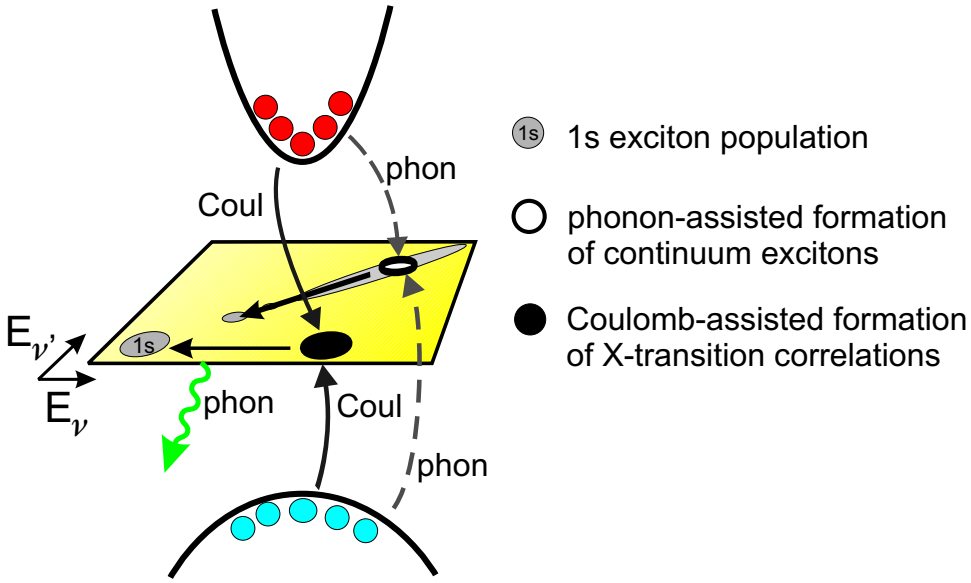

Figure 4.5: Schematic sketch of the two possible formation channels. In the incoherent regime, only indirect formation via off-diagonal transition correlations is possible. Under coherent excitation conditions, coherent polarization can be transformed directly into incoherent exciton populations.

$\Delta\langle N_{\nu,q}\rangle$ remain zero without the six-point scattering contribution. This shows that the formation of exciton populations in the incoherent regime has only one possible Coulombic channel. First, off-diagonal transition correlations $\Delta\langle X^\dagger_{\nu,q} X_{\nu'\neq\nu,q}\rangle$ are created. Then populations are formed from them via the six-point scattering in a second step. Direct formation of populations is only possible during a coherent excitation when phonon scattering can create excitonic populations out of the coherent polarization [41, 59]. Both formation channels are shown schematically in Fig. 4.5. Therefore, it is crucial to include both excitonic transition and population correlations in the formation analysis. In the k basis used in all computations, they are automatically included. When excitonic models are used with restriction to the diagonal populations, the formation channel via the transition correlations is completely omitted. Only with strong phonon scattering and with the assumption of non-vanishing population correlations right from the beginning [41], one gets phonon assisted formation directly along the excitonic dispersion.

The efficiency and the character of the indirect formation channel are analyzed in Fig. 4.6. This Figure compares the build-up of the integrated exciton population correlation $\Delta\langle N_{1s}\rangle$ for two different cases: The reference run shows a short segment of the exciton formation dynamics similar to Fig. 4.4 under good formation conditions of $n = 2\times10^4\,\mathrm{cm}^{-1}$ and with the initial carrier and lattice temperatures set to $T = 10\,\mathrm{K}$. In the other computation, we have manually reset all the off-diagonal transition correlations $\Delta\langle X^\dagger_\nu X_{\nu'\neq\nu}\rangle$ to zero in the middle of the computation. Thereto, the exciton correlations $c_{\mathrm{X}}^{q,k',k}$ are transformed into the excitonic basis and all off-diagonal correlations are set to zero. After transforming back into k space, the computation regularly continues. Figure 4.6 shows the total population corre-

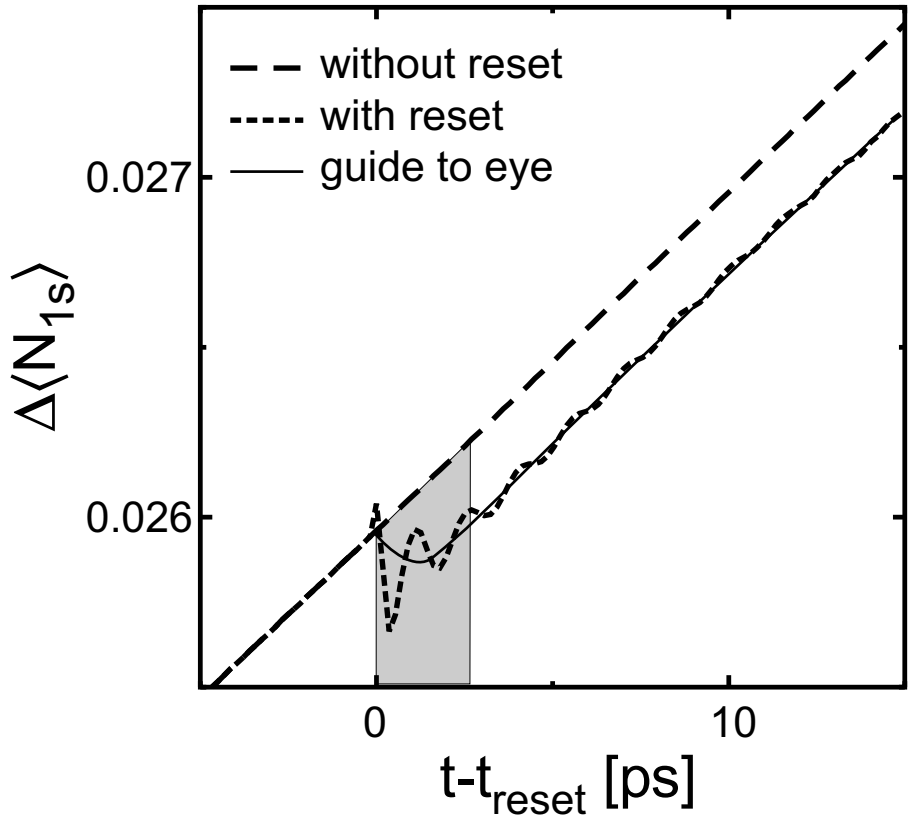

Figure 4.6: Total exciton population correlation $\sum_q \Delta\langle N_{1\mathrm{s},q}\rangle$ for two computations with and without reset of off-diagonal transition correlations. The thin solid line is given as guide to the eye.

lations during and after this reset. It is important to mention that no phonon-enhancement factor was used in this computation because we want to investigate Coulomb and phonon dynamics for equally short time scales. Exactly at the moment where the off-diagonal correlations are reset, the formation dynamics stops. No more exciton correlations can build up. On the contrary, the amount of 1s populations is even slightly decreased since the phonon scattering tends to transfer some of the diagonal populations back to off-diagonal transition correlations. Already around 3 ps after the reset, however, the off-diagonal transition correlations are fully recovered again. After some transient dynamics, the formation continues with the previous formation rate around 5 ps after the reset. Also in other quantities, as for example in the correlated Coulomb energy, this fast recovery of the transition correlations is confirmed. This behavior indicates that off-diagonal transition correlations build up extremely quickly compared to the formation rate of diagonal populations. As a result, the indirect formation channel is crucially important for the incoherent exciton formation.

The importance of the off-diagonal exciton transitions can also be seen in the equation of motion of the electron density. By expressing the right hand side of Eq. (3.36) with the help

of Eq. (4.24), one obtains

$$\frac{\partial}{\partial t} f_k^{\mathrm{e}}\Big|_{\mathrm{X-corrs}} = \sum_{\nu,\nu',q} (E_{\nu',q} - E_{\nu,q})(\phi^{\mathrm{l}}_{\nu',q}(k-q^{\mathrm{e}}))^* \phi^{\mathrm{r}}_{\nu,q}(k-q^{\mathrm{e}}) \Delta\langle X^\dagger_{\nu,q} X_{\nu',q}\rangle \,. \tag{4.32}$$

Thus, diagonal exciton populations do not change the carrier densities. Excitonic transitions are required in order to describe the full dynamics and the correct heating of the carrier plasma due to exciton formation.

4.4 Transition Correlations

In order to understand the general nature of the off-diagonal transition correlations, it is sufficient to investigate Eq. (4.31) where the triplet scattering is approximated by constant dephasing, i.e.,

$$\left[\hbar \frac{\partial}{\partial t} \langle X^\dagger_{\nu,q} X_{\nu',q}\rangle\right]_{\mathrm{T-scatt}} \approx -\gamma \,\langle X^\dagger_{\nu,q} X_{\nu',q}\rangle \,. \tag{4.33}$$

Since this term leads to a simple decay, Eq. (4.31) has a steady-state solution

$$\Delta\langle X^\dagger_{\nu,q} X_{\nu',q}\rangle\Big|_{\mathrm{steady-state}} = -\frac{E_{\nu',q} - E_{\nu,q}}{E_{\nu',q} - E_{\nu,q} - i\gamma} \langle X^\dagger_{\nu,q} X_{\nu',q}\rangle_{\mathrm{S}} \,. \tag{4.34}$$

For sufficiently small γ, we find

$$\Delta\langle X^\dagger_{\nu,q} X_{\nu',q}\rangle = (\delta_{\nu,\nu'} - 1)\langle X^\dagger_{\nu,q} X_{\nu',q}\rangle_{\mathrm{S}} \,. \tag{4.35}$$

For $\nu \neq \nu'$, the off-diagonal correlations $\Delta\langle X^\dagger_{\nu,q} X_{\nu',q}\rangle = -\langle X^\dagger_{\nu,q} X_{\nu',q}\rangle_{\mathrm{S}}$ fully cancel with the singlet (two-point) contribution when the total $\langle X^\dagger_{\nu,q} X_{\nu',q}\rangle$ is evaluated. The diagonal part $\langle X^\dagger_{\nu,q} X_{\nu,q}\rangle$, however, is determined by the mere singlet contribution. In other words, we obtain

$$\langle X^\dagger_{\nu,q} X_{\nu',q}\rangle \approx \delta_{\nu,\nu'} \langle X^\dagger_{\nu,q} X_{\nu,q}\rangle_{\mathrm{S}} = \delta_{\nu,\nu'} \sum_k |\phi^{\mathrm{l}}_{\nu,q}(k)|^2 f^{\mathrm{e}}_{k+q^{\mathrm{e}}} f^{\mathrm{h}}_{k-q^{\mathrm{h}}} \,, \tag{4.36}$$

where the solution is expressed with the help of Eq. (4.30). This result can be interpreted as follows: off-diagonal transition correlations build up quickly to compensate the off-diagonal two-point contributions whereas diagonal populations $\langle X^\dagger_{\nu,q} X_{\nu,q}\rangle$ have a non-vanishing and observable fermionic plasma contribution $\langle X^\dagger_{\nu,q} X_{\nu',q}\rangle_{\mathrm{S}}$.

These observations are valid also for more general cases where the six-point phonon scattering is included microscopically. Figure 4.7 shows the absolute value of the total exciton correlations $|\langle X^\dagger_{1\mathrm{s},q=0} X_{\nu,q=0}\rangle|$ as a function of the exciton energy E_ν for such a general calculation with microscopic phonon scattering. The marker at the lowest energy gives the diagonal 1s exciton population whereas the other markers indicate the magnitude of the off-diagonal transitions. Once again, these excitonic expectation values are calculated from the correlations and the carrier densities in k-space which are obtained directly from the computations. While the factorized contribution of the off-diagonal transitions is appreciable (open squares), the full exciton-exciton correlations are more than an order of magnitude smaller

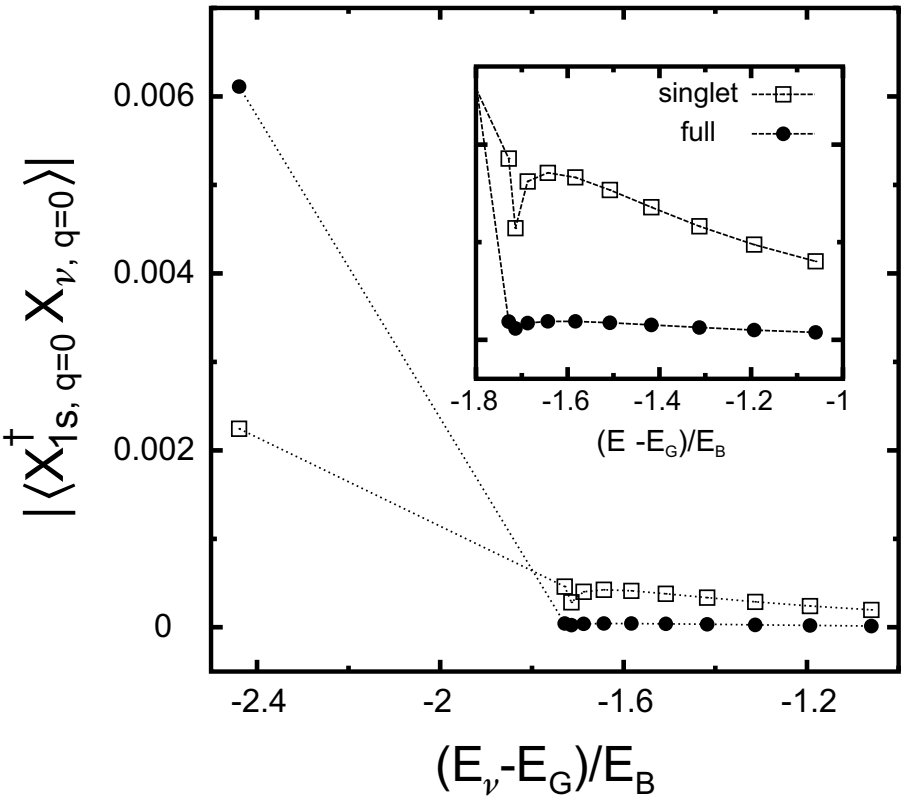

Figure 4.7: Exciton correlations $\langle X^\dagger_{1\mathrm{s},q=0} X_{\nu,q=0}\rangle$ as function of energy E_ν after 720 ps of computation for the same parameters as in Fig. 4.1. The inset magnifies the region for energies higher than $E_\mathrm{G} - 1.8E_\mathrm{B}$. While off-diagonal correlations are largely reduced in the full computation, the diagonal exciton population increases in time due to genuine exciton formation.

(full circles) which indicates almost a perfect cancellation as predicted by Eq. (4.36). Due to the very fast build-up of off-diagonal correlations compared to the slow phonon scattering, the steady-state result Eq. (4.35) for off-diagonal exciton transitions is still a good approximation for the full calculation. The main change to the simplified analysis which led to Eq. (4.36) is that under true formation conditions the diagonal exciton populations can grow and exceed their singlet contribution. Due to the formation dynamics, this diagonal population may increase in time and the difference to the plasma level determines the amount of true populations. This difference can also be seen in Fig. 4.7.

Even though the final correlations $\langle X^\dagger_{\nu,q} X_{\nu',q}\rangle$ are to a very good approximation diagonal in the exciton basis, the distinction between factorized and correlated part is absolutely necessary because the consistent theory shows that: i) only the truly correlated part of the off-diagonal exciton correlations leads to a significant contribution to the formation of excitons out of an incoherent plasma, ii) only the off-diagonal correlations influence the time evolution of the carrier distributions, and iii) even under good formation conditions, the correlated contribution to the exciton population is still of the same order of magnitude as

its factorized counterpart. Both contributions certainly influence experiments and must be carefully distinguished. As we will see in Chapter 5, the photoluminescence spectrum of a semiconductor is one example of an experimental quantity which is determined by the total exciton population $\langle X^\dagger_{\nu,q} X_{\nu,q}\rangle$, not just by its correlated part.

Whereas in excitonic theories often a thermal distribution of excitons is assumed without further proof, our analysis clearly shows that all measurements which are related to the total expectation value $\langle X^\dagger_{\nu,q} X_{\nu,q}\rangle$ and not only to the correlated exciton populations should in general lead to intrinsically nonthermal results due to the plasma contribution, Eq. (4.30). Even though the excitonic correlations may tend to equilibrate under the influence of scattering processes with phonons and other carriers, the carrier densities typically change very slowly, once they are close to their equilibrium distribution. Consequently, their contribution to the total exciton "number" $\langle X^\dagger_{\nu,q} X_{\nu,q}\rangle$ can be nonthermal in the sense that these exciton populations do not obey simple Bose-Einstein statistics. This can be understood directly from Eq. (4.30) which is an overlap integral between the product of the one-particle distributions $f^{\mathrm{e}}_k f^{\mathrm{h}}_k$ and the square of the modulus of the exciton wave function $|\phi^{\mathrm{l}}_{\nu,q}|^2$. If the carriers are at a low temperature, their distributions and thus also the product $f^{\mathrm{e}}_k f^{\mathrm{h}}_k$ is strongly peaked around $k = 0$. In that case, the wave functions of bound excitons can be significantly broader than $f^{\mathrm{e}}_k f^{\mathrm{h}}_k$, such that $\langle X^\dagger_{\nu,q} X_{\nu,q}\rangle_{\mathrm{S}}$ can be approximated by

$$\langle X^\dagger_{\nu,q} X_{\nu,q}\rangle_{\mathrm{S}} \approx |\phi^{\mathrm{l}}_{\nu,q}(k=0)|^2 \sum_k f^{\mathrm{e}}_k f^{\mathrm{h}}_k \,. \tag{4.37}$$

Since the 2p exciton typically has a larger extension in real space than the 1s exciton, its k dependent exciton wave function is narrower. Hence, the peak value $|\phi^{\mathrm{l}}_{\nu,q}(k=0)|^2$ can be larger for the 2p than for the 1s exciton and for sufficiently low temperatures one finds $\langle X^\dagger_{1\mathrm{s},q} X_{1\mathrm{s},q}\rangle_{\mathrm{S}} < \langle X^\dagger_{2\mathrm{p},q} X_{2\mathrm{p},q}\rangle_{\mathrm{S}}$, which is just opposite to the result expected from simple thermodynamic arguments.

For the continuum states, the exciton wave functions are sufficiently close to δ-functions in k-space such that even the plasma part behaves thermally according to

$$\sum_k |\phi^{\mathrm{l}}_\nu(k)|^2 f^{\mathrm{e}}_k f^{\mathrm{h}}_k \approx f^{\mathrm{e}}_{k_\nu} f^{\mathrm{h}}_{k_\nu} \approx \frac{1}{\mathrm{e}^{\frac{1}{kT}(E_\nu - \mu)} - 1} \tag{4.38}$$

with the chemical potential $\mu = \mu_{\mathrm{e}} + \mu_{\mathrm{h}}$ if the carrier occupations are given by thermal Fermi-Dirac distributions of temperature T. Therefore, also the singlet contribution $\langle X^\dagger_{\nu,q} X_{\nu,q}\rangle_{\mathrm{S}}$ behaves nearly thermal for continuum states ν when the carriers are in quasi-equilibrium.

Figure 4.8 confirms these results from our computations. We show the full diagonal exciton-exciton correlations with vanishing center-of-mass momentum including singlet and correlated contribution for the same parameters as in Fig. 4.1. The shaded area indicates the energies where continuum excitons exist. The factorized contribution to the exciton number is indeed nonthermal for bound excitons; the contribution of the second exciton is larger than that of the first one. During the formation, the $\langle X^\dagger_{\nu,q} X_{\nu,q}\rangle$ develops towards a thermal distribution. However, this thermalization takes place so slowly that even after 1.2 ns the system is still far from equilibrium. This is illustrated by the thermal distribution which correctly fits the tail of the continuum excitons and is plotted for comparison.

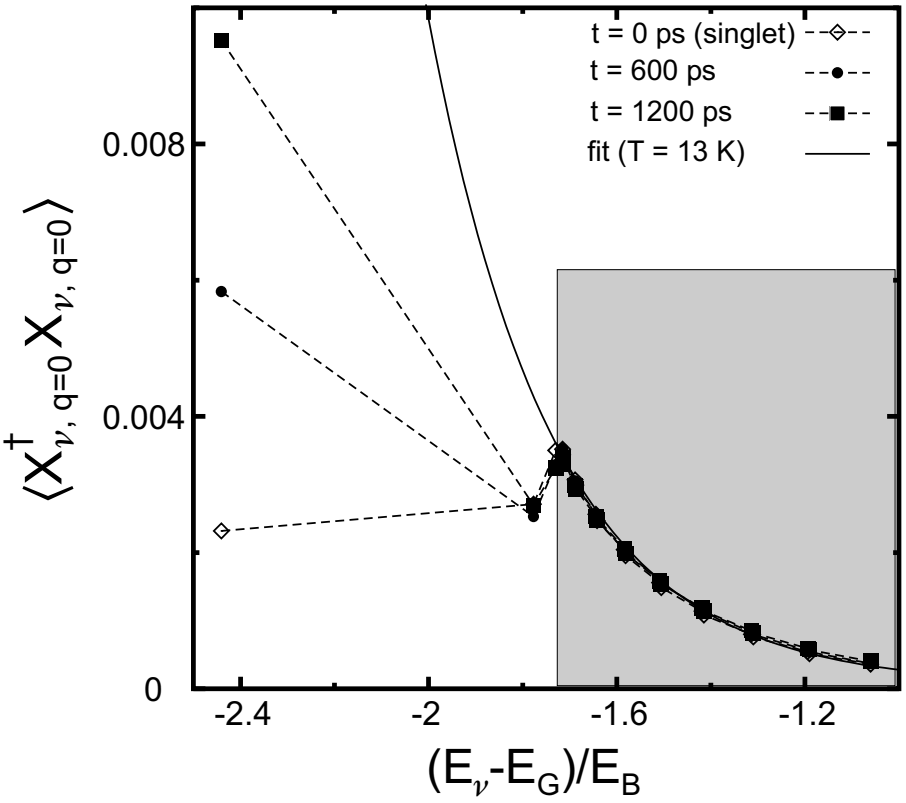

Figure 4.8: Diagonal exciton population correlation $\Delta\langle N_{\nu,q=0}\rangle$ for excitons with vanishing center-of-mass momentum given at t=0 (Hartree-Fock result) and at two subsequent times. A thermal distribution with a temperature of $T = 13\,\mathrm{K}$ fitting the high energy tail of the initial distribution is given for comparison.

4.5 Exciton Numbers

In general, it is an old question how to obtain a well defined quantum-mechanical number for non-elementary bosons [32]. Therefore, we investigate when and how the exciton population correlations, introduced in the previous Section, can be interpreted as exciton numbers.

First of all, we note that the total expectation value $\langle X^{\dagger}_{\nu,q} X_{\nu,q}\rangle$ cannot be interpreted as a number since the exciton basis is overcomplete such that

$$\begin{aligned}
\sum_{\nu,q}\langle X^{\dagger}_{\nu,q} X_{\nu,q}\rangle &= \sum_{\nu,q}\sum_{k,k'} \left(\phi^{\mathrm{l}}_{\nu,q}(k)\right)^{*} \phi^{\mathrm{l}}_{\nu,q}(k')\langle c^{\dagger}_{k+q^{\mathrm{e}}} v_{k-q^{\mathrm{h}}} v^{\dagger}_{k'-q^{\mathrm{h}}} c_{k'+q^{\mathrm{e}}}\rangle \\
&= \sum_{k,q}(1 - f^{\mathrm{e}}_{k+q^{\mathrm{e}}} - f^{\mathrm{h}}_{k-q^{\mathrm{h}}})^{-1}\langle c^{\dagger}_{k+q^{\mathrm{e}}} v_{k-q^{\mathrm{h}}} v^{\dagger}_{k-q^{\mathrm{h}}} c_{k+q^{\mathrm{e}}}\rangle \\
&= \sum_{k,p}(1 - f^{\mathrm{e}}_{k} - f^{\mathrm{h}}_{p})^{-1}\langle c^{\dagger}_{k} c_{k} v_{p} v^{\dagger}_{p}\rangle
\end{aligned} \tag{4.39}$$

which for low densities gives the operator product between the total number of electrons

and the total number of holes[2]. For a state with N electron-hole pairs in low density, this expectation value is normalized to N^2. Thus, the operator $X^\dagger_{\nu,q}X_{\nu,q}$ is not a number operator but rather counts the number of excitons multiplied with the possible holes which can be associated with every electron. Related problems have been treated in earlier publications [82–84]. There, it has been investigated in how far a mapping from the original many-fermion space to a bosonic Hilbert space can be introduced. It is possible to find such a mapping which gives the correct eigenvalues of the stationary Schrödinger equation [82]. The difficulty still comes at the point where expectation values have to be computed because one has to define a non-trivial norm-operator in connection with such a mapping [84].

In spite of those difficulties, it is intuitively clear that the state

$$|\Psi\rangle_{\mathrm{X}} = |\nu_1, q_1 \ldots \nu_N, q_N\rangle = \left(\prod_{j=1}^{N} X^\dagger_{\nu_j,q_j}\right)|0\rangle\,, \tag{4.40}$$

where N excitons are created from the semiconductor vacuum state, should be very close to describing a purely excitonic system, whereas

$$|\Psi\rangle_{\mathrm{pl}} = |k_1, p_1 \ldots k_N, p_N\rangle = \left(\prod_{j=1}^{N} c^\dagger_{k_j} v_{p_j}\right)|0\rangle \tag{4.41}$$

should be a good approximation of a plasma state with N uncorrelated electrons and holes. If one computes the expectation value of the operator $X^\dagger_{\nu,q}X_{\nu',q}$ for such a state with only two excitons, one finds

$$\begin{aligned}
\langle X^\dagger_{\nu,q}X_{\nu',q}\rangle\Big|_{\mathrm{X}} &= \langle \nu_1, q_1, \nu_2, q_2 | X^\dagger_{\nu,q}X_{\nu',q} | \nu_1, q_1, \nu_2, q_2\rangle \\
&= \delta_{\nu,\nu'}(\delta_{q,q_1}\delta_{\nu,\nu_1} + \delta_{q,q_2}\delta_{\nu,\nu_2}) \\
&\quad + \sum_{\substack{n,m=1\\ n\neq m}}^{2} \sum_{k} \phi_{\nu,q}(k-q^{\mathrm{e}})(\phi_{\nu',q}(k-q^{\mathrm{e}}))^* \\
&\qquad\qquad |\phi_{\nu_n,q_n}(k-q^{\mathrm{e}}_n)|^2 |\phi_{\nu_m,q_m}(k+q^{\mathrm{h}}_m-q)|^2\,,
\end{aligned} \tag{4.42}$$

where we have dropped the distinction between left and right-handed wave functions for simplicity and have used the commutation relation

$$\begin{aligned}
[X_{\nu,q}, X^\dagger_{\nu',q'}] &= \delta_{\nu,\nu'}\delta_{q,q'} - \sum_k \phi_{\nu,q}(k+q^{\mathrm{h}})\left(\phi_{\nu',q'}(k+q'^{\mathrm{h}})\right) c^\dagger_{k+q}c_{k+q'} \\
&\quad - \sum_k \phi_{\nu,q}(k-q^{\mathrm{e}})\left(\phi_{\nu',q'}(k-q'^{\mathrm{e}})\right) v_{k-q}v^\dagger_{k-q'}
\end{aligned} \tag{4.43}$$

between two excitonic states. This commutation relation is not totally bosonic due to the internal structure of an exciton as being composed of two fermions. Consequently, also

[2]One can avoid the phase-space filling factor completely by using one left- and one right handed exciton operator in the left-hand side of Eq. (4.39).

Eq. (4.42) can be separated into two contributions. The δ-functions in the first line can be identified as the bosonic contribution which would be obtained also for perfect bosons. The corrections in the second and third line of Eq. (4.42) are due to the underlying fermionic character. For the special case where the excitonic labels ν_1 and ν_2 denote bound excitons, the fermionic part is proportional to $1/\mathcal{L}^d$ where $\mathcal{L}$ denotes the extension of the d dimensional semiconductor structure. Hence, the fermionic part provides only a small correction to the expectation value $\langle X^\dagger_{\nu,q} X_{\nu,q}\rangle$ for each individual exciton state (ν, q). This correction vanishes with increasing system size. Only if we perform the infinite summation over all these small corrections, they add up to

$$\begin{aligned}\sum_{\nu,q}\langle X^\dagger_{\nu,q}X_{\nu,q}\rangle\Big|_{\mathrm{X,ferm}} =& \sum_{k,q}\big(|\phi_{\nu_1,q_1}(k-q_1^{\mathrm{e}})|^2|\phi_{\nu_2,q_2}(k+q_2^{\mathrm{h}}-q)|^2 \\ &+|\phi_{\nu_2,q_2}(k-q_2^{\mathrm{e}})|^2|\phi_{\nu_1,q_1}(k+q_1^{\mathrm{h}}-q)|^2\big)=2,\end{aligned} \tag{4.44}$$

which is equally big as the total bosonic contribution for the two-exciton state. In a general N-exciton state, the integrated bosonic contribution gives N whereas the fermionic contribution adds up to $N(N-1)$.

If we compute the singlet approximation of Eq. (4.42), we obtain

$$\begin{aligned}\langle X^\dagger_{\nu,q}X_{\nu',q}\rangle_{\mathrm{S}}\Big|_{\mathrm{X}} =& \sum_{n,m=1}^{2}\Big(\sum_k \phi_{\nu,q}(k-q^{\mathrm{e}})(\phi_{\nu',q}(k-q^{\mathrm{e}}))^* \\ &|\phi_{\nu_n,q_n}(k-q_n^{\mathrm{e}})|^2|\phi_{\nu_m,q_m}(k+q_m^{\mathrm{h}}-q)|^2\Big),\end{aligned} \tag{4.45}$$

which is very similar to the fermionic part. Compared to Eq. (4.42), the summation contains the additional term for $n=m$ and is thus normalized to $N^2=4$. Using Eq. (4.42) together with Eq. (4.45) we see that the correlated contribution of $\langle X^\dagger_{\nu,q}X_{\nu',q}\rangle$ for a two-exciton state is given by

$$\begin{aligned}\Delta\langle X^\dagger_{\nu,q}X_{\nu',q}\rangle\Big|_{\mathrm{X}} &= \langle X^\dagger_{\nu,q}X_{\nu',q}\rangle\Big|_{\mathrm{X}} - \langle X^\dagger_{\nu,q}X_{\nu',q}\rangle_{\mathrm{S}}\Big|_{\mathrm{X}} \\ &= \delta_{\nu,\nu'}(\delta_{q,q_1}\delta_{\nu,\nu_1}+\delta_{q,q_2}\delta_{\nu,\nu_2}) \\ &\quad -\sum_{n=1}^{2}\Big(\sum_k \phi_{\nu,q}(k-q^{\mathrm{e}})(\phi_{\nu',q}(k-q^{\mathrm{e}}))^* \\ &\qquad |\phi_{\nu_n,q_n}(k-q_n^{\mathrm{e}})|^2|\phi_{\nu_n,q_n}(k+q_n^{\mathrm{h}}-q)|^2\Big),\end{aligned} \tag{4.46}$$

which again differs from the genuine bosonic contribution only by an infinitesimal part, as long as the test function (4.40) contains only bound excitons.

For the plasma state $|\Psi_{\mathrm{pl}}\rangle$, both full and factorized contribution lead to the identical result

$$\langle X^\dagger_{\nu,q}X_{\nu',q}\rangle\Big|_{\mathrm{pl}} = \sum_{n,m=1}^{2}\phi_{\nu,q}(k_n-q^{\mathrm{e}})(\phi_{\nu',q}(k-q^{\mathrm{e}}))^*\delta_{q-k_n,p_m}\,. \tag{4.47}$$

Therefore, the correlated part as well as the bosonic part for such a state is strictly zero.

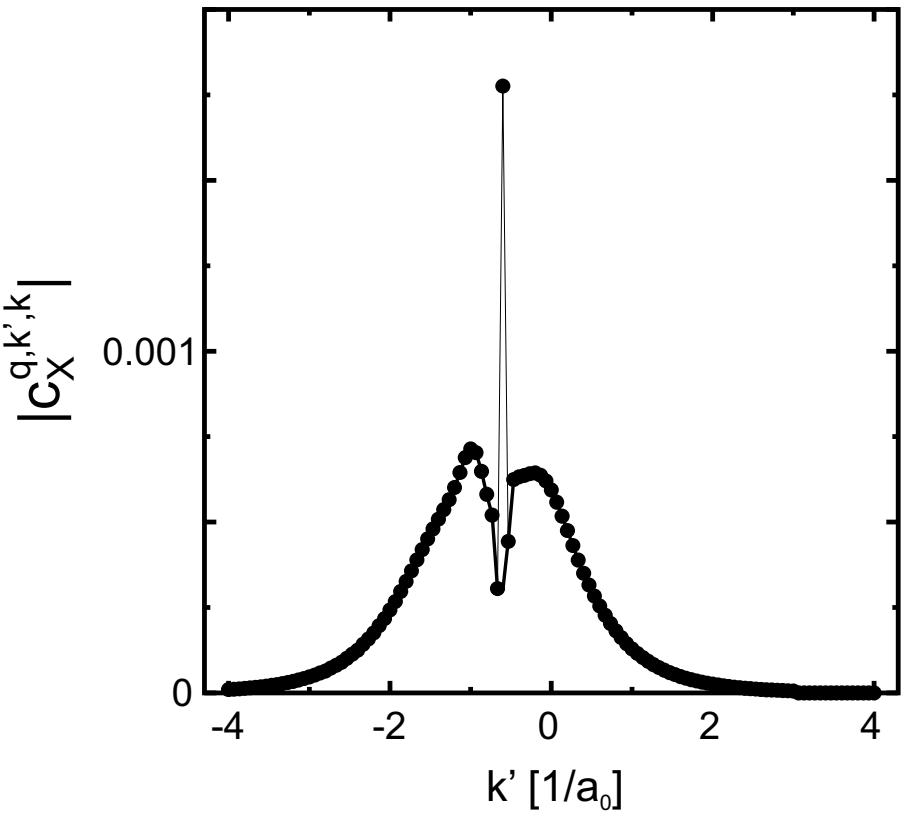

Figure 4.9: Typical cross section through exciton correlation $c_{\mathrm{X}}^{q,k',k}$ as function of k' for $q\,a_0 = 1$ and $k\,a_0 = 0.4$. For $k'\,a_0 = -0.6$ a strong discontinuity occurs.

The results obtained for the test functions, Eqs. (4.40) and (4.41), are clear evidence that the distinction between singlet and correlated contribution to a four-point operator is more than just a formal way to solve the hierarchy problem. Since correlated and bosonic contribution differ only by an infinitesimal amount, this separation is physically meaningful. In the numerical computations, however, the finite Δk corresponds to a fictitious sample length $\mathcal{L} = 2\pi/\Delta k$. Therefore, in the numerical results, the difference is not infinitesimal but depends on the quality of the k-grid we use. In order to remove the grid-dependent parts, we note that the fermionic contribution is continuous with respect to both ν and q and thus discontinuous in k space. The bosonic part of a bound exciton state, on the contrary, is discontinuous with respect to ν and q and thus smooth in k space. Indeed, a closer look at Eq. (3.32) reveals that for the special index combination $k = k' + q$ the right-hand-side of the equation is completely real. Thus, no phase cancellation effects can take place and a discontinuous contribution can evolve in time. This is demonstrated in Fig. 4.9 where we show a typical cross section of the exciton correlation $c_{\mathrm{X}}^{q,k',k}$ as function of k' for fixed q and k. We find the expected discontinuity at $k' = k - q$. Interestingly, this index combination is the one, where also the factorized part $\langle c_k^\dagger v_{k'}^\dagger c_{k'+q} v_{k-q}\rangle_{\mathrm{S}}$ of the full expectation value has its only non-vanishing contribution under incoherent conditions. Using the interpolated function after the removal of the discontinuity for the computation of physical quantities instead of

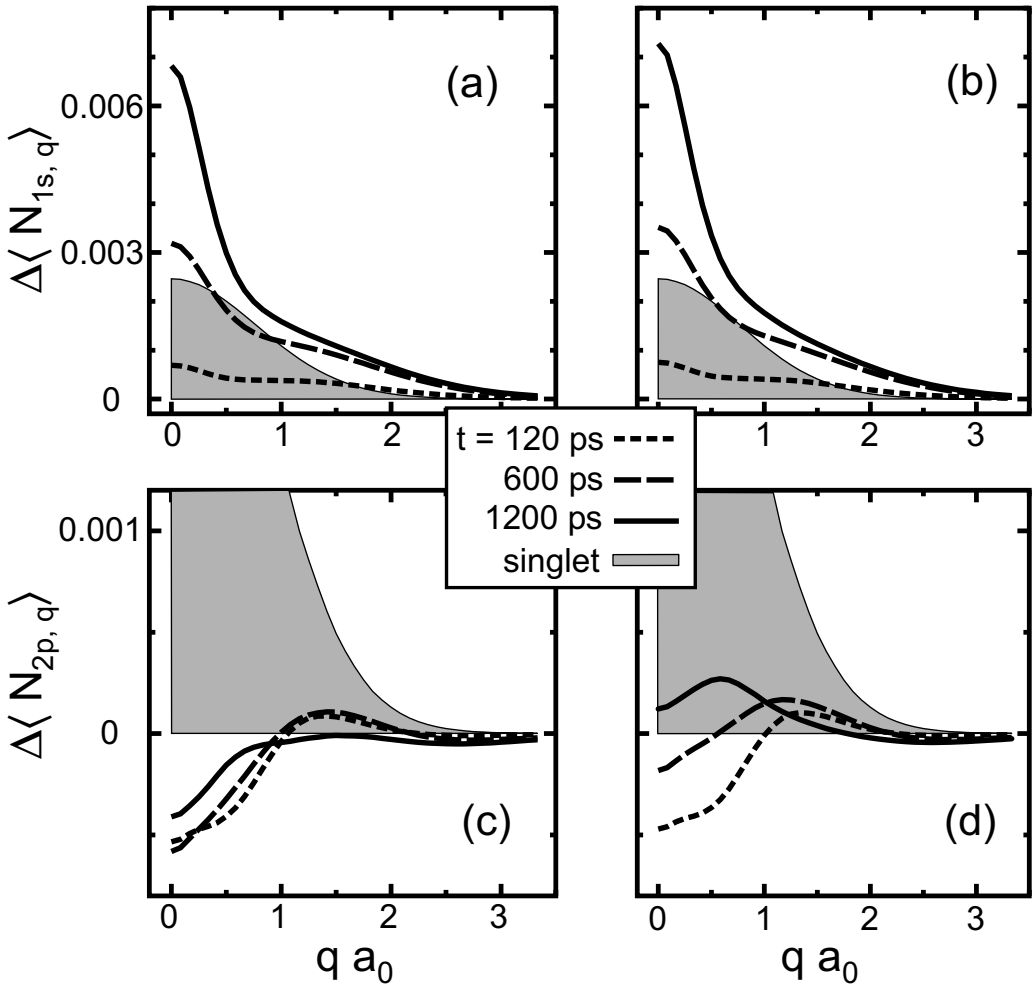

Figure 4.10: Center of mass distribution $\Delta\langle X^\dagger_{\nu,q} X_{\nu,q}\rangle$ for the lowest two exciton states at subsequent times for the same parameters as in Fig. 4.1. For the lowest exciton, the distributions obtained from the raw data (a) and after using the interpolation of the singular terms (b) are compared. For the second exciton, part (c) and (d) compare the results obtained without and with interpolation, respectively.

the original $c_{\mathrm{X}}^{q,k',k}$ leads to results which are independent of the numerical grid and much closer to the bosonic contributions discussed above.

The influence of such an interpolation is investigated in Fig. 4.10 where the difference between computations of exciton center-of-mass distributions with and without previous interpolation of the k dependent correlations are compared. The center-of-mass distributions $\Delta\langle N_{\nu,q}\rangle$ of the lowest two exciton states are shown at different times. In part (a) the distribution of the 1s exciton is obtained from the raw data. In part (b) the interpolation has been used. It is obvious that the difference is only minute. This is due to the fact that the fermionic correction is indeed small for bound excitons. In both cases, the distribution is completely positive and can be interpreted as an exciton number. Since these excitons are

created with a finite center-of-mass momentum, they exhibit a broad shoulder even at the final time of computation. Only after the creation of the excitons with finite center-of-mass momentum, they are cooled by the coupling to the phonon bath. Since the acoustic phonons are more effective for low wave numbers with a small energy transfer, the distributions at small k already follow a thermal distribution with a temperature close to the lattice temperature of 10 K even though the overall shape is still completely nonthermal and depends on the time scales of the relevant scattering processes. We also point out that the factorized part, which is given for comparison as a shaded area, is much broader than the Bose-Einstein distribution at 10 K and thus nonthermal as well.

As one can see in Fig. 4.8, the second exciton is already pretty close to the continuum. Therefore, fermionic and bosonic part can be of equal order of magnitude. In part (c) the distribution functions of the second exciton as obtained from the raw data are shown. They change very slowly and are almost completely negative even at the end of the calculations. The use of the interpolation scheme in Fig. 4.8(d) changes the picture drastically. Now the final distribution is almost completely positive and starts to be interpretable as a number of excitons. At earlier times, when the exciton number is still small, the correlations are dominated by the fermionic contribution such that the interpolation routine does not help and one gets basically identical results with or without interpolation. Moreover, the correlated contribution for the second exciton is very small compared to the factorized part $\langle X^\dagger_{2\mathrm{p},q} X_{2\mathrm{p},q}\rangle_\mathrm{S}$ shown for comparison.

We want to point out, though, that these computations of exciton "numbers" are nothing but a useful tool for the interpretation of results. All physical quantities like pair-correlation functions or different energy contributions can be obtained without the use of the exciton basis. We have seen that the positive exciton "number" $\langle X^\dagger_{\nu,q} X_{\nu,q}\rangle$ always contains a contribution related to the carrier plasma, leading to its wrong normalization properties. Furthermore, there is no fundamental reason why the exciton population correlations $\Delta\langle X^\dagger_{\nu,q} X_{\nu,q}\rangle$ should be positive. In a complicated system with many charge carriers, where different interaction processes take place simultaneously and different correlations influence each other, the true physical state is much more complicated than the simple wave functions in Eq. (4.40) or (4.41) used for motivation. Only when a dominant amount of excitons has formed in the system, the exciton population correlations are strictly positive and can be interpreted as exciton numbers.

Finally, we want to stress that the formation of excitons is not related to a question of particle species as suggested by simplified theories which establish rate equations between excitons and electrons and holes [85]. In these models, a free electron-hole pair is destroyed whenever an exciton is formed. In reality and in our theory, electrons and holes are always present and can be either correlated or not. The formation of excitons is nothing but a build-up of correlations which does not change the number of electrons and holes in the system. It is the build-up of the pair-correlation function or the build-up of the diagonal elements of the exciton population correlations which can answer the question whether excitons have formed or not. An atomic interpretation of excitons as entities only makes sense under very restricted conditions of a dilute gas where a small density of excitons interacts only very weakly with the remaining carriers. Under those conditions, our theory gives positive exciton numbers as was shown for the lowest bound exciton in Fig. 4.10. For the more

general condition, our theory can be used without making any ad-hoc assumptions about the nature of excitons.

4.6 Pair-Correlation Function

We return to the pair-correlation function to present its properties in connection with the exciton basis and the interpolation scheme introduced in the previous Section. First, by using Eq. (4.2), the integral over the pair-correlation function can be obtained as

$$\begin{aligned}\int g^{\mathrm{eh}}(r)\mathrm{d}r &= \int \frac{1}{\mathcal{L}^2}\sum_{k,k',q} \mathrm{e}^{i(k-k'-q)r}\langle c_k^\dagger v_{k-q} v_{k'}^\dagger c_{k'+q}\rangle \mathrm{d}r \\ &= \frac{1}{\mathcal{L}}\sum_{k,p}\langle c_k^\dagger c_k v_p v_p^\dagger\rangle\,. \end{aligned} \tag{4.48}$$

Thus, it is equal to the expectation value of the product between the total electron and hole number operators. As long as one neglects the coupling to the light field, this value is constant such that the integral over g and consequently also over Δg is conserved. Under incoherent conditions and for a fixed number of electron-hole pairs, one finds

$$\frac{1}{\mathcal{L}}\int g^{\mathrm{eh}}(r)\mathrm{d}r = n^{\mathrm{e}} n^{\mathrm{h}} = \frac{1}{\mathcal{L}}\int g_{\mathrm{S}}^{\mathrm{eh}}(r)\mathrm{d}r \tag{4.49}$$

such that the integral over the purely correlated part $\int \Delta g^{\mathrm{eh}}\mathrm{d}r$ vanishes in a mathematical sense. In other words, this represents the fact that the probability of finding the electron anywhere has to be conserved. From that point of view, only the total pair correlation is a positive-definite quantity whereas the correlated part becomes negative at certain values.

However, the integral $\int \Delta g^{\mathrm{eh}}\mathrm{d}r$ is not necessarily vanishing in the physical sense. In the early time behavior in Fig. 4.1, the pair-correlation function approaches its factorized value at large distances, i.e., the correlated contribution approaches zero. In that case, positive and negative parts in $\Delta g^{\mathrm{eh}}(r)$ can obviously cancel. After a sufficiently long time of evolution, however, when a major fraction of 1s excitons has formed, the pair-correlation function follows the distribution of a 1s exciton wave function. As shown in Fig. 4.11a, in this case the total pair-correlation function at large distances lies *infinitesimally* below its factorized value. Therefore, the correlated contribution Δg^{eh} is shifted by an infinitesimal amount such that the constant level lies below zero. More precisely, the negative level is proportional to $1/\mathcal{L}$ such that only an integration over the whole crystal yields the vanishing integral value. In all numerical computations, this shift is not vanishing but proportional to the inverse of the fictitious sample length $2\pi/\Delta k$ defined by the distance Δk between equally spaced grid points. Varying the number of grid points leads to different negative shifts for otherwise identical results. Based on Eq. (4.4), such a constant shift must be related to the index combination $k'+q-k=0$, i.e., exactly the same index combination which has been involved in the interpolation routine in the previous Section for the removal of the infinitesimal error in evaluating the bosonic contribution $\Delta\langle X^\dagger X\rangle$. And indeed, using this interpolation routine naturally

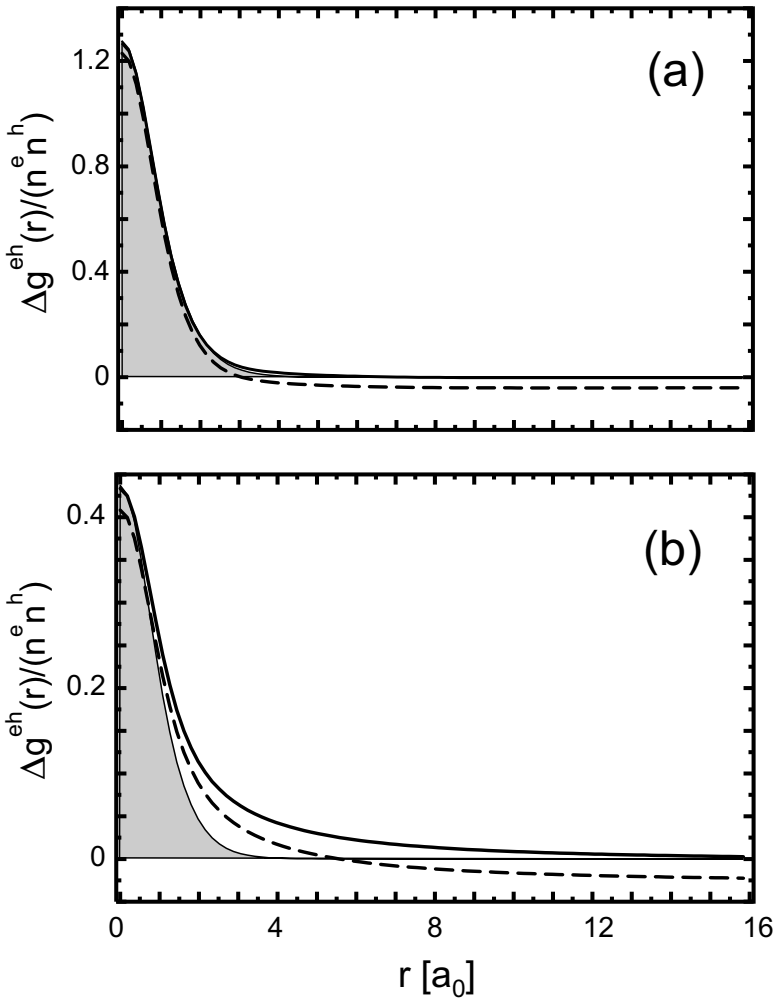

Figure 4.11: Comparison of pair-correlation function with (solid line) and without (dashed line) interpolation at the singular values of $c_{\mathrm{X}}^{q,k',k'+q}$. After removal of the singularity, the correlated part of the pair-correlation function correctly approaches the zero line at large densities. Therefore this interpolation procedure helps to extract the true bosonic part of the exciton number. Results are shown for $n = 2 \times 10^4\,\mathrm{cm}^{-}1$ at $T = 10\,\mathrm{K}$ (a) and $T = 50\,\mathrm{K}$ (b). For comparison, the 1s-exciton wave funciton is given as shaded area.

moves the pair-correlation function back to positive values, as also shown in Fig. 4.11a. After the interpolation, the pair-correlation function Δg^{eh} correctly approaches zero, such that the shape is independent of the numerical grid in use. Thus, the integral $\int \Delta g^{\mathrm{eh}} \mathrm{d}r$ becomes a physically meaningful quantity by the removal of the infinitesimal contribution. It is well defined and positive and can be interpreted as an exciton number. This interpolation has been used in Fig. 4.1. However, we should mention that the pair-correlation function at early times is genuinely negative and not changed by the use of the interpolation scheme.

In general, the integral over $\Delta g^{\mathrm{eh}}(r)$ cannot distinguish between different exciton states.

With the help of Eq. (4.24), the pair-correlation function can be expressed via

$$g^{\mathrm{eh}}(r) = \frac{1}{\mathcal{L}^2} \sum_{\nu,\nu',q} \left(\phi^{\mathrm{r}}_{\nu,q}(r)\right)^* \phi^{\mathrm{r}}_{\nu',q}(r) \langle X^\dagger_{\nu,q} X_{\nu',q} \rangle \,. \tag{4.50}$$

Using the results from Sec. 4.4, this double sum over ν and ν' can approximately be reduced to a single sum such that it simplifies to

$$g^{\mathrm{eh}}(r) \approx \frac{1}{\mathcal{L}^2} \sum_{\nu,q} |\phi^{\mathrm{l}}_{\nu,q}(r)|^2 \langle X^\dagger_{\nu,q} X_{\nu,q} \rangle \,. \tag{4.51}$$

Consequently, the pair-correlation function in general does not follow the 1s-exciton wave function when higher order correlations are important. As shown in Fig. 4.11b, the deviations become more important for elevated temperatures. But the interpolation scheme still works perfectly.

The integral over distance r gives the sum over all diagonal exciton correlations. Using Eq. (4.50), one directly obtains

$$\begin{aligned} \int g^{\mathrm{eh}}(r)\mathrm{d}r &= \frac{1}{\mathcal{L}^2} \int \sum_{\nu,\nu',q} \left(\phi^{\mathrm{r}}_{\nu,q}(r)\right)^* \phi^{\mathrm{r}}_{\nu',q}(r) \langle X^\dagger_{\nu,q} X_{\nu',q} \rangle \mathrm{d}r \\ &\approx \frac{1}{\mathcal{L}} \sum_{\nu,q} \langle X^\dagger_{\nu,q} X_{\nu,q} \rangle \,, \end{aligned} \tag{4.52}$$

where the last step is rigorously true only for low densities when the difference between right- and left handed wave functions is not yet relevant. After the removal of the singularity or, equivalently, after shifting the pair correlation obtained from the original data infinitesimally upwards, the integration over $\Delta g^{\mathrm{eh}}(r)$ is well-defined and can be taken as a measure of how many excitons have formed. Clearly, the infinitesimal contribution of Δg^{eh} and the infinitesimal error in the bosonic part of $\Delta\langle X^\dagger X \rangle$ have the same mathematical origin. Physically, a proper number can be defined by removing the singularity from $c_{\mathrm{X}}^{q,k',k}$ (see Fig. 4.11). And again, the distinction between correlated and factorized contribution proves to be helpful because the correlated part of the correlation function, in connection with the interpolation scheme, can provide a unique measure of the amount of bound excitons.

As a last detail, we want to mention that the abstract conservation law from Eq. (3.52) gets a physical interpretation. Equation (4.4) shows that the sum over exciton correlations,

$$\frac{1}{\mathcal{L}^2} \sum_{k,k',q} c_{\mathrm{X}}^{q,k',k} = \Delta g^{\mathrm{eh}}(r=0) \,, \tag{4.53}$$

is precisely the pair-correlation function at $r = 0$. Thus, Eq. (3.52) expresses the fact that this value is unchanged by the phonon interaction in its present form. The phonon interaction may change the shape of the pair-correlation function and can lead to a redistribution of the probability of finding an electron close to a hole. But only the coupled dynamics of phonon and Coulomb interaction can lead to an overall increase of the pair correlation as observed in Fig. 4.1.

5 Photoluminescence

Photoluminescence spectra have been the focus of extensive research in the past. In particular, it is often believed that photoluminescence experiments can serve as a measure of incoherent excitons. Several experimental publications directly conclude an exciton formation time from time-resolved photoluminescence spectra [27–30, 86]. One typical experimental situation is to excite carriers off-resonantly high in the band and to follow the subsequent dynamics, as illustrated in Fig. 1.1. The observed formation times in the literature vary between 20 ps and several hundred picoseconds. However, the deduction of such an exciton-formation time from luminescence experiments is not unambiguous, as we will show in this Chapter. Already with the results of the previous Chapter, one has to conclude that phonon assisted exciton formation for lattice and carrier temperatures below 50 K takes place on a relatively long time scale of at least several hundreds of picoseconds. Furthermore, it is not a priori clear in how far the exciton formation is altered if spontaneous emission processes of these excitons are considered. Especially since the radiative decay time of coherent excitons in two-dimensional quantum-well structures is known to be of the order of several picoseconds only [12], one can expect also incoherent excitons to decay equally fast. In that case, spontaneous emission should deplete excitonic populations much faster than they can build up.

In order to compare to the experiments, the effect of spontaneous emission onto carriers and exciton correlations has thus to be taken into account. Current theoretical approaches are sometimes formulated and solved in an exciton basis, often implicitly postulating the presence of excitons by neglecting the possibility of an uncorrelated electron-hole plasma [40, 41, 59]. For off-resonant excitation, however, the presence of the long-range Coulomb interaction which is not included in these approaches is expected to play an important role. In other theories, the so-called Kubo-Martin-Schwinger relation is used in order to compute photoluminescence spectra [25, 87]. This relation is strictly valid only under thermal equilibrium conditions and we will observe in the following that the actual exciton distributions are typically far from equilibrium. In fact, we show that for the computation of luminescence spectra it is often a reasonable approximation to neglect bound excitons completely.

We investigate the full numerical solution including the coupling to the quantized light field in Sec. 5.1. We show that most of the excitons are in dark states which do not couple to the light field. Using these results, we derive an analytical expression to compute photoluminescence spectra in direct analogy to the famous Elliott formula for absorption. This formula presents the fundamental features of semiconductor luminescence in a transparent manner such that one is able to understand and explain plasma vs. population features

in emission spectra. Furthermore, the formula can be used to avoid part of the numerical complexity. It thus allows us to compute luminescence spectra also for two dimensional quantum-well systems.

5.1 Numerical Solution

In Chapter 4, we have studied the build up of correlations out of an incoherent electron-hole plasma for a semiconductor structure with vanishing coupling to the light field. Since a strong suppression of spontaneous emission can be achieved by inserting a semiconductor structure inside a photonic bandgap material [35–37], these computations can be viewed as modeling a realistic setup. Even though in practice the detection of the weak photoluminescence signal might be difficult just because of the strong suppression of the spontaneous emission and the corresponding slow emission rate of photons, it is in principle possible to obtain photoluminescence spectra also in this case. Therefore, we compare the computed photoluminescence spectra of our full numerical simulation with and without the suppression of the dipole coupling.

The description of the quantized light field is obtained by including the dynamics according to Eqs. (3.54)–(3.58). All photoluminescence spectra are computed via Eq. (3.53), assuming a perfect energetic detector resolution. A set of computed photoluminescence spectra is shown in Fig. 5.1. In this set of figures, spectra at three different times after the begin of the computations for various lattice temperatures and carrier densities are displayed. As in the previous Chapter, all computations are initialized with vanishing correlations and quasi-equilibrium Fermi-Dirac distributions at the lattice temperature for carriers. Right from the beginning, the spectra are peaked at the excitonic resonance. This fact has been explained in terms of the Coulomb sum in Eq. (3.58) which introduces the excitonic resonance independently of the fact whether or not exciton correlations are formed [31]. Whereas for low densities and temperatures a growth of the photoluminescence peak by almost a factor of three is observed, this growth becomes negligible for high carrier densities and appreciably weaker for elevated temperatures.

In general, the source term, Eq. (3.60), shows that dynamic changes of the photoluminescence spectrum can equally well be due to changes in the exciton correlations $c_{\mathrm{X}}^{q,k',k}$ or to changing carrier distributions $f_k^{\mathrm{e/h}}$. Since the carrier distributions do not change appreciably during the computations, the growth of the peak height in Fig. 5.1 is directly related to the formation of exciton population correlations. For comparison, we also show the Hartree-Fock result of the steady-state spectrum obtained by including only the factorized source term $f_k^{\mathrm{e}} f_k^{\mathrm{h}}$ in Eq. (3.60). Whereas this approximation is in principle inconsistent according to the concept of the cluster expansion, it nevertheless gives reasonable results for the highest densities and temperatures shown in Fig. 5.1. In particular, it gives the main contribution at the lowest exciton resonance and underestimates mainly the luminescence at the higher bound states and in the continuum. For very low temperatures, this can even result in a negative luminescence signal around the renormalized band-edge. This possibility of a negative photoluminescence signal is unphysical and has been interpreted as a major limitation of our approach [87, 88]. Therefore, we want to point out that the inclusion of

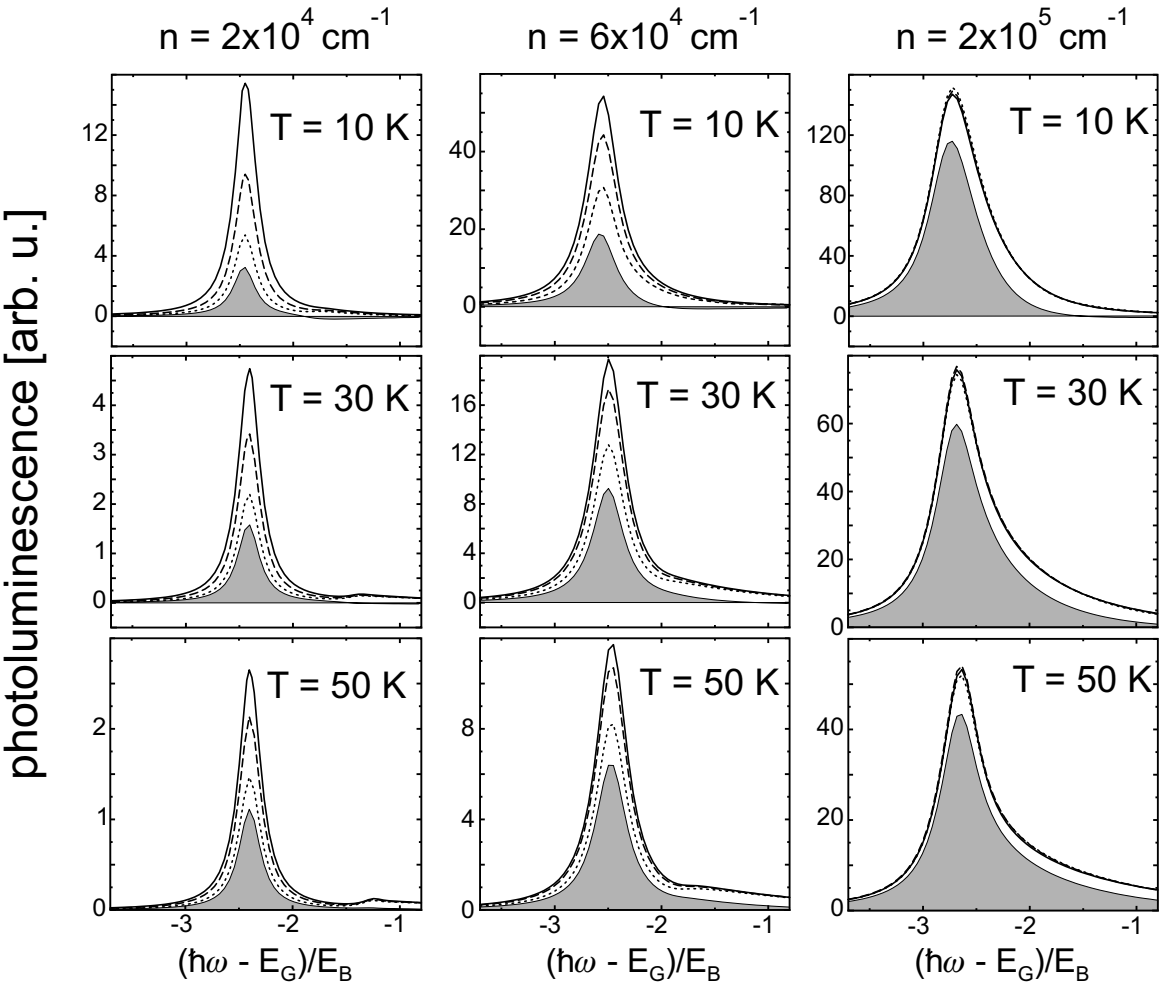

Figure 5.1: Set of computed photoluminescence spectra for different carrier densities and lattice temperatures. In each figure the spectrum is shown 120 ps (dotted line), 600 ps (dashed line) and 1200 ps (solid line) after the start of the computation. The Hartree-Fock spectrum is shown for comparison as a shaded area.

the full source term (3.60) guarantees a positive signal for any carrier distribution. This is nicely demonstrated from the numerical results in Fig. 5.2 where the luminescence spectra for different carrier densities at a lattice temperature of $T = 30\,\mathrm{K}$ are shown. The continuum luminescence shows a perfect exponential decay. The temperature fitted from this tail is approximately 40 K which is close to the initial carrier temperature. The deviation can be understood because the carriers are subject to a slow heating process in the course of their dynamic evolution.

When the computation is repeated without the suppression of spontaneous emission, the result obtained in Fig. 5.1 drastically changes. Figure 5.3 shows the result for a computation with an initial carrier density $n = 2 \times 10^4\,\mathrm{cm}^{-1}$ and a lattice temperature of 10 K. Now the excitonic peak of the photoluminescence spectrum even drops within a nanosecond. This drop is mainly due to heating of the carrier distributions. In order to see which role the

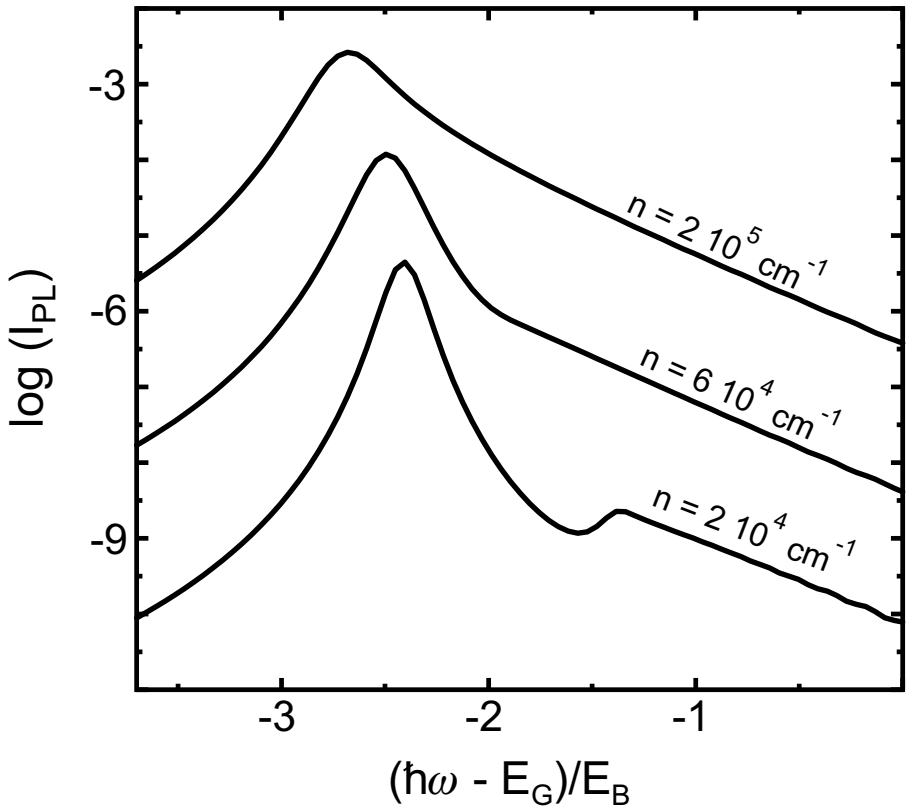

Figure 5.2: Computed photoluminescence spectrum for different carrier densities at a lattice temperature of 30 K in semi-logarithmic scale.

correlated part of the source term, Eq. (3.60), plays and to understand how the spontaneous emission influences the excitonic correlations, we compute the center-of-mass distribution of the lowest exciton population correlation. A comparison between the two computations with and without suppressed spontaneous emission is shown in Fig. 5.4. Compared to the case without spontaneous emission, the momentum dependent exciton distribution exhibits a very strong hole burning at center-of-mass momenta within the radiative cone, i.e., for all wave vectors

$$q < q_{\text{photon}} \approx \frac{E_G}{\hbar c_0}\,, \tag{5.1}$$

when the spontaneous emission is not suppressed. Since the parallel component of the wave vector is conserved according to Eq. (3.57), only excitons which fulfill Eq. (5.1) can emit photons which can propagate outside the substrate to the experimental detection. Since the photon momentum is at most $q_{\text{photon}} \approx 0.1 a_0^{-1}$, the radiative cone is very small compared to the full extent of the exciton distribution. Thus, we conclude that even under good formation conditions the dominant fraction of excitons is in dark states with a momentum too large to be transferred to a photon. Only after additional scattering processes into the radiative cone these excitons can be emitted. In general, the exact strength of the hole-burning effect depends on the balance between the spontaneous emission rate and the rate with which the

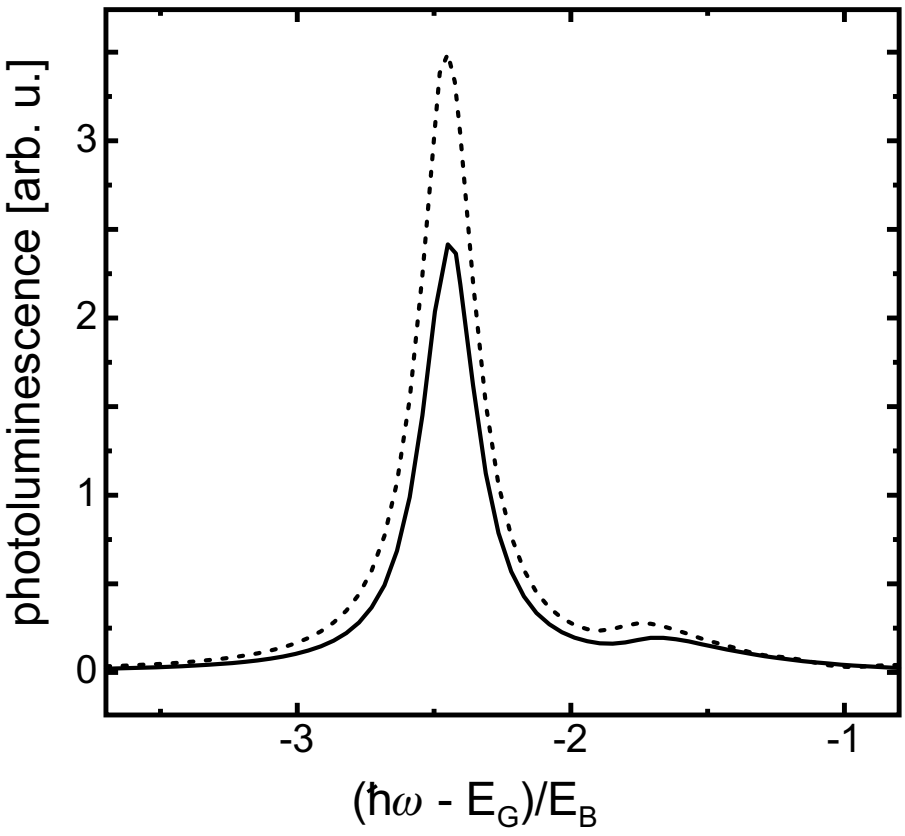

Figure 5.3: Computed photoluminescence spectra for the case of full dipole coupling. The spectra are taken directly after the start of the computation (dotted line) and after 1 ns (solid line). Instead of a growing signal, one gets a reduction of the spectrum in time.

hole is refilled via phonon or Coulomb scattering processes. It is known that the radiative life time of coherent excitons is on a picosecond time scale [13,70,89]. In principle, incoherent excitons should decay on the same picosecond time scale. Thus, the hole burning is always a dominant process in GaAs-like materials.

The electron and hole distributions do not exhibit a similar depletion at certain k values and their recombination does not have any preferred k value. More specifically, we can transform Eq. (3.55) and (3.56) into the exciton basis and obtain

$$\left[\frac{\partial}{\partial t} f_k^{\mathrm{e}}\right]_{H_{\mathrm{D}}} = \frac{2}{\hbar}\mathrm{Re}\left[\sum_{q,q_\perp,\nu} \mathcal{E}_{\mathbf{q}} \bar{u}_{\mathbf{q}}^* d_{\mathbf{q}}^* \phi_{\nu,q}^{\mathrm{r}}(k - q^{\mathrm{e}}) \Delta\langle b_{q,q_\perp}^\dagger X_{\nu,q}\rangle\right] \tag{5.2}$$

and an analogous equation for the hole distribution. In Eq. (5.8) we will see that the emission of a photon at the exciton energy E_ν is driven by the photon-assisted polarization $\Delta\langle b_{q,q_\perp}^\dagger X_{\nu,q}\rangle$ with the same exciton quantum number ν. Therefore, this emission process depletes the electrons according to the k dependence of the wave function of that specific exciton. This is confirmed by our numerical calculations. The resulting carrier distributions

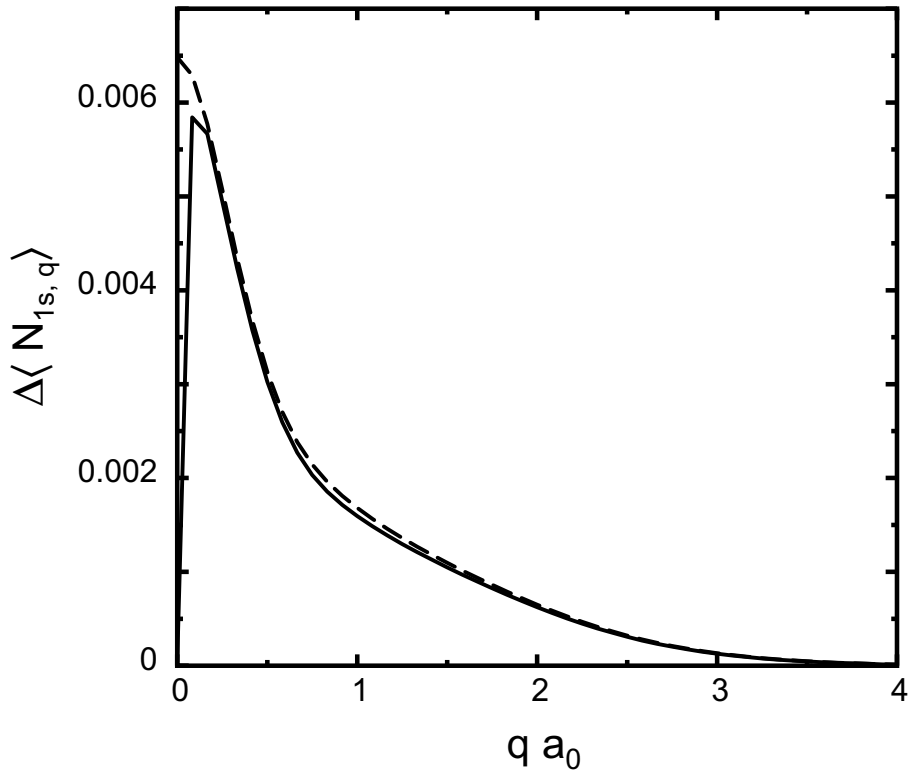

Figure 5.4: Center-of-mass distribution of the lowest exciton population correlation $\Delta\langle N_{1s,q}\rangle$ with full spontaneous emission (solid line) or with strongly suppressed spontaneous emission (dashed line) for the same conditions as in Fig. 5.3. The coupling results in a strong hole burning at momenta within the radiative cone.

corresponding to Fig. 5.4 are shown in Fig. 5.5. They only exhibit a weak heating but no traces of hole burning.

In summary, we have observed that the main consequence of the coupling of a semiconductor heterostructure to the quantum field of light is the exclusive depletion of exciton population correlations with small momenta within the radiative cone. Thus, even under conditions favorable for the build-up of excitonic correlations, the dominant part of all excitons occupies dark states and therefore does not contribute to the measured photoluminescence spectrum.

5.2 Elliott Formula for Photoluminescence

In order to understand the nature of semiconductor luminescence more clearly and to derive an analytical expression for the computation of photoluminescence spectra, we start by transforming Eqs. (3.54) and (3.58) into the generalized exciton basis. The photolumines-

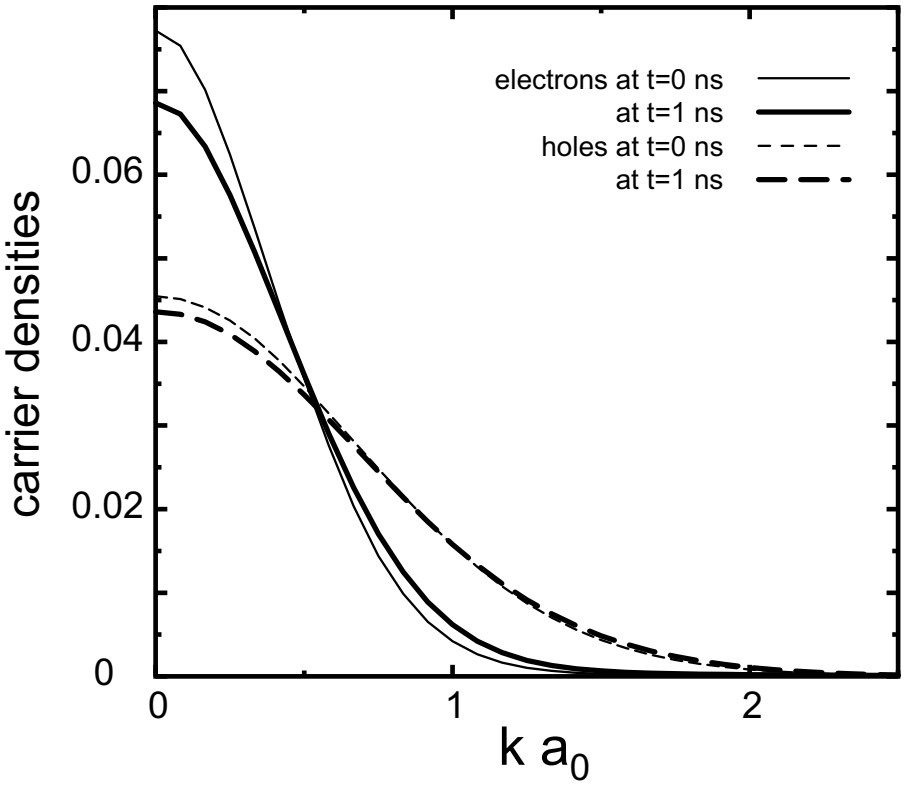

Figure 5.5: Carrier distributions initially and after one nanosecond of computed time for identical parameters as in Fig. 5.3. The main effect is a slow heating, especially for the lighter electrons, whereas strong effects due to recombination are not visible.

cence spectrum is thus given by

$$I_{\mathrm{PL}}(\omega_{\mathbf{q}}) = \frac{2}{\hbar}\mathrm{Re}\left[\mathcal{F}^{*}_{\mathbf{q}}\sum_{\nu}\phi^{\mathrm{r}}_{\nu,q}(r=0)\Delta\langle b^{\dagger}_{q_{\perp},q}X_{\nu,q}\rangle\right], \tag{5.3}$$

where the effective matrix element

$$\mathcal{F}_{\mathbf{q}} = \mathcal{E}_{\mathbf{q}}\bar{u}_{\mathbf{q}}d_{\mathbf{q}} \tag{5.4}$$

has been introduced. In Eq. (5.3), the vector $\mathbf{q}$ includes not only the information about the energy of the emitted photon $\hbar|\mathbf{q}|/c_0$, but also about the emission angle depending on the ratio between $q_\perp$ and q along the semiconductor structure. In Eq. (3.58) for the photon-assisted polarizations, the stimulated term can be neglected for systems without a cavity [44]. As a result, one obtains

$$\begin{aligned} i\hbar\frac{\partial}{\partial t}\Delta\langle b^{\dagger}_{q_{\perp},q}X_{\nu,q}\rangle &= (E_{\nu,q}+E_{\mathrm{G}}-\hbar\omega_{\mathbf{q}}-i\gamma)\Delta\langle b^{\dagger}_{q_{\perp},q}X_{\nu,q}\rangle \\ &\quad + i\mathcal{F}_{\mathbf{q}}\sum_{k}\phi^{\mathrm{l}}_{\nu,q}(k)\left[f^{\mathrm{e}}_{k+q^{\mathrm{e}}}f^{\mathrm{h}}_{k-q^{\mathrm{h}}}+\sum_{k'}\Delta\langle c^{\dagger}_{k'+q^{\mathrm{e}}}v^{\dagger}_{k-q^{\mathrm{h}}}c_{k+q^{\mathrm{e}}}v_{k'-q^{\mathrm{h}}}\rangle\right] \\ &= (E_{\nu,q}+E_{\mathrm{G}}-\hbar\omega_{\mathbf{q}}-i\gamma)\Delta\langle b^{\dagger}_{q_{\perp},q}X_{\nu,q}\rangle \end{aligned}$$

$$+ i\mathcal{F}_{\mathbf{q}} \sum_{\nu'} \phi^{\mathrm{r}}_{\nu',q}(r=0) \left[\langle X^{\dagger}_{\nu',q} X_{\nu,q} \rangle_{\mathrm{S}} + \Delta\langle X^{\dagger}_{\nu',q} X_{\nu,q} \rangle \right] . \tag{5.5}$$

In this equation, the total exciton energy, Eq. (4.20), includes the center-of-mass kinetic energy. The form of Eq. (5.5) furthermore assumes that the exciton wave functions change slowly in time. This adiabatic approximation is well valid since the carrier distributions typically do change slowly (see Fig. 5.5).

We proceed by solving Eq. (5.5) in Markov approximation,

$$\Delta\langle b^{\dagger}_{q_{\perp},q} X_{\nu,q} \rangle = \frac{i\mathcal{F}_{\mathbf{q}} \sum_{\nu'} \phi^{\mathrm{r}}_{\nu',q}(r=0) \left[\langle X^{\dagger}_{\nu',q} X_{\nu,q} \rangle_{\mathrm{S}} + \Delta\langle X^{\dagger}_{\nu',q} X_{\nu,q} \rangle \right]}{\hbar\omega_{\mathbf{q}} - E_{\mathrm{G}} - E_{\nu,q} + i\gamma} . \tag{5.6}$$

Inserting this solution into Eq. (5.3) results in

$$I_{\mathrm{PL}}(\omega_{\mathbf{q}}) = -\frac{2}{\hbar} \mathrm{Im} \left[|\mathcal{F}_{\mathbf{q}}|^2 \sum_{\nu,\nu'} \phi^{\mathrm{r}}_{\nu,q}(0) \phi^{\mathrm{r}}_{\nu',q}(0) \frac{\langle X^{\dagger}_{\nu',q} X_{\nu,q} \rangle_{\mathrm{S}} + \Delta\langle X^{\dagger}_{\nu',q} X_{\nu,q} \rangle}{\hbar\omega_{\mathbf{q}} - E_{\mathrm{G}} - E_{\nu,q} + i\gamma} \right] , \tag{5.7}$$

which nicely shows that in general luminescence at a certain excitonic energy depends not only on the corresponding exciton population, but also on the correlated carrier plasma via the term $\langle X^{\dagger}_{\nu',q} X_{\nu,q} \rangle_{\mathrm{S}}$ and on all off-diagonal transition correlations $\Delta\langle X^{\dagger}_{\nu',q} X_{\nu,q} \rangle$. From this fundamental derivation one can already conclude that a photoluminescence experiment never detects exclusively exciton populations. A careful analysis and a comparison to a microscopic theory is thus very important.

Now we recall the results of Sec. 4.3 that Coulomb processes typically lead to a very fast build-up of the off-diagonal transition correlations until they exactly cancel the singlet contribution. Thus, it is justified to assume that this process is fast compared to all other time scales of interest and Eq. (5.7) can be further simplified to

$$I_{\mathrm{PL}}(\omega_{\mathbf{q}}) = -\frac{2}{\hbar} \mathrm{Im} \left[|\mathcal{F}_{\mathbf{q}}|^2 \sum_{\nu} |\phi^{\mathrm{r}}_{\nu,q}(0)|^2 \frac{\langle X^{\dagger}_{\nu,q} X_{\nu,q} \rangle_{\mathrm{S}} + \Delta\langle X^{\dagger}_{\nu,q} X_{\nu,q} \rangle}{\hbar\omega_{\mathbf{q}} - E_{\mathrm{G}} - E_{\nu,q} + i\gamma} \right] . \tag{5.8}$$

This *Elliott Formula for Photoluminescence* summarizes all important aspects of semiconductor luminescence: i) the total luminescence spectrum has resonances given by the solution of the generalized Wannier equation due to the energy denominator, ii) these resonances are independent of the source term and a standard photoluminescence experiment cannot distinguish between contributions from exciton correlations and Coulomb correlated plasma; even with vanishing exciton correlations, the pure singlet source results in a strong peak at the 1s exciton resonance due to the large oscillator strength $|\phi^{\mathrm{r}}_{1\mathrm{s},q}(r=0)|^2$, iii) a typical photoluminescence spectrum is highly nonthermal in the sense that the Kubo-Martin-Schwinger relation [25], which relates photoluminescence to absorption measurements by a Bose-Einstein distribution via

$$I_{\mathrm{PL}}(\omega) = \alpha(\omega)\, g(\hbar\omega) , \tag{5.9}$$

cannot be applied in general.

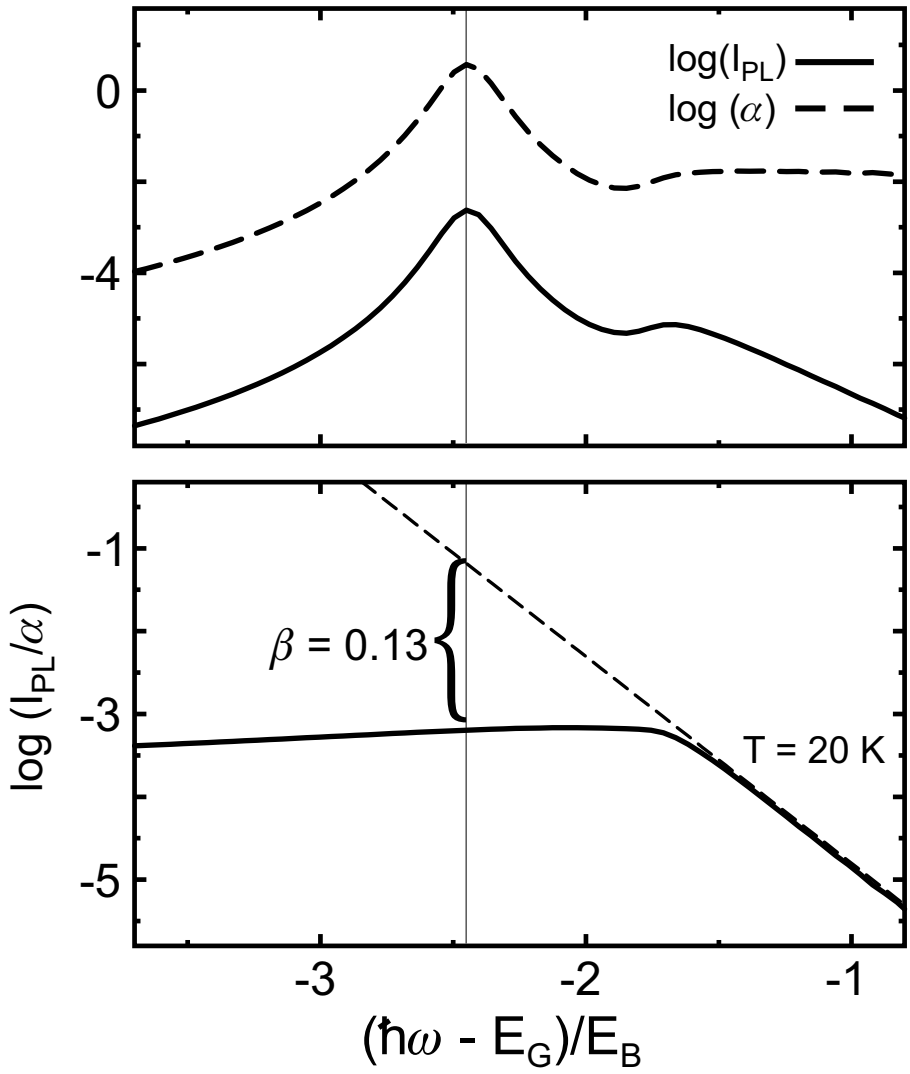

Figure 5.6: Top: Absorption and photoluminescence spectra for a computation with an initial carrier distribution of $n = 2 \times 10^4\,\mathrm{cm}^{-1}$ at 10 K in semi-logarithmic scale. Bottom: ratio I_{PL}/α between photoluminescence spectrum and absorption spectrum. The dashed line indicates a Bose-Einstein distribution of $T = 20\,\mathrm{K}$ corresponding to the temperature obtained from the high energy tail. For bosons in thermal equilibrium, the ratio should coincide with this line.

In Fig. 5.6 we investigate how important the deviations are compared to the result expected from Eq. (5.9). For the same computation as in Fig. 5.3, absorption and photoluminescence spectra in a semi-logarithmic plot are shown in the upper picture, and the ratio between both in the lower picture. According to Eq. (5.9), this ratio would have to follow the dashed line which was obtained by fitting a temperature from the high-energy tail. In contrast, we observe an emission which lies below the thermal result by a factor of $\beta = 0.13$. This value is in agreement with experiments [90] where such an attenuation factor β had

been introduced as a fitting parameter. Our theory explains β to be a fundamental physical quantity, related to the strong hole burning of excitons exposed to spontaneous emission. Due to this hole burning which is shown in Fig. 5.4, the emission according to Eq. (5.8) is typically dominated by the plasma contribution even under good formation conditions of low temperatures and low carrier densities. The nonthermal nature of the plasma contribution discussed in Sec. 4.4 leads to the deviation from the naively expected thermal emission properties.

Equation (5.8) also reveals why the Hartree-Fock approximation of the source term works well for elevated temperatures [31]. Compared to Eq. (5.7), the main effect of the population correlations is to reduce the double sum over exciton states to a single sum where only diagonal exciton correlations enter. After that, it is obvious from Eq. (5.8) that the calculated photoluminescence including the effect of exciton correlations is positive for all frequencies.

If we assume for a moment identical electron and hole temperatures, we can rewrite the singlet source, Eq. (4.30), as

$$\begin{aligned}
\langle X^\dagger_{\nu,q} X_{\nu',q} \rangle_{\mathrm{S}} &= \sum_k \phi^{\mathrm{l}}_{\nu,q}(k) \left(\phi^{\mathrm{l}}_{\nu',q}(k)\right)^* f^{\mathrm{e}}_{k+q^{\mathrm{e}}} f^{\mathrm{h}}_{k-q^{\mathrm{h}}} \\
&= \sum_k \phi^{\mathrm{r}}_{\nu,q}(k) \left(\phi^{\mathrm{l}}_{\nu',q}(k)\right)^* \frac{f^{\mathrm{e}}_{k+q^{\mathrm{e}}} f^{\mathrm{h}}_{k-q^{\mathrm{h}}}}{1 - f^{\mathrm{e}}_{k+q^{\mathrm{e}}} - f^{\mathrm{h}}_{k-q^{\mathrm{h}}}} \\
&= \sum_k \phi^{\mathrm{r}}_{\nu,q}(k) \left(\phi^{\mathrm{l}}_{\nu',q}(k)\right)^* g(E_{k,q}) \qquad (5.10)
\end{aligned}$$

with a Bose-Einstein distribution

$$g(E) = \frac{1}{e^{\frac{E-\mu}{kT}} - 1}\,, \qquad (5.11)$$

evaluated at the total kinetic energy $E_{k,q} = \frac{\hbar^2 k^2}{2\mu} + \frac{\hbar^2 q^2}{2M}$ of the electron-hole pair with the sum of the chemical potentials $\mu = \mu^{\mathrm{e}} + \mu^{\mathrm{h}}$. In the second line of Eq. (5.10), we have used a property of the exciton functions. For low temperatures, this expression confirms the nonthermal nature of the source term. For elevated temperatures, however, the Bose-Einstein distribution is sufficiently broad such that already the singlet source term can be approximated as

$$\langle X^\dagger_{\nu,q} X_{\nu',q} \rangle_{\mathrm{S}} \approx g(E_{k=0,q}) \sum_k \phi^{\mathrm{r}}_{\nu,q}(k) \left(\phi^{\mathrm{l}}_{\nu',q}(k)\right)^* = g(E_{k=0,q}) \delta_{\nu,\nu'}\,. \qquad (5.12)$$

Thus, also the pure singlet term is diagonal in the high temperature limit. As one can observe from Fig. 5.6, the Kubo-Martin-Schwinger relation is fully valid for the continuum emission.

5.3 Quantum-Well Luminescence

As we have seen in the previous section, the photoluminescence signal can very well be calculated from the Elliott formula for photoluminescence (5.8) once the source term is known. In order to simplify the further analysis and to extend our treatment to the computation of

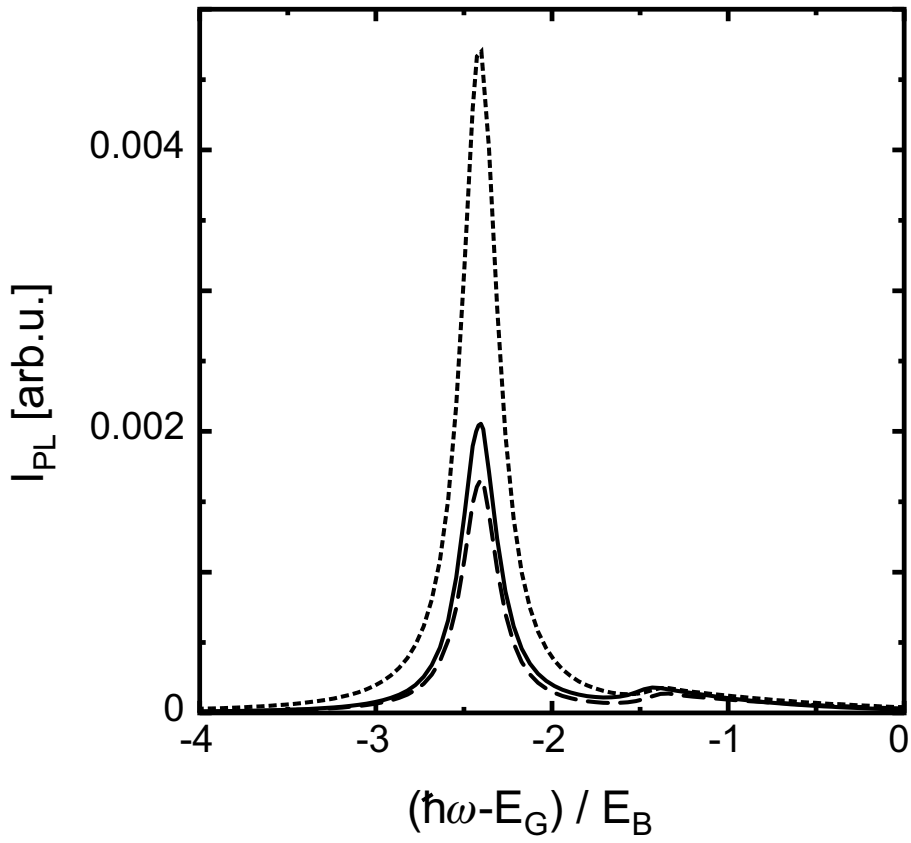

Figure 5.7: Comparison between the photoluminescence spectrum obtained from the Elliott formula (solid line) and from the full dynamical computation with spontaneous emission (dashed line) or with a suppressed spontaneous emission (dotted line). The dynamic spectra are taken after 1 ns of evolution. All calculations are performed for a carrier density of $n = 2 \times 10^4$ cm^1 and a lattice temperature of 30 K.

quantum-well photoluminescence spectra, we make use of the basic results obtained from the coupling of the semiconductor to the quantized light field: Since the dominant feature is the strong hole burning in the exciton distributions such that practically no excitons within the radiative cone are present, we assume from now on that the contribution from the exciton population correlations to the numerator of Eq. (5.8) are identical to zero. If we furthermore assume that the carrier densities are in thermal equilibrium with the lattice, we can compute photoluminescence spectra for various carrier temperatures and densities.

First, we show that these approximations are justified. In Fig. 5.7, the spectrum obtained from the Elliott formula is compared with the result of the full computation. And indeed, the Elliott formula result is in very close agreement with the case of full coupling to the quantized light field. It even overestimates the emission at the 1s resonance. But this small difference can be explained by the fact that the carrier distributions in the dynamical computation have heated up slightly such that the final carrier distributions are not exactly the ones used in the Elliott formula.

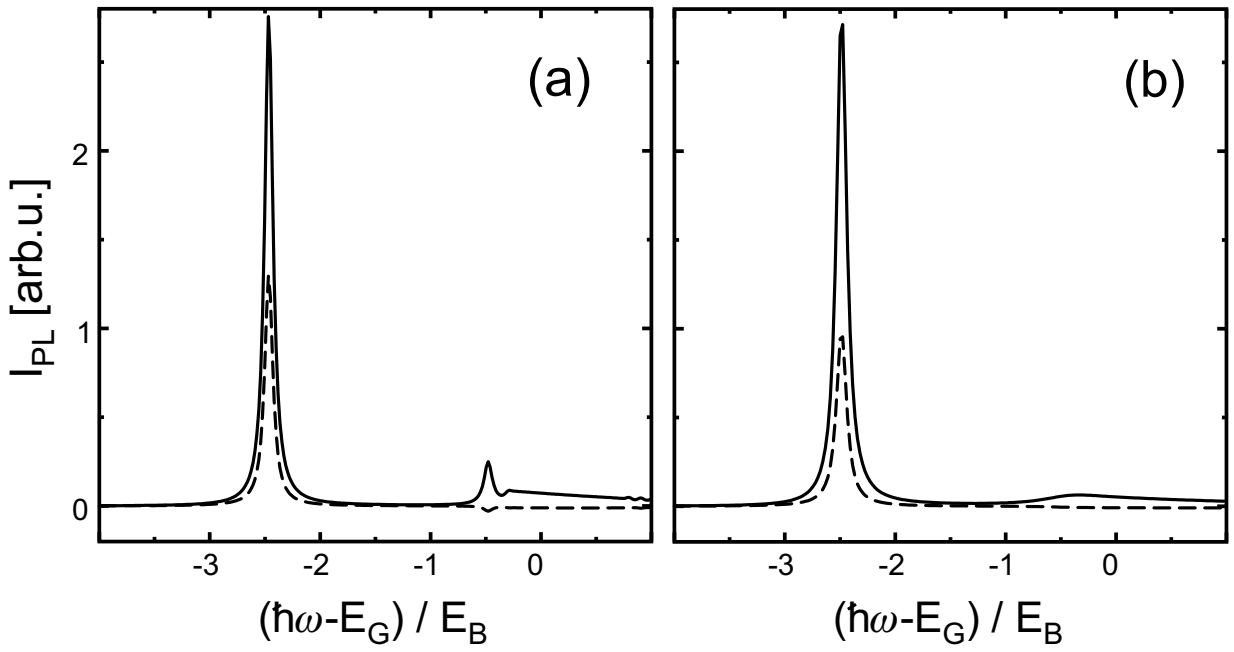

Figure 5.8: (a) Photoluminescence spectrum obtained from Eq. (5.8) for a quantum-well at a temperature of $T = 70\,\mathrm{K}$ and a carrier density of $n = 1 \times 10^9\,\mathrm{cm}^{-2}$. The full result (solid line) is compared with the computation where the total factorized part of the source term (3.60) is included (dashed line). (b) Same as (a) but with microscopic scattering contributions due to higher order Coulomb scattering.

With the same assumptions, the computation of luminescence spectra for two-dimensional quantum-well systems is now straight forward. We solve the generalized Wannier equation (C.3) in two dimensions, assume Fermi-Dirac distributions for electrons and holes and vanishing exciton population correlations, and apply Eq. (5.8) to compute the spectrum. The result is shown in Fig. 5.8(a). As in the one-dimensional case, the Elliott formula leads to a strong resonance at the 1s exciton, and also higher order excitons are still resolved with the small constant broadening γ which is used in the denominator of Eq. (5.8). A more realistic computation also includes microscopic Coulomb scattering of the photon assisted polarizations. In fact, one can generalize Eq. (C.3) to include this microscopic scattering on a level of a second Born approximation [16, 44]. In this case, no constant γ is needed and the microscopic mechanism of Coulomb scattering leads to the spectrum which is shown in Fig. 5.8(b). Whereas the 1s peak does hardly change at all, we want to point out the strong broadening of the higher order excitonic resonances. Therefore, we have to conclude that even in the so-called "linear regime" higher order excitons can already exhibit typical nonlinear behavior.

Finally, we investigate the validity of the Kubo-Martin-Schwinger relation in two dimensions. Figure 5.9 shows the result of a computation with the same parameters as in Fig. 5.8. As in the one-dimensional case (see Fig. 5.6), one obtains a very strong suppression of the 1s luminescence peak compared to the result expected from simple thermodynamic

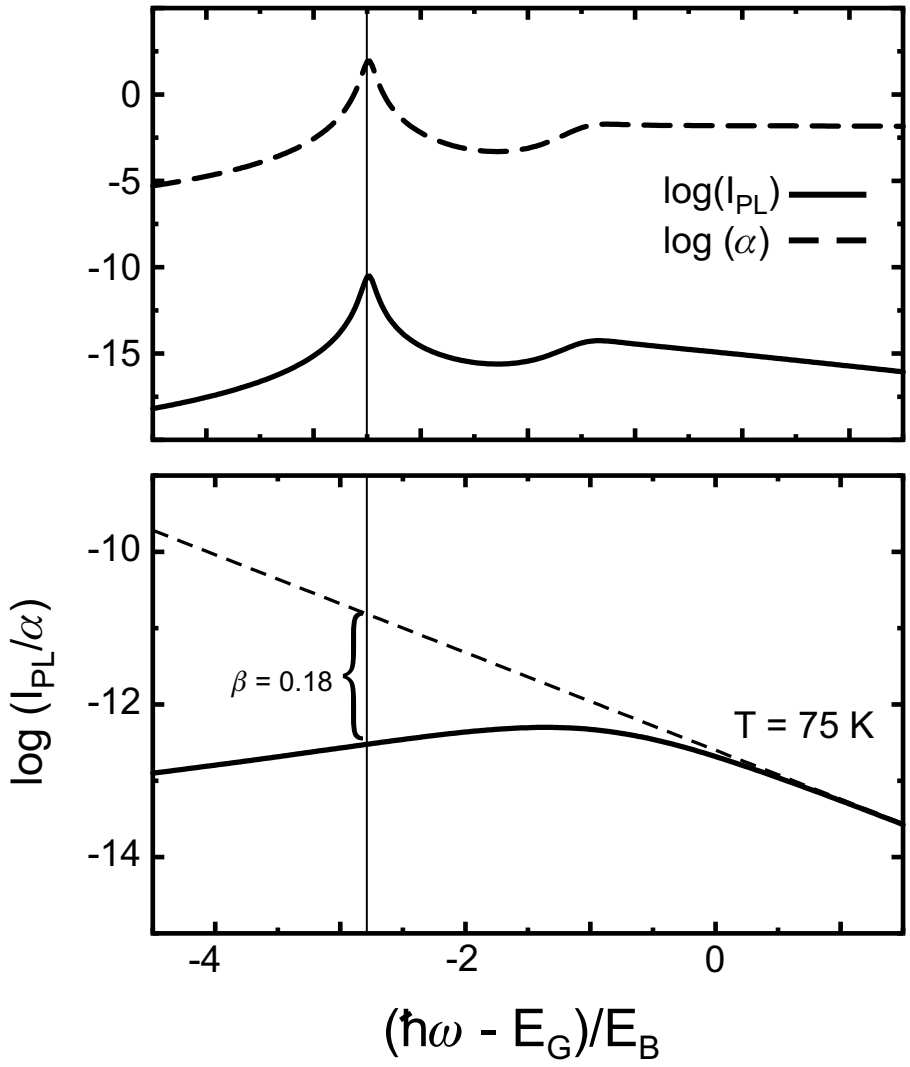

Figure 5.9: Analogous Figure to Fig. 5.6, but now computed for a quantum-well system computed for the same parameters as in Fig. 5.8.

arguments. Therefore, we must conclude that the nonequilibrium character of photoluminescence in the sense of a violation of the Kubo-Martin-Schwinger relation also holds in two dimensions. It is a challenge of the near future to measure time resolved absorption and emission spectra very precisely, using the same setup, in order to confirm these predictions experimentally.

6 Conclusion and Outlook

This thesis work presents the latest development on a microscopic theory which can be applied to study a variety of interesting many-body and quantum-optical problems in semiconductors. The main focus has been to include the full dynamics of the many-body system of a semiconductor with all its Coulomb correlated charge carriers and its coupling to a quantized electromagnetic field (photons) and to lattice vibrations (phonons).

The presented theoretical approach modifies the concept of the cluster expansion which is used in quantum chemistry in order to approximate the full electronic wave function of complicated atoms or molecules. There, the basic idea is to separate the many-electron wave function into parts consisting of uncorrelated carriers, clusters consisting of correlated doublets, triplets, and so forth. In a semiconductor, the same idea is applied to the density matrix of the interacting carrier-photon-phonon system. While the coupling of electrons to photons or phonons leads to a similar hierarchy problem as known from the Coulomb interaction, the cluster expansion scheme introduces the possibility to truncate the resulting infinite hierarchy of coupled differential equations in a controlled and physically meaningful way. Due to the formal correspondence of one photon (phonon) operator to a product of two electron operators, the truncation scheme provides the basis for the simultaneous consistent treatment not only of the many-body Coulomb correlations but also of the mixed carrier-photon (phonon) correlations. Hence, carrier, photon, and phonon correlations are treated on the same microscopic level. The resulting system of coupled differential equations is numerically highly demanding. Even with today's supercomputers, the full solution including all correlations up to the level of correlated pairs is numerically feasible only for a one-dimensional model system .

As a first application, the exciton formation out of a totally incoherent electron-hole plasma has been investigated for such a one-dimensional model system. The analysis determines carrier densities and lattice temperatures favorable for the formation of excitons. Even for cold lattices of around 10 K, exciton formation times of the order of nanoseconds have been obtained. The interesting interplay between diagonal exciton population correlations and off-diagonal transition correlations has been investigated in detail. While the diagonal population correlations can often be interpreted as exciton numbers, the off-diagonal transition correlations are shown to be crucial for the formation of excitons under incoherent conditions.

In the second part, the theory has been applied to describe photoluminescence properties of a semiconductor heterostructure. In addition to the full numerical solution, we have

derived the *Elliott Formula for Photoluminescence*

$$I_{\mathrm{PL}}(\omega_{\mathbf{q}}) = -\mathrm{Im}\left[\sum_{\nu} \mathcal{A}_{\nu,\mathbf{q}} \frac{N_{\mathrm{S}}(\nu,q) + \Delta N(\nu,q)}{\hbar\omega_{\mathbf{q}} - E_{\mathrm{G}} - E_{\nu,q} + i\gamma}\right] ,$$

in direct analogy to the famous Elliott formula for absorption. This formula summarizes the key aspects of semiconductor photoluminescence: i) The source of photoluminescence always consists of a sum of two terms, ΔN and N_{S}, where ΔN is related to genuine incoherent exciton populations and N_{S} corresponds to a Coulomb correlated electron-hole plasma. These two sources cannot be distinguished in a standard photoluminescence experiment such that one cannot determine whether or not the luminescence is due to exciton correlations because the spectrum will always exhibit distinct excitonic resonances, as shown by the energy denominator. This simply reflects the fact that the emission process itself is Coulomb correlated. In fact, even under good formation conditions most excitons are "dark" excitons with a momentum too large to be transferred to a photon. These excitons cannot directly emit light and must first be scattered into the radiative cone. Therefore, photoluminescence is often dominated by the contribution from the electron-hole plasma, which explains why simplistic assumptions about excitons in thermal equilibrium must fail when describing photoluminescence measurements.

The investigations of this thesis focus on the incoherent regime, where all calculations are started with completely uncorrelated carrier densities, and study the formation of excitons and the light emission under these conditions. A very promising task for the near future is to describe the full excitation process with its transition from the coherent to the incoherent regime also on a microscopic level. In order to do so, a large number of additional coherent four-point correlations must be evaluated. Also the description of the phonons should be improved and at least include optical phonons which play an important role in the early cooling of hot carrier distributions. Such an extended analysis could give valuable information of how the transition to the incoherent regime takes place, what amount of incoherent excitons can be created during the first picoseconds after the exciting pulse, and how this fraction depends on the detailed excitation conditions.

Another goal for the future is to use the same method in order to address more quantum-optical questions. Due to the large variety of possible interaction processes, many interesting results are to be expected. As far as the investigation of true quantum properties of light in semiconductors is concerned, we are just at the beginning of a promising scientific future.

A General Set of Equations of Motion

A semiconductor is a true many-body system with a vast number of Coulomb interacting carriers. Most physical quantities of interest, in contrast, are one or two-particle quantities. For example, the kinetic energies of carriers, the carrier densities themselves, or the coherent polarization are examples for one-particle quantities; the Coulomb energy or pair-correlations between charge carriers are examples of a two-particle interaction. In the language of second quantization, the one-particle quantities can be obtained from expectation values of the form $\langle a^\dagger_{\lambda_1,k_1} a_{\lambda_2,k_2}\rangle$ involving only one pair of creation and destruction operators. Hence, they are often referred to as two-point quantities. For the computation of a two-particle quantity, the knowledge of true four-point quantities of the form $\langle a^\dagger_{\lambda_1,k_1} a^\dagger_{\lambda_2,k_2} a_{\lambda_3,k_3} a_{\lambda_4,k_4}\rangle$ is necessary.

A widespread theoretical approach is to compute equations of motion for matrix elements of the reduced density matrix. In all interacting systems, this method inevitably introduces an infinite hierarchy of equations which has to be suitably truncated to a level which is numerically solvable. In this Appendix, we derive the complete set of equations for the interacting carrier-photon-phonon system up to the two-particle level according to Sec. 3.2. This set of equations can be used to derive the incoherent equations from Chapter 3. It is by far more general, though, and can also serve as a starting point for future investigations of quantum-optical properties of semiconductors.

A.1 Two-Body Carrier Interaction

General starting point for the investigation of the Coulomb interaction, Eq. (2.8), or the dipole self-energy, Eq. (2.46), is a Hamiltonian of the form

$$H_{\mathrm{C/dip}} = \frac{1}{2}\sum_{\nu,\mu}\sum_{l,l',q'\neq 0} f_{q'}\, a^\dagger_{\mu,l} a^\dagger_{\nu,l'} a_{\bar{\nu},l'+q'} a_{\bar{\mu},l-q'} \,. \tag{A.1}$$

Here, ν and μ denote the different bands and are assumed to be either c or v. In principle, it is straightforward to include also different spins. In the case of the Coulomb interaction, f_q denotes the Coulomb matrix element and the band $\bar{\mu}$ is equal to the band μ as can be seen by comparison to Eq. (2.8). More details about the Coulomb matrix element V_q are given in appendix E. For the dipole self-interaction, the comparison to Eq. (2.46) determines the coupling strength $f_q = \frac{\bar{g}|d_q|^2}{\epsilon_0 n^2 \mathcal{L}^d}$ and the definition of $\bar{\mu}$ as $\bar{c}(\bar{v}) = v(c)$.

The basic equation of motion is the operator equation for a single annihilation operator

given by

$$\left[i\hbar\frac{\partial}{\partial t}a_{\lambda,k}\right]_{H_{\mathrm{C/dip}}} = [a_{\lambda,k}, H_{\mathrm{C/dip}}] = \sum_{\nu,l,q} f_q\, a^\dagger_{\nu,l} a_{\bar{\nu},l+q} a_{\bar{\lambda},k-q}\,. \tag{A.2}$$

Together with the Hermitian conjugate operator dynamics

$$\left[i\hbar\frac{\partial}{\partial t}a^\dagger_{\lambda,k}\right]_{H_{\mathrm{C/dip}}} = (-1)\sum_{\nu,l,q} f_q\, a^\dagger_{\bar{\lambda},k-q} a^\dagger_{\bar{\nu},l+q} a_{\nu,l}\,, \tag{A.3}$$

we can easily derive the equation of motion for a general one particle (i.e. 2-point) operator $a^\dagger_{\lambda,k}a_{\tilde{\lambda},k+q}$. Using Eqs. (A.2) and (A.3), we obtain

$$\begin{aligned}\left[i\hbar\frac{\partial}{\partial t}a^\dagger_{\lambda,k}a_{\tilde{\lambda},k+q}\right]_{H_{\mathrm{C/dip}}} &= \sum_{\nu,l,q'} f_{q'}\, a^\dagger_{\lambda,k} a^\dagger_{\nu,l} a_{\bar{\nu},l+q'} a_{\bar{\tilde{\lambda}},k+q-q'} \\ &\quad - \sum_{\nu,l,q'} f_{q'}\, a^\dagger_{\bar{\lambda},k-q'} a^\dagger_{\bar{\nu},l+q'} a_{\nu,l} a_{\tilde{\lambda},k+q}\,.\end{aligned} \tag{A.4}$$

This operator equation can be used to directly compute the equations of motion for the single particle expectation values as electron and hole densities and interband polarizations. Equally well we can use the equation in order to derive the equations of motion for two-particle expectation values and photon- or phonon assisted one-particle variables.

For the relevant one-particle correlations we define

$$P^{\lambda,\tilde{\lambda}}_k = \langle a^\dagger_{\lambda,k} a_{\tilde{\lambda},k}\rangle\,, \tag{A.5}$$

where we assume that an incident laser pulse homogeneously excites the disorderless sample in normal direction. In that case, only diagonal two-point quantities with equal k-index as defined in Eq. (A.5) can be non-vanishing. The resulting equation of motion for $P^{\lambda,\tilde{\lambda}}_k$ is given by

$$\begin{aligned}\left[i\hbar\frac{\partial}{\partial t}P^{\lambda,\tilde{\lambda}}_k\right]_{H_{\mathrm{C/dip}}} &= \sum_{\nu,l,q'} f_{q'}\, \left(\langle a^\dagger_{\lambda,k} a^\dagger_{\nu,l} a_{\bar{\nu},l+q'} a_{\bar{\tilde{\lambda}},k-q'}\rangle - \langle a^\dagger_{\bar{\lambda},k-q'} a^\dagger_{\bar{\nu},l+q'} a_{\nu,l} a_{\tilde{\lambda},k}\rangle\right) \\ &= \sum_{\nu,l} f_0\, \left(P^{\lambda,\bar{\tilde{\lambda}}}_k - P^{\bar{\lambda},\tilde{\lambda}}_k\right) P^{\nu,\bar{\nu}}_l + \sum_{\nu,q'} f_{q'}\, \left(P^{\bar{\lambda},\nu}_{k-q'} P^{\bar{\nu},\tilde{\lambda}}_k - P^{\lambda,\bar{\nu}}_k P^{\nu,\bar{\tilde{\lambda}}}_{k-q'}\right) \\ &\quad + \sum_{\nu,l,q'} f_{q'}\, \left(\Delta\langle a^\dagger_{\lambda,k} a^\dagger_{\nu,l} a_{\bar{\nu},l+q'} a_{\bar{\tilde{\lambda}},k-q'}\rangle - \Delta\langle a^\dagger_{\bar{\lambda},k-q'} a^\dagger_{\bar{\nu},l+q'} a_{\nu,l} a_{\tilde{\lambda},k}\rangle\right)\,,\end{aligned} \tag{A.6}$$

where we have used the expansion in terms of correlations as discussed in Sec. 3.2. The term proportional to f_0 is only present for the dipole self-energy. In the case of Coulomb interaction, the respective term is canceled against the Coulomb contribution of the positive background.

The first quantities formally equivalent to four-point terms are photon- or phonon assisted two-point correlations which are obtained as

$$\begin{aligned}
\left[i\hbar\frac{\partial}{\partial t}\Delta\langle O^\dagger_{q_\perp,q}a^\dagger_{\lambda,k}a_{\tilde{\lambda},k+q}\rangle\right]_{H_{\mathrm{C/dip}}} &= \left[i\hbar\frac{\partial}{\partial t}\langle O^\dagger_{q_\perp,q}a^\dagger_{\lambda,k}a_{\tilde{\lambda},k+q}\rangle\right]_{H_{\mathrm{C/dip}},q\neq 0}\\
&= \sum_{\nu,l,q'} f_{q'}\Big(\langle O^\dagger_{q_\perp,q}a^\dagger_{\lambda,k}a^\dagger_{\nu,l}a_{\bar{\nu},l+q'}a_{\bar{\tilde{\lambda}},k+q-q'}\rangle\Big|_{q\neq 0}\\
&\qquad -\langle O^\dagger_{q_\perp,q}a^\dagger_{\bar{\lambda},k-q'}a^\dagger_{\bar{\nu},l+q'}a_{\nu,l}a_{\tilde{\lambda},k+q}\rangle\Big|_{q\neq 0}\Big)\\
&= f_0\left(\sum_{\nu,l}P^{\nu,\bar{\nu}}_l\right)\left(\Delta\langle O^\dagger_{q_\perp,q}a^\dagger_{\lambda,k}a_{\bar{\tilde{\lambda}},k+q}\rangle - \Delta\langle O^\dagger_{q_\perp,q}a^\dagger_{\bar{\lambda},k}a_{\tilde{\lambda},k+q}\rangle\right)\\
&+f_q\left(\sum_{\nu,l}\Delta\langle O^\dagger_{q_\perp,q}a^\dagger_{\nu,l}a_{\bar{\nu},l+q}\rangle\right)\left(P^{\lambda,\bar{\tilde{\lambda}}}_k - P^{\bar{\lambda},\tilde{\lambda}}_{k+q}\right)\\
&+\sum_\nu\left(\sum_{q'}f_{q'}\,\Delta\langle O^\dagger_{q_\perp,q}a^\dagger_{\bar{\tilde{\lambda}},k-q'}a_{\nu,k+q-q'}\rangle\right)P^{\bar{\nu},\tilde{\lambda}}_{k+q}\\
&-\sum_\nu\left(\sum_{q'}f_{q'}\Delta\langle O^\dagger_{q_\perp,q}a^\dagger_{\nu,k-q'}a_{\bar{\tilde{\lambda}},k+q-q'}\rangle\right)P^{\lambda,\bar{\nu}}_k\\
&-\sum_\nu\left(\sum_{q'}f_{q'}P^{\nu,\bar{\tilde{\lambda}}}_{k+q-q'}\right)\Delta\langle O^\dagger_{q_\perp,q}a^\dagger_{\lambda,k}a_{\bar{\nu},k+q}\rangle\\
&+\sum_\nu\left(\sum_{q'}f_{q'}\,P^{\bar{\lambda},\nu}_{k-q'}\right)\Delta\langle O^\dagger_{q_\perp,q}a^\dagger_{\bar{\nu},k}a_{\tilde{\lambda},k+q}\rangle. \qquad (A.7)
\end{aligned}$$

In this derivation, we use the fact that the correlated part $\Delta\langle O^\dagger_{q_\perp,q}a^\dagger_{\lambda,k}a_{\tilde{\lambda},k+q}\rangle$ is equal to the full correlation $\langle O^\dagger_{q_\perp,q}a^\dagger_{\lambda,k}a_{\tilde{\lambda},k+q}\rangle$ for all index combinations except for $q=0$. By deriving the equation of motion for the full correlation under the restriction $q\neq 0$, we thus directly obtain the equation for the pure correlated part.

The most tedious four-point term is the product of four Fermion operators. Here, we get

$$\begin{aligned}
\left[i\hbar\frac{\partial}{\partial t}\Delta\langle a^\dagger_{\lambda,k}a^\dagger_{\lambda',k'}a_{\tilde{\lambda}',k'+q}a_{\tilde{\lambda},k-q}\rangle\right]_{H_{\mathrm{C/dip}}} &= \left[i\hbar\frac{\partial}{\partial t}\Delta\langle a^\dagger_{\lambda,k}a_{\tilde{\lambda},k-q}a^\dagger_{\lambda',k'}a_{\tilde{\lambda}',k'+q}\rangle\right]_{H_{\mathrm{C/dip}}}\\
&= \sum_{\nu,l,q'}f_{q'}\,\langle a^\dagger_{\lambda,k}a^\dagger_{\nu,l}a_{\bar{\nu},l+q'}a_{\bar{\tilde{\lambda}},k-q-q'}a^\dagger_{\lambda',k'}a_{\tilde{\lambda}',k'+q}\rangle\Big|_{q,k'+q-k\neq 0}\\
&\quad -\sum_{\nu,l,q'}f_{q'}\,\langle a^\dagger_{\bar{\lambda},k-q'}a^\dagger_{\bar{\nu},l+q'}a_{\nu,l}a_{\tilde{\lambda},k-q}a^\dagger_{\lambda',k'}a_{\tilde{\lambda}',k'+q}\rangle\Big|_{q,k'+q-k\neq 0}\\
&\quad +\sum_{\nu,l,q'}f_{q'}\,\langle a^\dagger_{\lambda,k}a_{\tilde{\lambda},k-q}a^\dagger_{\lambda',k'}a^\dagger_{\nu,l}a_{\bar{\nu},l+q'}a_{\bar{\tilde{\lambda}}',k'+q-q'}\rangle\Big|_{q,k'+q-k\neq 0}
\end{aligned}$$

$$- \sum_{\nu,l,q'} f_{q'} \left\langle a^\dagger_{\lambda,k} a_{\tilde{\lambda},k-q} a^\dagger_{\bar{\tilde{\lambda}}',k'-q'} a^\dagger_{\bar{\nu},l+q'} a_{\nu,l} a_{\tilde{\lambda}',k'+q} \right\rangle \Big|_{q,k'+q-k\neq 0} . \tag{A.8}$$

Again, this result can be used to obtain the equation of motion for the correlated part, if in the expansion of Eq. (A.8) in terms of singlets and doublets we neglect all possible combinations with $q = 0$ or $k' + q - k = 0$. Examining the different parts of Eq. (A.8) one by one and factorizing it under these restrictions, we obtain the singlet contribution

$$\begin{aligned}
&\sum_{\nu,l,q'} f_{q'} \left\langle a^\dagger_{\lambda,k} a^\dagger_{\nu,l} a_{\bar{\nu},l+q'} a_{\bar{\tilde{\lambda}},k-q-q'} a^\dagger_{\lambda',k'} a_{\tilde{\lambda}',k'+q} \right\rangle_{\mathrm{S}} = \\
&\qquad \sum_{\nu} \left[f_q P^{\lambda,\bar{\tilde{\lambda}}}_k \left(\delta_{\lambda',\bar{\nu}} - P^{\lambda',\bar{\nu}}_{k'} \right) - f_{k-q-k'} P^{\lambda,\bar{\nu}}_k \left(\delta_{\lambda',\bar{\tilde{\lambda}}} - P^{\lambda',\bar{\tilde{\lambda}}}_{k'} \right) \right] P^{\nu,\tilde{\lambda}'}_{k'+q} , \\
&\sum_{\nu,l,q'} f_{q'} \left\langle a^\dagger_{\bar{\tilde{\lambda}},k-q'} a^\dagger_{\bar{\nu},l+q'} a_{\nu,l} a_{\tilde{\lambda},k-q} a^\dagger_{\lambda',k'} a_{\tilde{\lambda}',k'+q} \right\rangle_{\mathrm{S}} = \\
&\qquad \sum_{\nu} \left[f_q P^{\bar{\lambda},\tilde{\lambda}}_{k-q} P^{\bar{\nu},\tilde{\lambda}'}_{k'+q} - f_{k-q-k'} P^{\bar{\lambda},\tilde{\lambda}'}_{k'+q} P^{\bar{\nu},\tilde{\lambda}}_{k-q} \right] \left(\delta_{\lambda',\nu} - P^{\lambda',\nu}_{k'} \right) , \\
&\sum_{\nu,l,q'} f_{q'} \left\langle a^\dagger_{\lambda,k} a_{\tilde{\lambda},k-q} a^\dagger_{\lambda',k'} a^\dagger_{\nu,l} a_{\bar{\nu},l+q'} a_{\bar{\tilde{\lambda}}',k'+q-q'} \right\rangle_{\mathrm{S}} = \\
&\qquad \sum_{\nu} \left[f_q P^{\lambda,\bar{\nu}}_k P^{\lambda',\bar{\tilde{\lambda}}'}_{k'} - f_{k'+q-k} P^{\lambda,\bar{\tilde{\lambda}}'}_k P^{\lambda',\bar{\nu}}_{k'} \right] \left(\delta_{\nu,\tilde{\lambda}} - P^{\nu,\tilde{\lambda}}_{k-q} \right) , \\
&\sum_{\nu,l,q'} f_{q'} \left\langle a^\dagger_{\lambda,k} a_{\tilde{\lambda},k-q} a^\dagger_{\bar{\tilde{\lambda}}',k'-q'} a^\dagger_{\bar{\nu},l+q'} a_{\nu,l} a_{\tilde{\lambda}',k'+q} \right\rangle_{\mathrm{S}} = \\
&\qquad \sum_{\nu} \left[f_q \left(\delta_{\bar{\nu},\tilde{\lambda}} - P^{\bar{\nu},\tilde{\lambda}}_{k-q} \right) P^{\bar{\tilde{\lambda}}',\tilde{\lambda}'}_{k'+q} - f_{k'+q-k} \left(\delta_{\bar{\tilde{\lambda}}',\tilde{\lambda}} - P^{\bar{\tilde{\lambda}}',\tilde{\lambda}}_{k-q} \right) P^{\bar{\nu},\tilde{\lambda}'}_{k'+q} \right] P^{\lambda,\nu}_k .
\end{aligned} \tag{A.9}$$

If we insert the last four equations into Eq. (A.8) we obtain the complete singlet contributions to the equation of motion

$$\begin{aligned}
&\left[i\hbar \frac{\partial}{\partial t} \Delta \langle a^\dagger_{\lambda,k} a^\dagger_{\lambda',k'} a_{\tilde{\lambda}',k'+q} a_{\tilde{\lambda},k-q} \rangle \right]_{H_{\mathrm{C/dip}},\mathrm{S}} = \\
&\quad f_q \left(P^{\lambda,\bar{\tilde{\lambda}}}_k P^{\lambda',\bar{\tilde{\lambda}}'}_{k'} - P^{\bar{\lambda}',\tilde{\lambda}'}_{k'+q} P^{\bar{\lambda},\tilde{\lambda}}_{k-q} \right) - f_{k-q-k'} \left(P^{\lambda,\bar{\tilde{\lambda}}'}_k P^{\lambda',\bar{\tilde{\lambda}}}_{k'} - P^{\bar{\lambda},\tilde{\lambda}'}_{k'+q} P^{\bar{\lambda}',\tilde{\lambda}}_{k-q} \right) \\
&\quad + \sum_{\nu} f_{k-q-k'} \left[\left(P^{\lambda',\bar{\tilde{\lambda}}}_{k'} - P^{\bar{\lambda}',\tilde{\lambda}}_{k-q} \right) P^{\lambda,\bar{\nu}}_k P^{\nu,\tilde{\lambda}'}_{k'+q} + \left(P^{\lambda,\bar{\tilde{\lambda}}'}_k - P^{\bar{\lambda},\tilde{\lambda}'}_{k'+q} \right) P^{\bar{\nu},\tilde{\lambda}}_{k-q} P^{\lambda',\nu}_{k'} \right] \\
&\quad - \sum_{\nu} f_q \left[\left(P^{\lambda,\bar{\tilde{\lambda}}}_k - P^{\bar{\lambda},\tilde{\lambda}}_{k-q} \right) P^{\lambda',\bar{\nu}}_{k'} P^{\nu,\tilde{\lambda}'}_{k'+q} + \left(P^{\lambda',\bar{\tilde{\lambda}}'}_{k'} - P^{\bar{\lambda}',\tilde{\lambda}'}_{k'+q} \right) P^{\lambda,\bar{\nu}}_k P^{\nu,\tilde{\lambda}}_{k-q} \right] .
\end{aligned} \tag{A.10}$$

In the same way, all doublet contributions from Eq. (A.8) must be collected. If we treat the terms one after the other, we obtain

$$\begin{aligned}
&\sum_{\nu,l,q'} f_{q'} \left\langle a^\dagger_{\lambda,k} a^\dagger_{\nu,l} a_{\bar{\nu},l+q'} a_{\bar{\tilde{\lambda}},k-q-q'} a^\dagger_{\lambda',k'} a_{\tilde{\lambda}',k'+q} \right\rangle_{\mathrm{D}} = \\
&\qquad f_0 \left(\sum_{\nu,l} P^{\nu,\bar{\nu}}_l \right) \Delta \langle a^\dagger_{\lambda,k} a^\dagger_{\lambda',k'} a_{\tilde{\lambda}',k'+q} a_{\bar{\tilde{\lambda}},k-q} \rangle
\end{aligned}$$

$$
\begin{aligned}
&+ f_q P_k^{\lambda,\bar{\tilde{\lambda}}} \left(\sum_{\nu,l} \Delta \langle a^\dagger_{\nu,l} a^\dagger_{\lambda',k'} a_{\tilde{\lambda}',k'+q} a_{\bar{\nu},l-q} \rangle \right) \\
&+ f_{k-q-k'} \left(\delta_{\lambda',\bar{\tilde{\lambda}}} - P_{k'}^{\lambda',\bar{\tilde{\lambda}}} \right) \left(\sum_{\nu,l} \Delta \langle a^\dagger_{\lambda,k} a^\dagger_{\nu,l} a_{\bar{\nu},l+k-q-k'} a_{\tilde{\lambda}',k'+q} \rangle \right) \\
&- \sum_{\nu} \left(\sum_{q'} f_{k-q-q'} P_{q'}^{\nu,\bar{\tilde{\lambda}}} \right) \Delta \langle a^\dagger_{\lambda,k} a^\dagger_{\lambda',k'} a_{\tilde{\lambda}',k'+q} a_{\bar{\nu},k-q} \rangle \\
&- \sum_{\nu} P_k^{\lambda,\bar{\nu}} \left(\sum_{q'} f_{q'} \Delta \langle a^\dagger_{\nu,k-q'} a^\dagger_{\lambda',k'} a_{\tilde{\lambda}',k'+q} a_{\bar{\tilde{\lambda}},k-q-q'} \rangle \right) \\
&- \sum_{\nu} P_{k'+q}^{\nu,\tilde{\lambda}'} \left(\sum_{q'} f_{q'} \Delta \langle a^\dagger_{\lambda,k} a^\dagger_{\lambda',k'} a_{\bar{\nu},k'+q+q'} a_{\bar{\tilde{\lambda}},k-q-q'} \rangle \right) \\
&- \sum_{\nu} P_{k'}^{\lambda',\bar{\nu}} \left(\sum_{q'} f_{q'} \Delta \langle a^\dagger_{\lambda,k} a^\dagger_{\nu,k'-q'} a_{\tilde{\lambda}',k'+q} a_{\bar{\tilde{\lambda}},k-q-q'} \rangle \right) \\
&+ \sum_{q'} f_{q'} \Delta \langle a^\dagger_{\lambda,k} a^\dagger_{\tilde{\lambda}',k'-q'} a_{\tilde{\lambda}',k'+q} a_{\bar{\tilde{\lambda}},k-q-q'} \rangle \,,
\end{aligned}
\tag{A.11}
$$

$$
\sum_{\nu,l,q'} f_{q'} \langle a^\dagger_{\bar{\tilde{\lambda}},k-q'} a^\dagger_{\bar{\nu},l+q'} a_{\nu,l} a_{\tilde{\lambda},k-q} a^\dagger_{\lambda',k'} a_{\tilde{\lambda}',k'+q} \rangle_{\mathrm{D}} =
$$

$$
\begin{aligned}
&f_0 \left(\sum_{\nu,l} P_l^{\nu,\bar{\nu}} \right) \Delta \langle a^\dagger_{\bar{\tilde{\lambda}},k} a^\dagger_{\lambda',k'} a_{\tilde{\lambda}',k'+q} a_{\tilde{\lambda},k-q} \rangle \\
&+ f_q P_{k-q}^{\bar{\tilde{\lambda}},\tilde{\lambda}} \left(\sum_{\nu,l} \Delta \langle a^\dagger_{\bar{\nu},l} a^\dagger_{\lambda',k'} a_{\tilde{\lambda}',k'+q} a_{\nu,l-q} \rangle \right) \\
&- f_{k-q-k'} P_{k'+q}^{\bar{\tilde{\lambda}},\tilde{\lambda}'} \left(\sum_{\nu,l} \Delta \langle a^\dagger_{\lambda',k'} a^\dagger_{\nu,l} a_{\bar{\nu},l+k'+q-k} a_{\tilde{\lambda},k-q} \rangle \right) \\
&- \sum_{\nu} \left(\sum_{q'} f_{k-q'} P_{q'}^{\bar{\tilde{\lambda}},\nu} \right) \Delta \langle a^\dagger_{\bar{\nu},k} a^\dagger_{\lambda',k'} a_{\tilde{\lambda}',k'+q} a_{\tilde{\lambda},k-q} \rangle \\
&- \sum_{\nu} P_{k-q}^{\bar{\nu},\tilde{\lambda}} \left(\sum_{q'} f_{q'} \Delta \langle a^\dagger_{\bar{\tilde{\lambda}},k-q'} a^\dagger_{\lambda',k'} a_{\tilde{\lambda}',k'+q} a_{\nu,k-q-q'} \rangle \right) \\
&- \sum_{\nu} P_{k'+q}^{\bar{\nu},\tilde{\lambda}'} \left(\sum_{q'} f_{q'} \Delta \langle a^\dagger_{\bar{\tilde{\lambda}},k-q'} a^\dagger_{\lambda',k'} a_{\nu,k'+q-q'} a_{\tilde{\lambda},k-q} \rangle \right) \\
&- \sum_{\nu} P_{k'}^{\lambda',\nu} \left(\sum_{q'} f_{q'} \Delta \langle a^\dagger_{\bar{\tilde{\lambda}},k-q'} a^\dagger_{\bar{\nu},k'+q'} a_{\tilde{\lambda}',k'+q} a_{\tilde{\lambda},k-q} \rangle \right)
\end{aligned}
$$

$$+ \sum_{q'} f_{q'} \Delta \langle a^\dagger_{\tilde{\lambda},k-q'} a^\dagger_{\tilde{\lambda}',k'+q'} a_{\tilde{\lambda}',k'+q} a_{\tilde{\lambda},k-q} \rangle \,, \tag{A.12}$$

$$\begin{aligned}
&\sum_{\nu,l,q'} f_{q'} \, \langle a^\dagger_{\lambda,k} a_{\tilde{\lambda},k-q} a^\dagger_{\lambda',k'} a^\dagger_{\nu,l} a_{\bar{\nu},l+q'} a_{\bar{\tilde{\lambda}}',k'+q-q'} \rangle_{\mathrm{D}} = \\
&\qquad f_0 \left(\sum_{\nu,l} P^{\nu,\bar{\nu}}_{l} \right) \Delta \langle a^\dagger_{\lambda,k} a^\dagger_{\lambda',k'} a_{\bar{\tilde{\lambda}}',k'+q} a_{\tilde{\lambda},k-q} \rangle \\
&+ f_q P^{\lambda',\bar{\tilde{\lambda}}'}_{k'} \left(\sum_{\nu,l} \Delta \langle a^\dagger_{\lambda,k} a^\dagger_{\nu,l} a_{\bar{\nu},l+q} a_{\tilde{\lambda},k-q} \rangle \right) \\
&- f_{k'+q-k} P^{\lambda,\bar{\tilde{\lambda}}'}_{k} \left(\sum_{\nu,l} \Delta \langle a^\dagger_{\lambda',k'} a^\dagger_{\nu,l} a_{\bar{\nu},l+k'+q-k} a_{\tilde{\lambda},k-q} \rangle \right) \\
&- \sum_{\nu} \left(\sum_{q'} f_{k'+q-q'} P^{\nu,\bar{\tilde{\lambda}}'}_{q'} \right) \Delta \langle a^\dagger_{\lambda,k} a^\dagger_{\lambda',k'} a_{\bar{\nu},k'+q} a_{\tilde{\lambda},k-q} \rangle \\
&- \sum_{\nu} P^{\lambda,\bar{\nu}}_{k} \left(\sum_{q'} f_{q'} \Delta \langle a^\dagger_{\nu,k-q'} a^\dagger_{\lambda',k'} a_{\bar{\tilde{\lambda}}',k'+q-q'} a_{\tilde{\lambda},k-q} \rangle \right) \\
&- \sum_{\nu} P^{\lambda',\bar{\nu}}_{k'} \left(\sum_{q'} f_{q'} \Delta \langle a^\dagger_{\lambda,k} a^\dagger_{\nu,k'-q'} a_{\bar{\tilde{\lambda}}',k'+q-q'} a_{\tilde{\lambda},k-q} \rangle \right) \\
&- \sum_{\nu} P^{\nu,\tilde{\lambda}}_{k-q} \left(\sum_{q'} f_{q'} \Delta \langle a^\dagger_{\lambda,k} a^\dagger_{\lambda',k'} a_{\bar{\tilde{\lambda}}',k'+q-q'} a_{\bar{\nu},k-q+q'} \rangle \right) \\
&+ \sum_{q'} f_{q'} \Delta \langle a^\dagger_{\lambda,k} a^\dagger_{\lambda',k'} a_{\bar{\tilde{\lambda}}',k'+q-q'} a_{\bar{\tilde{\lambda}},k-q+q'} \rangle \,,
\end{aligned} \tag{A.13}$$

$$\begin{aligned}
&\sum_{\nu,l,q'} f_{q'} \, \langle a^\dagger_{\lambda,k} a_{\tilde{\lambda},k-q} a^\dagger_{\tilde{\lambda}',k'-q'} a^\dagger_{\bar{\nu},l+q'} a_{\nu,l} a_{\tilde{\lambda}',k'+q} \rangle_{\mathrm{D}} = \\
&\qquad f_0 \left(\sum_{\nu,l} P^{\nu,\bar{\nu}}_{l} \right) \Delta \langle a^\dagger_{\lambda,k} a^\dagger_{\tilde{\lambda}',k'} a_{\tilde{\lambda}',k'+q} a_{\tilde{\lambda},k-q} \rangle \\
&+ f_q P^{\tilde{\lambda}',\tilde{\lambda}'}_{k'+q} \left(\sum_{\nu,l} \Delta \langle a^\dagger_{\lambda,k} a^\dagger_{\nu,l} a_{\bar{\nu},l+q} a_{\tilde{\lambda},k-q} \rangle \right) \\
&+ f_{k'+q-k} \left(\delta_{\tilde{\lambda}',\tilde{\lambda}} - P^{\tilde{\lambda}',\tilde{\lambda}}_{k-q} \right) \left(\sum_{\nu,l} \Delta \langle a^\dagger_{\lambda,k} a^\dagger_{\nu,l} a_{\bar{\nu},l+k-q-k'} a_{\tilde{\lambda}',k'+q} \rangle \right) \\
&- \sum_{\nu} \left(\sum_{q'} f_{k'-q'} P^{\bar{\tilde{\lambda}}',\nu}_{q'} \right) \Delta \langle a^\dagger_{\lambda,k} a^\dagger_{\bar{\nu},k'} a_{\tilde{\lambda}',k'+q} a_{\tilde{\lambda},k-q} \rangle
\end{aligned}$$

$$
\begin{aligned}
&- \sum_{\nu} P_{k}^{\lambda,\nu} \left(\sum_{q'} f_{q'} \Delta \langle a^{\dagger}_{\bar{\nu},k+q'} a^{\dagger}_{\bar{\lambda}',k'-q'} a_{\tilde{\lambda}',k'+q} a_{\tilde{\lambda},k-q} \rangle \right) \\
&- \sum_{\nu} P_{k'+q}^{\bar{\nu},\tilde{\lambda}'} \left(\sum_{q'} f_{q'} \Delta \langle a^{\dagger}_{\lambda,k} a^{\dagger}_{\bar{\lambda}',k'-q'} a_{\nu,k'+q-q'} a_{\tilde{\lambda},k-q} \rangle \right) \\
&- \sum_{\nu} P_{k-q}^{\bar{\nu},\tilde{\lambda}} \left(\sum_{q'} f_{q'} \Delta \langle a^{\dagger}_{\lambda,k} a^{\dagger}_{\bar{\lambda}',k'-q'} a_{\tilde{\lambda}',k'+q} a_{\nu,k-q-q'} \rangle \right) \\
&+ \sum_{q'} f_{q'} \Delta \langle a^{\dagger}_{\lambda,k} a^{\dagger}_{\bar{\lambda}',k'-q'} a_{\tilde{\lambda}',k'+q} a_{\bar{\tilde{\lambda}},k-q-q'} \rangle \,. \qquad \text{(A.14)}
\end{aligned}
$$

Putting everything together gives

$$
\left[i\hbar \frac{\partial}{\partial t} \Delta \langle a^{\dagger}_{\lambda,k} a^{\dagger}_{\lambda',k'} a_{\tilde{\lambda}',k'+q} a_{\tilde{\lambda},k-q} \rangle \right]_{H_{\mathrm{C/dip,D}}} = \sum_{\nu} \left(W^{\nu} + w^{\nu} + S^{\nu} + s^{\nu} \right) \,, \qquad \text{(A.15)}
$$

where we have defined

$$
\begin{aligned}
W^{\nu} \;=\; & \left(\sum_{q'} f_{k-q'} P_{q'}^{\bar{\lambda},\bar{\nu}} \right) \Delta \langle a^{\dagger}_{\nu,k} a^{\dagger}_{\lambda',k'} a_{\tilde{\lambda}',k'+q} a_{\tilde{\lambda},k-q} \rangle \qquad \text{(A.16)} \\
&+ \left(\sum_{q'} f_{k'-q'} P_{q'}^{\bar{\lambda}',\bar{\nu}} \right) \Delta \langle a^{\dagger}_{\lambda,k} a^{\dagger}_{\nu,k'} a_{\tilde{\lambda}',k'+q} a_{\tilde{\lambda},k-q} \rangle \\
&- \left(\sum_{q'} f_{k'+q-q'} P_{q'}^{\bar{\nu},\bar{\tilde{\lambda}}'} \right) \Delta \langle a^{\dagger}_{\lambda,k} a^{\dagger}_{\lambda',k'} a_{\nu,k'+q} a_{\tilde{\lambda},k-q} \rangle \\
&- \left(\sum_{q'} f_{k-q-q'} P_{q'}^{\bar{\nu},\bar{\tilde{\lambda}}} \right) \Delta \langle a^{\dagger}_{\lambda,k} a^{\dagger}_{\lambda',k'} a_{\tilde{\lambda}',k'+q} a_{\nu,k-q} \rangle \,,
\end{aligned}
$$

$$
\begin{aligned}
w^{\nu} \;=\; & f_0 \Big(\sum_{l} P_{l}^{\nu,\bar{\nu}} \Big) \qquad \text{(A.17)} \\
& \Big(\Delta \langle a^{\dagger}_{\lambda,k} a^{\dagger}_{\lambda',k'} a_{\tilde{\lambda}',k'+q} a_{\bar{\tilde{\lambda}},k-q} \rangle + \Delta \langle a^{\dagger}_{\lambda,k} a^{\dagger}_{\lambda',k'} a_{\bar{\tilde{\lambda}}',k'+q} a_{\tilde{\lambda},k-q} \rangle \\
& - \Delta \langle a^{\dagger}_{\lambda,k} a^{\dagger}_{\bar{\lambda}',k'} a_{\tilde{\lambda}',k'+q} a_{\tilde{\lambda},k-q} \rangle - \Delta \langle a^{\dagger}_{\bar{\lambda},k} a^{\dagger}_{\lambda',k'} a_{\tilde{\lambda}',k'+q} a_{\tilde{\lambda},k-q} \rangle \Big) \,,
\end{aligned}
$$

$$
\begin{aligned}
s^{\nu} \;=\; & f_q \left(P_{k}^{\lambda,\bar{\tilde{\lambda}}} - P_{k-q}^{\bar{\lambda},\tilde{\lambda}} \right) \left(\sum_{l} \Delta \langle a^{\dagger}_{\nu,l} a^{\dagger}_{\lambda',k'} a_{\tilde{\lambda}',k'+q} a_{\bar{\nu},l-q} \rangle \right) \qquad \text{(A.18)} \\
& + f_q \left(P_{k'}^{\lambda',\bar{\tilde{\lambda}}'} - P_{k'+q}^{\bar{\lambda}',\tilde{\lambda}'} \right) \left(\sum_{l} \Delta \langle a^{\dagger}_{\lambda,k} a^{\dagger}_{\nu,l} a_{\bar{\nu},l+q} a_{\tilde{\lambda},k-q} \rangle \right) \\
& - f_{k'+q-k} \left(P_{k'}^{\lambda',\bar{\tilde{\lambda}}} - P_{k-q}^{\bar{\lambda}',\tilde{\lambda}} \right) \left(\sum_{l} \Delta \langle a^{\dagger}_{\lambda,k} a^{\dagger}_{\nu,l} a_{\bar{\nu},l+k-q-k'} a_{\tilde{\lambda}',k'+q} \rangle \right)
\end{aligned}
$$

$$- f_{k'+q-k}\left(P_k^{\lambda,\bar{\tilde{\lambda}}'} - P_{k'+q}^{\bar{\lambda},\tilde{\lambda}'}\right)\left(\sum_l \Delta\langle a^\dagger_{\lambda',k'} a^\dagger_{\nu,l} a_{\bar{\nu},l+k'+q-k} a_{\tilde{\lambda},k-q}\rangle\right) ,$$

$$\begin{aligned}
S^\nu \;=\;& \left(P_k^{\lambda,\nu} - \delta_{\lambda,\nu}\right)\left(\sum_{q'} f_{q'}\Delta\langle a^\dagger_{\bar{\nu},k-q'} a^\dagger_{\tilde{\lambda}',k'+q'} a_{\tilde{\lambda}',k'+q} a_{\tilde{\lambda},k-q}\rangle\right) \\
&- P_k^{\lambda,\nu}\sum_{q'} f_{q'}\left(\Delta\langle a^\dagger_{\bar{\nu},k-q'} a^\dagger_{\lambda',k'} a_{\tilde{\lambda}',k'+q} a_{\bar{\tilde{\lambda}},k-q-q'}\rangle + \Delta\langle a^\dagger_{\bar{\nu},k-q'} a^\dagger_{\lambda',k'} a_{\bar{\tilde{\lambda}}',k'+q-q'} a_{\tilde{\lambda},k-q}\rangle\right) \\
&+ P_{k'}^{\lambda',\nu}\left(\sum_{q'} f_{q'}\Delta\langle a^\dagger_{\bar{\tilde{\lambda}},k+q'} a^\dagger_{\bar{\nu},k'-q'} a_{\tilde{\lambda}',k'+q} a_{\tilde{\lambda},k-q}\rangle\right) \\
&- P_{k'}^{\lambda',\nu}\sum_{q'} f_{q'}\left(\Delta\langle a^\dagger_{\lambda,k} a^\dagger_{\bar{\nu},k'-q'} a_{\tilde{\lambda}',k'+q} a_{\bar{\tilde{\lambda}},k-q-q'}\rangle + \Delta\langle a^\dagger_{\lambda,k} a^\dagger_{\bar{\nu},k'-q'} a_{\bar{\tilde{\lambda}}',k'+q-q'} a_{\tilde{\lambda},k-q}\rangle\right) \\
&- \left(P_{k'+q}^{\nu,\tilde{\lambda}'} - \delta_{\nu,\tilde{\lambda}'}\right)\left(\sum_{q'} f_{q'}\Delta\langle a^\dagger_{\lambda,k} a^\dagger_{\lambda',k'} a_{\bar{\nu},k'+q-q'} a_{\bar{\tilde{\lambda}},k-q+q'}\rangle\right) \\
&+ P_{k'+q}^{\nu,\tilde{\lambda}'}\sum_{q'} f_{q'}\left(\Delta\langle a^\dagger_{\lambda,k} a^\dagger_{\tilde{\lambda}',k'-q'} a_{\bar{\nu},k'+q-q'} a_{\tilde{\lambda},k-q}\rangle + \Delta\langle a^\dagger_{\bar{\tilde{\lambda}},k-q'} a^\dagger_{\lambda',k'} a_{\bar{\nu},k'+q-q'} a_{\tilde{\lambda},k-q}\rangle\right) \\
&- P_{k-q}^{\nu,\tilde{\lambda}}\left(\sum_{q'} f_{q'}\Delta\langle a^\dagger_{\lambda,k} a^\dagger_{\lambda',k'} a_{\bar{\tilde{\lambda}}',k'+q-q'} a_{\bar{\nu},k-q+q'}\rangle\right) \\
&+ P_{k-q}^{\nu,\tilde{\lambda}}\sum_{q'} f_{q'}\left(\Delta\langle a^\dagger_{\lambda,k} a^\dagger_{\bar{\tilde{\lambda}}',k'-q'} a_{\tilde{\lambda}',k'+q} a_{\bar{\nu},k-q-q'}\rangle + \Delta\langle a^\dagger_{\bar{\tilde{\lambda}},k-q'} a^\dagger_{\lambda',k'} a_{\tilde{\lambda}',k'+q} a_{\bar{\nu},k-q-q'}\rangle\right) .
\end{aligned} \tag{A.19}$$

Equations (A.6), (A.7), (A.10), and (A.15) together with Eqs. (A.16)–(A.19) have served as a starting point to derive the Coulomb contributions in the explicit equations of motion in Chapter 3.

A.2 Carrier-Boson Interaction

Similarly as in the case of two-particle carrier interactions, also the phonon and photon coupling can be treated at the same time. In this case, the general starting point is the Hamiltonian of the form

$$\begin{aligned}
H_{\mathrm{D/P}} &= \sum_{q_\perp,q,\nu,l} g^\nu_{q_\perp,q} B^\dagger_{q_\perp,q}\, a^\dagger_{\nu,l} a_{\bar{\nu},l+q} + \left(g^\nu_{q_\perp,q}\right)^* B_{q_\perp,-q}\, a^\dagger_{\nu,l} a_{\bar{\nu},l+q} \\
&= \sum_{q,\nu,l} \mathcal{B}^\dagger_{\nu,q}\, a^\dagger_{\nu,l} a_{\bar{\nu},l+q} ,
\end{aligned} \tag{A.20}$$

where we have defined the collective operator

$$\mathcal{B}^\dagger_{\nu,q} = \sum_{q_\perp} g^\nu_{q_\perp,q} B^\dagger_{q_\perp,q} + \left(g^\nu_{q_\perp,q}\right)^* B_{q_\perp,-q} , \tag{A.21}$$

which obeys the relation

$$\mathcal{B}^{\dagger}_{\nu,q} = \mathcal{B}_{\nu,-q}\,. \tag{A.22}$$

We note that again only the component $q_\perp$ perpendicular to the semiconductor structure is denoted explicitly. The components without index refer to vectors along the direction of the quantum well or quantum wire. In Eq. (A.20), the operator B can be either a photon or a phonon operator. For phonon interaction, we use $\bar{\nu} = \nu$ because it is an intraband interaction, while for the dipole interaction $\bar{c} = v$ and vice versa. The matrix element can be determined by comparing to Eqs. (2.43) and (2.64).

The general starting point are the three operator equations of motion

$$\left[i\hbar\frac{\partial}{\partial t}B_{q_\perp,q}\right]_{H_{\mathrm{D/P}}} = \sum_{\nu,l} g^{\nu}_{q_\perp,q}\, a^{\dagger}_{\nu,l}\, a_{\bar{\nu},l+q}\,, \tag{A.23}$$

$$\left[i\hbar\frac{\partial}{\partial t}B^{\dagger}_{q_\perp,q}\right]_{H_{\mathrm{D/P}}} = -\sum_{\nu,l} \left(g^{\nu}_{q_\perp,q}\right)^{*} a^{\dagger}_{\bar{\nu},l+q}\, a_{\nu,l}\,, \tag{A.24}$$

$$\begin{aligned}\left[i\hbar\frac{\partial}{\partial t}a^{\dagger}_{\lambda,k}a_{\tilde{\lambda},k+q}\right]_{H_{\mathrm{D/P}}} &= \sum_{q'} \mathcal{B}^{\dagger}_{\tilde{\lambda},q'}\, a^{\dagger}_{\lambda,k}\, a_{\bar{\tilde{\lambda}},k+q+q'} \\ &\quad - \sum_{q'} \mathcal{B}^{\dagger}_{\bar{\lambda},q'}\, a^{\dagger}_{\bar{\lambda},k-q'}\, a_{\tilde{\lambda},k+q}\,.\end{aligned} \tag{A.25}$$

The simplest expectation values formally corresponding to four-point operators are products of two bosonic operators. Without the need of approximations, we obtain

$$\begin{aligned}\left[i\hbar\frac{\partial}{\partial t}\Delta\langle B^{\dagger}_{q_\perp,q}B_{q'_\perp,q}\rangle\right]_{H_{\mathrm{D/P}}} &= \sum_{\nu,l}\Big(g^{\nu}_{q'_\perp,q}\Delta\langle B^{\dagger}_{q_\perp,q}a^{\dagger}_{\nu,l}a_{\bar{\nu},l+q}\rangle \\ &\quad - \left(g^{\nu}_{q_\perp,q}\right)^{*}\Delta\langle a^{\dagger}_{\bar{\nu},l+q}a_{\nu,l}B_{q'_\perp,q}\rangle\Big)\,,\end{aligned} \tag{A.26}$$

$$\begin{aligned}\left[i\hbar\frac{\partial}{\partial t}\Delta\langle B_{q_\perp,-q}B_{q'_\perp,q}\rangle\right]_{H_{\mathrm{D/P}}} &= \sum_{\nu,l}\Big(g^{\nu}_{q'_\perp,q}\Delta\langle B_{q_\perp,-q}a^{\dagger}_{\nu,l}a_{\bar{\nu},l+q}\rangle \\ &\quad + g^{\nu}_{q_\perp,q}\Delta\langle a^{\dagger}_{\nu,l}a_{\bar{\nu},l-q}B_{q'_\perp,q}\rangle\Big)\,.\end{aligned} \tag{A.27}$$

In the next step, we compute the equation of motion for the boson-assisted two-point operators and obtain

$$\begin{aligned}&\left[i\hbar\frac{\partial}{\partial t}\Delta\langle B^{\dagger}_{q_\perp,q}a^{\dagger}_{\lambda,k}a_{\tilde{\lambda},k+q}\rangle\right]_{H_{\mathrm{D/P}}} \\ &\quad= \sum_{q'}\Big(\langle B^{\dagger}_{q_\perp,q}\mathcal{B}^{\dagger}_{\tilde{\lambda},q'}a^{\dagger}_{\lambda,k}a_{\bar{\tilde{\lambda}},k+q+q'}\rangle\Big|_{q\neq 0} - \langle B^{\dagger}_{q_\perp,q}\mathcal{B}^{\dagger}_{\bar{\lambda},q'}a^{\dagger}_{\bar{\lambda},k-q'}a_{\tilde{\lambda},k+q}\rangle\Big|_{q\neq 0}\Big) \\ &\qquad - \sum_{\nu,l}\left(g^{\nu}_{q_\perp,q}\right)^{*}\langle a^{\dagger}_{\bar{\nu},l+q}a_{\nu,l}a^{\dagger}_{\lambda,k}a_{\tilde{\lambda},k+q}\rangle\Big|_{q\neq 0} \\ &= \quad \langle\mathcal{B}_{\tilde{\lambda},0}\rangle\Delta\langle B^{\dagger}_{q_\perp,q}a^{\dagger}_{\lambda,k}a_{\bar{\tilde{\lambda}},k+q}\rangle - \langle\mathcal{B}_{\bar{\lambda},0}\rangle\Delta\langle B^{\dagger}_{q_\perp,q}a^{\dagger}_{\bar{\lambda},k}a_{\tilde{\lambda},k+q}\rangle\end{aligned} \tag{A.28}$$

$$+\Delta\langle B^\dagger_{q_\perp,q}\mathcal{B}_{\tilde\lambda,q}\rangle P_k^{\lambda,\bar{\tilde\lambda}} - \Delta\langle B^\dagger_{q_\perp,q}\mathcal{B}_{\bar{\tilde\lambda},q}\rangle P_{k+q}^{\bar\lambda,\tilde\lambda}$$
$$-\sum_\nu \left(g^\nu_{q_\perp,q}\right)^* P_{k+q}^{\bar\nu,\tilde\lambda}\left(\delta_{\lambda,\nu} - P_k^{\lambda,\nu}\right) - \sum_{\nu,l}\left(g^\nu_{q_\perp,q}\right)^*\Delta\langle a^\dagger_{\lambda,k}a^\dagger_{\bar\nu,l+q}a_{\nu,l}a_{\tilde\lambda,k+q}\rangle\,.$$

The equation of motion for the expectation value $\Delta\langle B_{q_\perp,-q}a^\dagger_{\lambda,k}a_{\tilde\lambda,k+q}\rangle$ can be obtained either in the same way or by noting that

$$\Delta\langle B_{q_\perp,-q}a^\dagger_{\lambda,k}a_{\tilde\lambda,k+q}\rangle = \Delta\langle B^\dagger_{q_\perp,-q}a_{\tilde\lambda,k+q}a^\dagger_{\lambda,k}\rangle^* \tag{A.29}$$

and using Eq. (A.28).

Finally, we must examine the equation of motion for the four-point carrier correlations. It is given by

$$\begin{aligned}\left[i\hbar\frac{\partial}{\partial t}\Delta\langle a^\dagger_{\lambda,k}a^\dagger_{\lambda',k'}a_{\tilde\lambda',k'+q}a_{\tilde\lambda,k-q}\rangle\right]_{H_{\mathrm{D/P}}}&\\
= \sum_{q'}\langle\mathcal{B}^\dagger_{\tilde\lambda,q'}a^\dagger_{\lambda,k}a_{\bar{\tilde\lambda},k-q+q'}a^\dagger_{\lambda',k'}a_{\tilde\lambda',k'+q}\rangle\Big|_{q,k'+q-k\neq0}&\\
-\sum_{q'}\langle\mathcal{B}^\dagger_{\tilde\lambda,q'}a^\dagger_{\bar{\tilde\lambda},k-q'}a_{\tilde\lambda,k-q}a^\dagger_{\lambda',k'}a_{\tilde\lambda',k'+q}\rangle\Big|_{q,k'+q-k\neq0}&\\
+\sum_{q'}\langle\mathcal{B}^\dagger_{\tilde\lambda',q'}a^\dagger_{\lambda,k}a_{\tilde\lambda,k-q}a^\dagger_{\lambda',k'}a_{\bar{\tilde\lambda}',k'+q+q'}\rangle\Big|_{q,k'+q-k\neq0}&\\
-\sum_{q'}\langle\mathcal{B}^\dagger_{\bar{\tilde\lambda}',q'}a^\dagger_{\lambda,k}a_{\tilde\lambda,k-q}a^\dagger_{\bar{\tilde\lambda}',k'-q'}a_{\tilde\lambda',k'+q}\rangle\Big|_{q,k'+q-k\neq0}\,.&\end{aligned} \tag{A.30}$$

Singlet contributions to this equation do not exist such that the full equation of motion in the consistent singlet-doublet approximation is given by

$$\begin{aligned}\left[i\hbar\frac{\partial}{\partial t}\Delta\langle a^\dagger_{\lambda,k}a^\dagger_{\lambda',k'}a_{\tilde\lambda',k'+q}a_{\tilde\lambda,k-q}\rangle\right]_{H_{\mathrm{D/P}},D}&\\
= \langle\mathcal{B}_{\tilde\lambda,0}\rangle\Delta\langle a^\dagger_{\lambda,k}a^\dagger_{\lambda',k'}a_{\tilde\lambda',k'+q}a_{\bar{\tilde\lambda},k-q}\rangle&\\
+\langle\mathcal{B}_{\tilde\lambda',0}\rangle\Delta\langle a^\dagger_{\lambda,k}a^\dagger_{\lambda',k'}a_{\bar{\tilde\lambda}',k'+q}a_{\tilde\lambda,k-q}\rangle&\\
-\langle\mathcal{B}_{\tilde\lambda',0}\rangle\Delta\langle a^\dagger_{\lambda,k}a^\dagger_{\bar{\tilde\lambda}',k'}a_{\tilde\lambda',k'+q}a_{\tilde\lambda,k-q}\rangle&\\
-\langle\mathcal{B}_{\tilde\lambda,0}\rangle\Delta\langle a^\dagger_{\bar{\tilde\lambda},k}a^\dagger_{\lambda',k'}a_{\tilde\lambda',k'+q}a_{\tilde\lambda,k-q}\rangle&\\
+\Delta\langle\mathcal{B}^\dagger_{\tilde\lambda,q}a^\dagger_{\lambda',k'}a_{\tilde\lambda',k'+q}\rangle P_k^{\lambda,\bar{\tilde\lambda}} - \Delta\langle\mathcal{B}^\dagger_{\bar{\tilde\lambda},q}a^\dagger_{\lambda',k'}a_{\tilde\lambda',k'+q}\rangle P_{k-q}^{\bar\lambda,\tilde\lambda}&\\
+\Delta\langle\mathcal{B}_{\tilde\lambda',q}a^\dagger_{\lambda,k}a_{\tilde\lambda,k-q}\rangle P_{k'}^{\lambda',\bar{\tilde\lambda}'} - \Delta\langle\mathcal{B}_{\bar{\tilde\lambda}',q}a^\dagger_{\lambda,k}a_{\tilde\lambda,k-q}\rangle P_{k'+q}^{\bar\lambda',\tilde\lambda'}&\\
+\Delta\langle\mathcal{B}^\dagger_{\tilde\lambda,k'+q-k}a^\dagger_{\lambda,k}a_{\tilde\lambda',k'+q}\rangle\left(\delta_{\lambda',\bar{\tilde\lambda}} - P_{k'}^{\lambda',\bar{\tilde\lambda}}\right)&\\
-\Delta\langle\mathcal{B}^\dagger_{\bar{\tilde\lambda}',k'+q-k}a^\dagger_{\lambda,k}a_{\tilde\lambda',k'+q}\rangle\left(\delta_{\bar{\tilde\lambda}',\tilde\lambda} - P_{k-q}^{\bar{\tilde\lambda}',\tilde\lambda}\right)&\\
+\Delta\langle\mathcal{B}_{\tilde\lambda,k'+q-k}a^\dagger_{\lambda',k'}a_{\tilde\lambda,k-q}\rangle P_{k'+q}^{\bar\lambda,\tilde\lambda'}&\\
-\Delta\langle\mathcal{B}_{\tilde\lambda',k'+q-k}a^\dagger_{\lambda',k'}a_{\tilde\lambda,k-q}\rangle P_k^{\lambda,\bar{\tilde\lambda}'}\,.&\end{aligned} \tag{A.31}$$

The set of equations derived in this Appendix forms a general starting point for many quantum-optical and many-body investigations. It provides the means to compute the equations of motion for the coupled semiconductor-photon-phonon system on the consistent singlet-doublet level. In this thesis, we have used those equations to investigate the fully incoherent regime.

B Phonon Interaction

As we have shown in Chapter 4, a microscopic scattering mechanism is needed for excitonic correlations in order to study true exciton formation. As a simple and realistic candidate, phonon scattering was introduced. Since we consider long time scales in the order of nanoseconds, we are not interested in coherent phonons or memory effects and choose the simplest possible treatment for the description of phonons. They are treated as a reservoir and in Markov approximation. For all computations, we have included only terms proportional to the square of the phonon matrix elements. No Coulomb or light-matter interaction was included in the treatment of the phonon-assisted quantities.

In App. A, all equations up to the four-point level are derived in general notation. In the case of the phonon interaction Hamiltonian Eq. (2.64), the explicit equation of motion for the carrier densities are of the form

$$\left[i\hbar\frac{\partial}{\partial t}f_k^{\mathrm{e}}\right]_{H_{\mathrm{P}}} = \sum_p \Delta\langle \mathcal{G}_p c_k^\dagger c_{k-p}\rangle - \text{c.c.}\,, \tag{B.1}$$

where we have used the definition (2.65). To compute the right-hand side of Eq. (B.1), we have to establish the equations of motion for the phonon-assisted terms. In the case of the phonon-assisted electron density, this gives

$$\begin{aligned}\left[i\hbar\frac{\partial}{\partial t}\Delta\langle D_{p_\perp,p}c_k^\dagger c_{k-p}\rangle\right]_{H_{\mathrm{P}}} &= G_{p_\perp,p}f_{k-p}^{\mathrm{e}}(1-f_k^{\mathrm{e}}) \\ &\quad +\Delta\langle D_{p_\perp,p}\mathcal{G}_{-p}\rangle(f_k^{\mathrm{e}}-f_{k-p}^{\mathrm{e}}) \\ &\quad +G_{p_\perp,p}\sum_l\left(c_{\mathrm{e}}^{p,l,k}-c_{\mathrm{X}}^{k-p-l,l,k}\right),\end{aligned} \tag{B.2}$$

where we have already left out all terms proportional to the coherent transition amplitudes $P_k = \langle v_k^\dagger c_k\rangle$. In cases with coherent excitations, those terms can easily be included. In order to compute Eq. (B.1), we solve Eq. (B.2) in Markov approximation. In principle, the result of a Markov approximation is dependent on the basis one uses. In general, however, the influence of the basis is not crucial if the resulting terms are summed over as in the case of Eq. (B.1). By including only the kinetic energies in the equations of phonon-assisted densities in addition to Eq. (B.2), we effectively perform the Markov approximation in the one-particle basis of Bloch electrons and holes. We numerically confirmed that our result is independent of the precise choice of the basis. Furthermore assuming a reservoir of phonons, we neglect coherent phonons and off-diagonal phonon-phonon correlations, and

assume a Bose-Einstein distribution

$$\Delta\langle D^\dagger_{p_\perp,p} D_{p'_\perp}, p\rangle = \delta_{p_\perp,p'_\perp}\left(\mathrm{e}^{\frac{E_{p,p_\perp}}{kT}}-1\right)^{-1}, \tag{B.3}$$

for phonons at the corresponding energy $E_{p,p_\perp}$ given by the phonon dispersion. After those approximations, we obtain Eqs. (3.38) and (3.39) for the carrier densities.

Equation (B.2) and its counterpart for the phonon-assisted hole density suffice to compute the four-point correlation contribution to the correlation equations, given in Eqs. (3.40)–(3.42). In addition, phonon-assisted correlations of the form $\Delta\langle Da^\dagger a^\dagger aa\rangle$ are needed to provide a true dephasing mechanism for excitonic and carrier-carrier correlations. More specifically, the phonon contribution to the equation of motion for excitonic correlations is

$$\begin{aligned}
i\hbar\frac{\partial}{\partial t}\Delta\langle c^\dagger_k v^\dagger_{k'} c_{k'+q} v_{k-q}\rangle = \\
&\Delta\langle \mathcal{G}^\dagger_{k'+q-k} c^\dagger_k c_{k'+q}\rangle \left(f^{\mathrm{h}}_{k'} - f^{\mathrm{h}}_{k-q}\right) - \Delta\langle \mathcal{G}_{k'+q-k} v^\dagger_{k'} v_{k-q}\rangle \left(f^{\mathrm{e}}_{k} - f^{\mathrm{e}}_{k'+q}\right) \\
&+\sum_p \Delta\langle \mathcal{G}^\dagger_p c^\dagger_k v^\dagger_{k'} c_{k'+q} v_{k-q+p}\rangle - \sum_p \Delta\langle \mathcal{G}^\dagger_p c^\dagger_{k-p} v^\dagger_{k'} c_{k'+q} v_{k-q}\rangle \\
&+\sum_p \Delta\langle \mathcal{G}^\dagger_p c^\dagger_k v^\dagger_{k'} c_{k'+q+p} v_{k-q}\rangle - \sum_p \Delta\langle \mathcal{G}^\dagger_p c^\dagger_k v^\dagger_{k'-p} c_{k'+q} v_{k-q}\rangle\,,
\end{aligned} \tag{B.4}$$

where we again have restricted the derivation to the incoherent terms. Similar equations can be derived for the carrier-carrier correlations. The first row leads to Eq. (3.40) and involves the phonon-assisted densities solved in Eq. (B.2). The remaining terms are clearly beyond the four-point level. In the spirit of the cluster expansion of Sec. 3.2, they can be viewed as a scattering approximation of the triplet level. Also the equation

$$\begin{aligned}
i\hbar\frac{\partial}{\partial t}\Delta\langle D_{p_\perp,p} c^\dagger_k v^\dagger_{k'} c_{k'+q} v_{k-q-p}\rangle = \\
&G_{p_\perp,p}\left(N^{\mathrm{PH}}_{p_\perp,p} + f^{\mathrm{h}}_{k-q-p}\right)\Delta\langle c^\dagger_k v^\dagger_{k'} c_{k'+q} v_{k-q}\rangle \\
+&G_{p_\perp,p}\left(N^{\mathrm{PH}}_{p_\perp,p} + 1 - f^{\mathrm{e}}_{k'+q}\right)\Delta\langle c^\dagger_k v^\dagger_{k'} c_{k'+q+p} v_{k-q-p}\rangle \\
-&G_{p_\perp,p}\left(N^{\mathrm{PH}}_{p_\perp,p} + 1 - f^{\mathrm{h}}_{k'}\right)\Delta\langle c^\dagger_k v^\dagger_{k'-p} c_{k'+q} v_{k-q-p}\rangle \\
-&G_{p_\perp,p}\left(N^{\mathrm{PH}}_{p_\perp,p} + f^{\mathrm{e}}_{k}\right)\Delta\langle c^\dagger_{k-p} v^\dagger_{k'} c_{k'+q} v_{k-q-p}\rangle
\end{aligned} \tag{B.5}$$

together with the equations of similar phonon-assisted carrier-carrier correlations are therefore solved in Markov approximation. That way, one obtains Eqs. (3.45), (3.50) and (3.51) which describe the microscopic scattering between phonons and correlations.

C Exciton Basis

In this thesis, a generalized exciton basis is used to solve Eq. (4.14) analytically and find its steady state solution. Also for the interpretation of our results starting from Sec. 4.3, it is helpful to be able to compute the number of bound excitons within a certain excitonic state. Therefore, we must have a clear definition of the exciton eigenfunctions. In particular for non-vanishing densities, this definition is not trivial.

The excitonic eigenfunctions can be derived in several ways. The first way is to set up the Hamiltonian for a semiconductor and look for the *single*-pair state that minimizes the total energy of the system. Using a variational principle, the exciton wavefunctions are found to be the solutions. The second way is to set up the well known semiconductor Bloch equations [19] and to look for solutions of the homogeneous part in the low density limit. In both cases, the resulting equation in k-space representation is

$$(\frac{\hbar^2 k^2}{2\mu})\phi_\nu(k) - \sum_{k'} V_{k'-k}\phi_\nu(k') = \varepsilon_\nu \phi_\nu(k)\,. \tag{C.1}$$

After a Fourier transformation to real space, this leads to the equation

$$-\frac{\hbar^2\nabla^2}{2\mu}\phi_\nu(r) - V(r)\phi_\nu(r) = \varepsilon_\nu\phi_\nu(r)\,, \tag{C.2}$$

which is exactly the equation of the relative motion of the hydrogen atom. Hence, the spectrum consists of a series of bound states and a continuum of ionized states. Since the linear operator acting on ϕ is Hermitian, the set of eigenfunctions is a complete basis of orthogonal functions and can be used to expand the linearized semiconductor Bloch equation to obtain the Elliott formula of absorption as an analytical result [19].

In the more general case of non-vanishing but slowly varying carrier densities, this equation is changed. Instead of the low density limit (C.1), we rather use the equation

$$\begin{aligned} \bar{\varepsilon}_{k,q}\phi^{\mathrm{r}}_{\nu,q}(k) - \bar{f}_{k,q}\sum_{k'} V_{k'-k}\phi^{\mathrm{r}}_{\nu,q}(k') &= \varepsilon_{\nu,q}\phi^{\mathrm{r}}_{\nu,q}(k)\,, \\ \left(\phi^{\mathrm{l}}_{\nu,q}(k)\right)^* \bar{\varepsilon}_{k,q} - \sum_{k'}\left(\phi^{\mathrm{l}}_{\nu,q}(k')\right)^* \bar{f}_{k',q}V_{k'-k} &= \left(\phi^{\mathrm{l}}_{\nu,q}(k)\right)^*\varepsilon_{\nu,q}\,, \end{aligned} \tag{C.3}$$

with the definitions from Eqs. (4.17)–(4.19). The exciton energy of the relative motion can be explicitly expressed as

$$\bar{\varepsilon}_{k,q} = \frac{\hbar^2 k^2}{2\mu} - \sum_{k'} V_{k-k'}\left(f^{\mathrm{e}}_{k'+q^{\mathrm{e}}} + f^{\mathrm{h}}_{k'-q^{\mathrm{h}}}\right)\,. \tag{C.4}$$

Due to the filling factor $\bar{f}$, the equation is not Hermitian anymore and the more general derivation of left- and right handed eigenfunctions is required. We stress that Eq. (C.3) is the equation for the relative motion only. Nevertheless, as a consequence of the q-dependence of the phase-space filling factor and of the energy renormalization, center-of-mass and relative motion become coupled. The exciton wave function for the relative motion thus depends on the center-of-mass motion which simply gives a contribution of $\frac{\hbar^2 q^2}{2(m^{\mathrm{e}}+m^{\mathrm{h}})}$ to the total exciton energy.

For low densities where the phase-space filling stays positive, Eq. (C.3) can be cast into matrix form. For every center-of-mass momentum q, we find

$$\begin{aligned} \mathbf{F}\mathbf{M}\mathbf{\Phi}^{\mathrm{r}}_{\nu,q} &= E_{\nu,q}\mathbf{\Phi}^{\mathrm{r}}_{\nu,q}\,, \\ \left(\mathbf{\Phi}^{\mathrm{l}}_{\nu,q}\right)^t \mathbf{F}\mathbf{M} &= \left(\mathbf{\Phi}^{\mathrm{l}}_{\nu,q}\right)^t E_{\nu,q}\,, \end{aligned} \tag{C.5}$$

where the different matrices are given by

$$\mathbf{F}_{k,k'} = \delta_{k,k'}(1 - f^{\mathrm{e}}_{k+q^{\mathrm{e}}} - f^{\mathrm{h}}_{k-q^{\mathrm{h}}})\,, \tag{C.6}$$

$$\mathbf{M}_{k,k'} = \delta_{k,k'}\frac{\bar{\varepsilon}_{k,q}}{1 - f^{\mathrm{e}}_{k+q^{\mathrm{e}}} - f^{\mathrm{h}}_{k-q^{\mathrm{h}}}} + V_{k-k'}\,, \tag{C.7}$$

and $\mathbf{\Phi}^{\mathrm{r(l)}}_{\nu,q}$ is the vector of all the right(left)-handed eigenfunctions $\phi^{\mathrm{r(l)}}_{\nu,q}(k)$. We first note that for positive $\bar{f}_{k,q}$ the matrix $\mathbf{B} := \sqrt{\mathbf{F}}\mathbf{M}\sqrt{\mathbf{F}}$ is well defined and Hermitian. Therefore we know, that a unitary transformation matrix $\mathbf{T}$ exists such that

$$\mathbf{T}^\dagger\mathbf{B}\mathbf{T} = \mathbf{D} \tag{C.8}$$

becomes diagonal. In fact, this diagonal matrix contains the excitonic eigenenergies. With the help of the transformation matrix, one can easily show that

$$\mathbf{\Phi}^{\mathrm{r}}_{\nu,q} = \sqrt{\mathbf{F}}\mathbf{T}\mathbf{e}_\nu \tag{C.9}$$

is right-handed eigenfunction for all cartesian vectors $\mathbf{e}_\nu$. Namely,

$$\mathbf{F}\mathbf{M}\mathbf{\Phi}^{\mathrm{r}}_{\nu,q} = \mathbf{F}\mathbf{M}\left(\sqrt{\mathbf{F}}\mathbf{T}\mathbf{e}_\nu\right) = \sqrt{\mathbf{F}}\mathbf{B}\mathbf{T}\mathbf{e}_\nu = \sqrt{\mathbf{F}}\mathbf{T}\mathbf{D}\mathbf{e}_\nu = E_\nu\mathbf{\Phi}^{\mathrm{r}}_{\nu,q}\,. \tag{C.10}$$

Similarly, one can show that the corresponding left-handed eigenfunction is given by

$$\mathbf{\Phi}^{\mathrm{l}}_{\nu,q} = \sqrt{\mathbf{F}^{-1}}\mathbf{T}\mathbf{e}_\nu. \tag{C.11}$$

The set of left-handed eigenfunctions or the set of right-handed eigenfunctions alone is not orthogonal. But a generalized orthogonality relation,

$$\langle\mathbf{\Phi}^{\mathrm{l}}_{\nu,q}|\mathbf{\Phi}^{\mathrm{r}}_{\nu',q}\rangle = \langle\sqrt{\mathbf{F}^{-1}}\mathbf{T}\mathbf{e}_\nu|\sqrt{\mathbf{F}}\mathbf{T}\mathbf{e}_{\nu'}\rangle = \langle\mathbf{e}_\nu|\mathbf{T}^\dagger\sqrt{\mathbf{F}^{-1}}\sqrt{\mathbf{F}}\mathbf{T}|\mathbf{e}_{\nu'}\rangle = \delta_{\nu,\nu'}, \tag{C.12}$$

is valid, and the corresponding completeness relation is given by

$$\sum_\nu |\mathbf{\Phi}^{\mathrm{l}}_{\nu,q}\rangle\langle\mathbf{\Phi}^{\mathrm{r}}_{\nu,q}| = \mathbf{1}. \tag{C.13}$$

For sufficiently low densities, the matrix $\mathbf{F}$ becomes the identity matrix and we recover the usual zero-density exciton functions.

D Confinement Functions

In this Appendix, we derive the different confinement functions for a two-dimensional quantum well and for a one-dimensional quantum wire using different confinement potentials.

D.1 Quantum well with infinitely high walls

Using the envelope-function approximation [19], the Bloch functions, Eq. (2.2), for a quantum well are given by

$$\phi_{\mathbf{k}_\parallel,\lambda,n}(\mathbf{r}) = \xi_n(z)\frac{e^{i\,\mathbf{k}_\parallel\cdot\mathbf{r}_\parallel}}{\sqrt{\mathcal{S}}} w_{\lambda,\mathbf{k}\approx 0}(\mathbf{r}), \tag{D.1}$$

where we explicitly denote the index n for the different subbands due to the confinement and $\mathcal{S}$ is the quantization area of the quantum well. For a sufficiently strong step in the confinement potential, we can assume that ξ_n can be approximated by the eigenfunctions of a particle in an infinitely high box. If the width of that box is denoted a and the box is situated symmetrically from $-a/2$ to $a/2$, the eigenfunctions are

$$\xi_n(z) = \sqrt{\frac{2}{a}} \begin{cases} \cos(n\frac{\pi}{a}z) & n \text{ odd} \\ \text{if} & \\ \sin(n\frac{\pi}{a}z) & n \text{ even} \end{cases} \tag{D.2}$$

The corresponding energies are given by

$$E_n = \frac{\hbar^2}{2m}\frac{\pi^2}{a^2}n^2\,. \tag{D.3}$$

D.2 Quantum wire with square cross-section

In all cases of a one-dimensional semiconductor structure, the Bloch functions in envelope-function approximation are of the form

$$\phi_{k_\parallel,\lambda,n}(\mathbf{r}) = \xi_n(\mathbf{r}_\perp)\frac{e^{i\,k_\parallel r_\parallel}}{\sqrt{\mathcal{L}}} w_{\lambda,\mathbf{k}\approx 0}(\mathbf{r}), \tag{D.4}$$

where the quantum wire is extended along the $r_\parallel$-direction and $\xi_n(\mathbf{r}_\perp)$ is determined by the confinement perpendicular to the wire extension.

In the case of a quantum wire with square cross section, the solutions can be obtained directly from Sec. D.1. The eigenfunctions are simply products of the solutions from Eq. (D.2) and the corresponding eigenenergies are given by

$$E_{n,m} = \frac{\hbar^2}{2m}\frac{\pi^2}{a^2}(n^2 + m^2)\,. \tag{D.5}$$

We note that both n and m must be larger or equal than one. Therefore, the lowest energy is given for $n = m = 1$ and thus twice as large as in the case of a quantum well. The difference between the lowest two subbands is given by $\frac{3\hbar^2}{2m}\frac{\pi^2}{a^2}$ and thus identical to that of a quantum well.

D.3 Cylindrical quantum wire

More useful for practical derivations are cylindrical quantum wires with circular cross section. In order to compute the corresponding solutions, we first express the Hamiltonian of the free motion in polar coordinates. The Laplacian transforms according to

$$\begin{aligned}\Delta_{\text{polar}} &= \frac{1}{r}\frac{\partial}{\partial r}\left(r\,\frac{\partial}{\partial r}\right) + \frac{1}{r^2}\frac{\partial^2}{\partial \phi^2} \\ &= \frac{\partial^2}{\partial r^2} + \frac{1}{r}\frac{\partial}{\partial r} + \frac{1}{r^2}\frac{\partial^2}{\partial \phi^2}.\end{aligned} \tag{D.6}$$

If we make an ansatz for the wave function according to

$$\xi_{n,m}(r,\phi) = R_n(r)\; e^{i\,m\,\phi}\,, \tag{D.7}$$

the radial part must fulfill the equation

$$-\frac{1}{r}\frac{\partial}{\partial r}\left(r\,\frac{\partial}{\partial r}R_n(r)\right) + \frac{m^2}{r^2}R_n(r) = \frac{2mE_n}{\hbar^2}R_n(r). \tag{D.8}$$

If we furthermore introduce the dimensionless coordinate

$$\rho = \sqrt{\frac{2mE_n}{\hbar^2}}\; r\,, \tag{D.9}$$

the resulting equation simplifies to

$$\rho^2\;\frac{\partial^2 R_n(\rho)}{\partial \rho^2} + \rho\;\frac{\partial R_n(\rho)}{\partial \rho} + (\rho^2 - m^2)R_n(\rho) = 0, \tag{D.10}$$

which is the defining equation for Bessel functions. Since the Bessel functions of the second kind Y_n have a logarithmic divergence at $r = 0$, we only consider the Bessel functions of the first kind J_n. The different solutions in the original units are thus proportional to

$$\xi_{n,m}(r,\phi) = R_n(r)\; e^{i\,m\,\phi} = J_m\!\left(\sqrt{\frac{2mE_n}{\hbar^2}}\; r\right)\; e^{i\,m\,\phi}. \tag{D.11}$$

The various possible eigenenergies, i.e. the index n, is determined according to the condition that the wave function must vanish at the boundary of the quantum wire with radius R. The ground state is obtained for $m = 0$ and an energy E_0 chosen such that $\sqrt{\frac{2mE_0}{\hbar^2}}\, R$ is the first zero of the function J_0. Thus

$$E_0 = \frac{\hbar^2}{2mR^2}\alpha_0^2\,, \tag{D.12}$$

where $\alpha_0 \approx 2.405$ is the first zero of J_0. After proper normalization, we obtain

$$\xi_0(r,\phi) = \frac{J_0(\alpha_0 \frac{r}{R})}{\sqrt{\pi}\, R\, J_1(\alpha_0)}\,. \tag{D.13}$$

D.4 Cylindrical quantum wire with parabolic confinement

In practice, all computations of matrix elements are facilitated if we use a parabolic confinement instead of the infinitely high box of the last sections. Thus, we present here the derivation of the ground state of a particle in a parabolic confined quantum wire according to the equation

$$\frac{\hbar^2}{2m}\left(-\Delta + \frac{1}{4}\frac{r^2}{R^4}\right)\xi_n(r,\phi) = E_n\, \xi_n(r,\phi)\,. \tag{D.14}$$

The "radius" R is here nothing but a parameter to characterize the strength of the confinement. We can immediately solve the equation with the help of the standard textbook physics of the harmonic oscillator when we identify $\hbar^2/(8mR^4)$ with the usual prefactor $m\omega^2/2$. The ground state energy in two dimensions is then given by

$$E_0 = \hbar\omega = \frac{\hbar^2}{2\, m\, R^2}\,, \tag{D.15}$$

and the corresponding eigenfunction is

$$\xi_0(r,\phi) = \frac{1}{\sqrt{2\,\pi}}\frac{1}{R}e^{-\frac{r^2}{4R^2}}\,. \tag{D.16}$$

We see that the parameter R for parabolic confinement should be smaller by a factor of α_0 in order to produce the same ground state energy Eq. (D.12) as the infinite box. In that sense, one can interpret the quantity $R\,\alpha_0$ as the physical radius of the quantum wire.

E Coulomb Matrix Element in Quantum Wires

The Coulomb Hamiltonian, Eq. (2.8), of a one-dimensional structure is usually expressed as

$$H_{\mathrm{C}} = \frac{1}{2}\frac{\mathrm{e}^2}{4\pi\varepsilon_0}\sum_{\lambda,\lambda',k,k'}\sum_{q\neq 0}\left(\frac{1}{\mathcal{L}}\int V^{\mathrm{eff}}(z)e^{-i\,q\,z}\mathrm{d}z\right)\hat{a}^{\dagger}_{\lambda,k}\hat{a}^{\dagger}_{\lambda',k'}\hat{a}_{\lambda',k'+q}\hat{a}_{\lambda,k-q}\,, \tag{E.1}$$

where $V^{\mathrm{eff}}(z)$ is an effective Coulomb potential including the influence of the finite width of the quantum wire. It is given by

$$V^{\mathrm{eff}}(z-z') = \iiiint |\xi_0(x,y)|^2|\xi_0(x',y')|^2\; V^{\mathrm{3D}}(\mathbf{r}-\mathbf{r}')\;\mathrm{d}x\mathrm{d}y\mathrm{d}x'\mathrm{d}y' \tag{E.2}$$

with the confinement functions $\xi_0(x,y)$ depending on the geometry of the quantum wire. In the case of parabolic confinement introduced in App. D.4, the effective Coulomb matrix element is given by

$$\begin{aligned} V^{\mathrm{eff}}(z) &= \frac{1}{4\pi^2\,R^4}\iiiint e^{-\frac{x^2+y^2+x'^2+y'^2}{2\,R^2}} \\ &\qquad \left((x-x')^2+(y-y')^2+z^2\right)^{-\frac{1}{2}}\;\mathrm{d}x\mathrm{d}y\mathrm{d}x'\mathrm{d}y'. \end{aligned} \tag{E.3}$$

A transformation according to $X=(x+x')/2$ and $x^r = x-x'$ leads to

$$\begin{aligned} V^{\mathrm{eff}}(z) &= \frac{1}{4\pi^2\,R^4}\left[\int e^{-\frac{X^2}{R^2}}\mathrm{d}X\right]^2 \\ &\qquad \iint e^{-\frac{(x^r)^2+(y^r)^2}{4\,R^2}}\left((x^r)^2+(y^r)^2+z^2\right)^{-\frac{1}{2}}\;\mathrm{d}x^r\mathrm{d}y^r \\ &= \frac{1}{4\pi\,R^2}\int_0^{\infty}\int_0^{2\pi} e^{-\frac{r^2}{4\,R^2}}\left(r^2+z^2\right)^{-\frac{1}{2}}\;r\;\mathrm{d}r\mathrm{d}\phi \\ &= \int_0^{\infty} e^{-x}\left(4\,R^2\,x+z^2\right)^{-\frac{1}{2}}\;\mathrm{d}x \\ &= \frac{\sqrt{\pi}}{2\,R}\,e^{\left(\frac{z}{2\,R}\right)^2}\left(1-\mathrm{erf}(\frac{|z|}{2\,R})\right), \end{aligned} \tag{E.4}$$

where $\mathrm{erf}(z)$ is the error function. This functional form of the Coulomb potential can be approximated with the help of

$$\sqrt{\pi}e^{x^2}\left(1-\mathrm{erf}(x)\right) \approx \frac{1}{\sqrt{x^2+\gamma^2}} \tag{E.5}$$

with γ of the order of 0.6. Choosing $\gamma = \frac{2}{\pi}$, we obtain for the effective matrix element of the Coulomb potential

$$V^{\rm eff}(z) = \frac{1}{2R}\frac{1}{\sqrt{\left(\frac{z}{2R}\right)^2+\gamma^2}} = \frac{1}{\sqrt{z^2+\left(\frac{4}{\pi}R\right)^2}}\,. \tag{E.6}$$

In Eq. (E.1), the Fourier transformation of that effective matrix element is taken. We obtain

$$\begin{aligned}
V^{\rm eff}(q) &= \frac{1}{\mathcal{L}}\int_{-\mathcal{L}/2}^{\mathcal{L}/2}\frac{1}{\sqrt{z^2+\left(\frac{4}{\pi}R\right)^2}}e^{-i\,q\,z}{\rm d}z \\
&\approx \frac{1}{\mathcal{L}}\int_{-\infty}^{0}\frac{1}{\sqrt{z^2+\left(\frac{4}{\pi}R\right)^2}}e^{-i\,q\,z}{\rm d}z + \frac{1}{\mathcal{L}}\int_{0}^{\infty}\frac{1}{\sqrt{z^2+\left(\frac{4}{\pi}R\right)^2}}e^{-i\,q\,z}{\rm d}z \\
&= \frac{1}{\mathcal{L}}\int_{0}^{\infty}\frac{1}{\sqrt{z^2+\left(\frac{4}{\pi}R\right)^2}}\left(e^{i\,q\,z}+e^{-i\,q\,z}\right){\rm d}z \\
&= \frac{2}{\mathcal{L}}\int_{0}^{\infty}\frac{\cos(q\,z)}{\sqrt{z^2+\left(\frac{4}{\pi}R\right)^2}}{\rm d}z = \frac{1}{\mathcal{L}}\int_{-\infty}^{\infty}\frac{\cos(q\,z)}{\sqrt{z^2+\left(\frac{4}{\pi}R\right)^2}}{\rm d}z \\
&= \frac{2}{\mathcal{L}}K_0(|q|\frac{4}{\pi}\,R),
\end{aligned} \tag{E.7}$$

where K_0 is the modified Bessel function and can be approximated by

$$K_0(x) \approx \sqrt{\frac{\pi}{2\,x}}\,e^{-x}. \tag{E.8}$$

Thus, we finally obtain as an approximate Coulomb matrix element

$$V^{\rm eff}(q) \approx \frac{\pi}{\mathcal{L}}\sqrt{\frac{1}{2\,|q|\,R}}\,e^{-|q|\frac{4}{\pi}\,R}\,. \tag{E.9}$$

This matrix element is used in all numerical computations for one-dimensional systems throughout this Thesis.

F Markov Approximation

In this Appendix, we show the general solution of an equation of motion in Markov approximation when the driving term has also a dominant oscillation frequency. Thus, we consider the general equation

$$i\hbar\frac{\partial}{\partial t}X = (E_X - i\gamma)X + A\,. \tag{F.1}$$

The formal solution of that equation is given by

$$X(t) = -\frac{i}{\hbar}\int_{-\infty}^{t} A(t')\; e^{-\frac{i}{\hbar}(E_X - i\gamma)(t-t')}\mathrm{d}t'\,. \tag{F.2}$$

In order to separate strongly and weakly time dependent terms under the integral, we assume that A itself is mainly oscillating with a frequency $E_A/\hbar$ and can be written as

$$A(t) = A_0(t)\, e^{-\frac{i}{\hbar}E_A\, t}, \tag{F.3}$$

where $A_0(t)$ itself is slowly varying in time. Then we can take that slowly varying part out of the integral and obtain

$$\begin{aligned} X(t) &\approx -\frac{i}{\hbar}A(t)\int_{-\infty}^{t} e^{\frac{i}{\hbar}(E_A - E_X + i\gamma)(t-t')}\mathrm{d}t' \\ &= -\frac{i}{\hbar}A(t)\int_{0}^{\infty} e^{\frac{i}{\hbar}(E_A - E_X + i\gamma)t'}\mathrm{d}t' \\ &= -\frac{i}{\hbar}A(t)\frac{\hbar}{i(E_A - E_X + i\gamma)}e^{\frac{i}{\hbar}(E_A - E_X + i\gamma)t'}\Big|_0^{\infty} \\ &= \frac{A(t)}{E_A - E_X + i\gamma}\,. \end{aligned} \tag{F.4}$$

The result can easily be generalized to several driving terms to give

$$X(t) \approx \frac{A(t)}{E_A - E_X + i\gamma} + \frac{B(t)}{E_B - E_X + i\gamma} + \ldots \tag{F.5}$$

This formula is used in App. B to derive the expressions for the phonon assisted one and two-particle correlations.

G List of Parameters (GaAs)

Symbol	Value	Description
m_0	9.1×10^{-31} kg	free-electron mass
m_e	$0.077\, m_0$ ($0.0665\, m_0$)	effective electron mass
m_h	$0.232\, m_0$ ($0.457\, m_0$)	effective hole mass
μ	$0.058\, m_0$	reduced mass
ε_0	13.74	static dielectric constant
ε_∞	10.9	HF dielectric constant
a_0	12.4 nm	3D-Bohr radius
E_B	4.2 meV	3D-binding energy
E_G	1.519 eV	band-gap energy
c_LA	$4.79\, 10^3 m/s$	LA-velocity of sound
$D_\mathrm{e/h}$	8.6 eV	deformation constant

In all numerical computations, we have used a ratio of three between hole and electron mass in order to have less extended hole distributions and to reduce the required amount of grid points. The values are chosen such that the reduced mass is identical to the one obtained from the true effective masses given in brackets.

Bibliography

[1] A. H. Zewail. Laser femtochemistry. *Science*, **242**:1645, 1988.

[2] D. S. Chemla and J. Shah. Many-body and correlation effects in semiconductors. *Nature*, **411**:549–557, 2001.

[3] E. Moreau, I. Robert, L. Manin, V. Thierry-Mieg, J. M. Gérard, and I. Abram. Quantum cascade of photons in semiconductor quantum dots. *Phys. Rev. Lett.*, **87**:183601, 2001.

[4] O. Benson, C. Santori, M. Pelton, and Y. Yamamoto. Regulated and entangled photons from a single quantum dot. *Phys. Rev. Lett.*, **84**:2513, 2000.

[5] Y.-S. Lee, T. B. Norris, M. Kira, F. Jahnke, S. W. Koch, G. Khitrova, and H. M. Gibbs. Quantum correlations and intraband coherences in semiconductor cavity QED. *Phys. Rev. Lett.*, **83**:5338, 1999.

[6] C. Ell, P. Brick, M. Hübner, E. S. Lee, O. Lyngnes, J. P. Prineas, G. Khitrova, H. M. Gibbs, M. Kira, F. Jahnke, S. W. Koch, D. G. Deppe, and D. L. Huffaker. Quantum correlations in the nonperturbative regime of semiconductor microcavities. *Phys. Rev. Lett.*, **85**:5392–5395, 2000.

[7] D. R. Wake, H. W. Yoon, J. P. Wolfe, and H. Morkoc. Response of excitonic absorption spectra to photoexcited carriers in GaAs quantum wells. *Phys. Rev. B*, **46**:13452, 1992.

[8] C. Weisbuch, M. Nishioka, A. Ishikawa, and Y. Arakawa. Observation of the coupled exciton-photon mode splitting in a semiconductor quantum microcavity. *Phys. Rev. Lett.*, **69**:3314, 1992.

[9] T. B. Norris, J.-K. Rhee, C.-Y. Sung, Y. Arakawa, M. Nishioka, and C. Weisbuch. Time-resolved vacuum Rabi oscillations in a semiconductor quantum microcavity. *Phys. Rev. B*, **50**:14663, 1994.

[10] T. Rappen, U. G. Peter, M. Wegener, and W. Schäfer. Polarization dependence of dephasing processes: A probe for many-body effects. *Phys. Rev. B*, **49**:10774, 1994.

[11] P. Kner, W. Schäfer, R. Lövenich, and D. S. Chemla. Coherence of four-particle correlations in semiconductors. *Phys. Rev. Lett.*, **81**:5386, 1998.

[12] G. Khitrova, H. M. Gibbs, F. Jahnke, M. Kira, and S. W. Koch. Nonlinear optics of normal-mode-coupling semiconductor microcavities. *Rev. Mod. Phys.*, **71**:1591, 1999.

[13] F. Tassone, F. Bassani, and L. C. Andreani. Quantum-well reflectivity and exciton-polariton dispersion. *Phys. Rev. B*, **45**:6023, 1992.

[14] K. El Sayed, L. Bányai, and H. Haug. Coulomb quantum kinetics and optical dephasing on the femtosecond time scale. *Phys. Rev. B*, **50**:1541, 1994.

[15] T. Stroucken, A. Knorr, C. Anthony, A. Schulze, P. Thomas, S. W. Koch, M. Koch, S. T. Cundiff, J. Feldmann, and E. O. Göbel. Light propagation and disorder effects in semiconductor multiple quantum wells. *Phys. Rev. Lett.*, **74**:2391, 1995.

[16] F. Jahnke, M. Kira, and S. W. Koch. Linear and nonlinear optical properties of quantum confined excitons in semiconductor microcavities. *Z. Physik B*, **104**:559, 1997.

[17] C. Sieh, T. Meier, F. Jahnke, A. Knorr, S. W. Koch, P. Brick, M. Hübner, C. Ell, J. P. Prineas, G. Khitrova, and H. M. Gibbs. Coulomb memory signatures in the excitonic optical stark effect. *Phys. Rev. Lett.*, **82**(15):3112, 1999.

[18] H. Haug and E. Hanamura. Condensation effects of excitons. *Phys. Rep.*, **33**:209–284, 1977.

[19] H. Haug and S. W. Koch. *Quantum Theory of the Optical and Electronic Properties of Semiconductors*. World Scientific Publ., Singapore, 3. edition, 1994.

[20] D. Snoke. Coherent exciton waves. *Science*, **273**:1351–1352, 1996.

[21] D. G. Lidzey, D. D. C. Bradley, M. S. Skolnick, T. Virgili, S. Walker, and D. M. Whittaker. Strong exciton-photon coupling in an organic semiconductor microcavity. *Nature*, **395**:53–55, 1998.

[22] T. Lundstrom, W. Schoenfeld, H. Lee, and P. M. Petroff. Exciton storage in semiconductor self-assembled quantum dots. *Science*, **286**:2312–2314, 1999.

[23] M. Bayer, O. Stern, P. Hawrylak, S. Fafard, and A. Forchel. Hidden symmetries in the energy levels of excitonic 'artificial atoms'. *Nature*, **405**:923–926, 2000.

[24] S. Savasta and R. Girlanda. Signatures of the electromagnetic field quantization in the nonlinear optical response of excitons. *Journal of physics: Condensed matter*, **11**:6045, 1999.

[25] K. Hannewald, S. Glutsch, and F. Bechstedt. Quantum-kinetic theory of hot luminescence from pulse-excited semiconductors. *Phys. Rev. Lett.*, **86**:2451, 2001.

[26] F. Jahnke, M. Kira, W. Hoyer, and S. W. Koch. Influence of correlation effects on the excitonic semiconductor photoluminescence. *Phys. stat. sol. (b)*, **221**:189, 2000.

[27] B. Deveaud, F. Clérot, N. Roy, K. Satzke, B. Sermage, and D. S. Katzer. Enhanced radiative recombination of free excitons in GaAs quantum wells. *Phys. Rev. Lett.*, **67**:2355, 1991.

[28] P. W. M. Blom, P. J. Vanhall, C. Smit, J. P. Cuypers, and J. H. Wolter. Selective exciton formation in thin GaAs/Al_xGa_{1-x}As quantum wells. *Phys. Rev. Lett.*, **71**:3878, 1993.

[29] A. Vinattieri, J. Shah, T. C. Damen, D. S. Kim, L. N. Pfeiffer, M. Z. Maialle, and L. J. Sham. Exciton dynamics in GaAs quantum-wells under resonant excitation. *Phys. Rev. B*, **50**:10868, 1994.

[30] R. Kumar, A. S. Vengurlekar, A. V. Gopal, T. Melin, F. Laruelle, B. Etienne, and J. Shah. Exciton formation and relaxation dynamics in quantum wires. *Phys. Rev. Lett.*, **81**:2578, 1998.

[31] M. Kira, F. Jahnke, and S. W. Koch. Microscopic theory of excitonic signatures in semiconductor photoluminescence. *Phys. Rev. Lett.*, **81**:3263, 1998.

[32] T. Usui. Excitations in a high density electron gas. *Prog. Theor. Phys.*, **23**:787, 1960.

[33] D. Snoke, J. P. Wolfe, and A. Mysyrowicz. Quantum saturation of a Bose gas: Excitons in Cu_2O. *Phys. Rev. Lett.*, **59**:827, 1987.

[34] K. Johnson and G. M. Kavoulakis. Probing Bose-Einstein condensation of excitons with electromagnetic radiation. *Phys. Rev. Lett.*, **86**:858, 2001.

[35] E. Yablonovitch. Inhibited spontaneous emission in solid-state physics and electronics. *Phys. Rev. Lett.*, **58**:2059–2062, 1987.

[36] S. John. Strong localization of photons in certain disordered dielectric superlattices. *Phys. Rev. Lett.*, **58**:2486–2489, 1987.

[37] D. Labilloy, H. Benisty, C. Weisbuch, T. F. Krauss, R. M. De La Rue, V. Bardinal, R. Houdré, U. Oesterle, D. Cassagne, and C. Jouanin. Quantitative measurement of transmission, reflection, and diffraction of two-dimensional photonic band gap structures at near-infrared wavelengths. *Phys. Rev. Lett.*, **79**:4147, 1997.

[38] J. Hader, P. Thomas, and S. W. Koch. Optoelectronics of semiconductor superlattices. *Prog. in Quant. Electr.*, **22**:123, 1998.

[39] H. Haug and A.-P. Jauho. *Quantum Kinetics in Transport & Optics of Semiconductors*. Springer-Verlag, Berlin, 1. edition, 1996.

[40] C. Piermarocchi, F. Tassone, V. Savona, A. Quattropani, and P. Schwendimann. Nonequilibrium dynamics of free quantum-well excitons in time-resolved photoluminescence. *Phys. Rev. B*, **53**:15834, 1996.

[41] K. Siantidis, V. M. Axt, and T. Kuhn. Dynamics of exciton formation for near band-gap excitations. *Phys. Rev. B*, **65**:035303, 2001.

[42] S. R. Bolton, U. Neukirch, L. J. Sham, D. S. Chemla, and V. M. Axt. Demonstration of sixth-order coulomb correlations in a semiconductor single quantum well. *Phys. Rev. Lett.*, **85**:2002, 2000.

[43] C. Cohen-Tannoudji, J. Dupont-Roc, and G. Grynberg. *Photons & Atoms*. Wiley, New York, 3. edition, 1989.

[44] M. Kira, F. Jahnke, W. Hoyer, and S. W. Koch. Quantum theory of spontaneous emission and coherent effects in semiconductor microstructures. *Prog. in Quant. Electr.*, **23**:189, 1999.

[45] W. Vogel and D.-G. Welsch. *Quantum optics*. Akademie Verlag, Berlin, 1. edition, 1994.

[46] M. O. Scully and M. S. Zubairy. *Quantum Optics*. Cambridge University Press, Cambridge, 1. edition, 1997.

[47] K. Huang. *Quarks, Leptons, and Gauge Fields*. World Scientific, Singapore, 2. edition, 1992.

[48] N. W. Ashcroft and N. D. Mermin. *Solid State Physics*. Saunders College Publishing, New York, 1. edition, 1976.

[49] G. D. Mahan. *Many-Particle Physics*. Plenum, New York, 2. edition, 1990.

[50] I.-K. Oh and J. Singh. Excitonic relaxation involving exciton-acoustic phonon interactions in quantum wells. *Journal of Luminescence*, **87**:219–221, 2000.

[51] M. Born and R. Oppenheimer. *Ann. Phys.*, **84**:457, 1927.

[52] H. Haken. *Quantenfeldtheorie des Festkörpers*. Teubner, Stuttgart, 2. edition, 1993.

[53] F. Jahnke, M. Kira, S. W. Koch, G. Khitrova, E. K. Lindmark, T. R. Nelson Jr., D. V. Wick, J. D. Berger, O. Lyngnes, H. M. Gibbs, and K. Tai. Excitonic nonlinearities of semiconductor microcavities in the nonperturbative regime. *Phys. Rev. Lett.*, **77**:5257, 1996.

[54] P. Borri, W. Langbein, J. M. Hvam, and F. Martelli. Well-width dependence of exciton-phonon scattering in $In_xGa_{1-x}As$/GaAs single quantum wells. *Phys. Rev. B*, **59**:2215, 1999.

[55] B. Mieck, H. Haug, W. A. Hügel, M. F. Heinrich, and M. Wegener. Quantum-kinetic dephasing in resonantly excited semiconductor quantum wells. *Phys. Rev. B*, **62**:2686, 2000.

[56] L. C. Andreani. Exciton-polaritons in superlattices. *Phys. Lett. A*, **192**:99, 1994.

[57] M. Gulia, F. Rossi, E. Molinari, P. E. Selbmann, and P. Lugli. Phonon-assisted exciton formation and relaxation in GaAs/$Al_xGa_{1-x}As$ quantum wells. *Phys. Rev. B*, **55**:16049, 1997.

[58] A. L. Ivanov, P. B. Littlewood, and H. Haug. Bose-Einstein statistics in thermalization and photoluminescence of quantum-well excitons. *Phys. Rev. B*, **59**:5032, 1999.

[59] A. Thränhardt, S. Kuckenburg, A. Knorr, T. Meier, and S. W. Koch. Quantum theory of phonon-assisted exciton formation and luminescence in semiconductor quantum wells. *Phys. Rev. B*, **62**(4):2706, 2000.

[60] W. Schäfer and M. Wegener. *Semiconductor Optics and Transport Phenomena*. Springer-Verlag, Berlin, 1. edition, 2002.

[61] see e.g. articles in *The Hubbard Model*, ed. by M. Rasetti, Series on Advances in Statistical Mechanics, World Scientific Publ. (1991).

[62] J. Cízek. On correlation problem in atomic and molecular systems. calculation of wavefunction components in ursell-type expansion using quantum-field theoretical methods. *J. Chem. Phys.*, **45**:4256, 1966.

[63] G. D. Purvis and R. J. Bartlett. A full coupled-cluster singles and doubles model: The inclusion of disconnected triples. *J. Chem. Phys.*, **76**:1910, 1982.

[64] F. E. Harris, H. J. Monkhorst, and D. L. Freeman. *Algebraic and Diagrammatic Methods in Many-Fermion Theory*. Oxford Press, New York, 1. edition, 1992.

[65] J. Fricke. Transport equations including many-particle correlations for an arbitrary quantum system: A general formalism. *Annals of Physics*, **252**:479, 1996.

[66] M. Lindberg, Y. Z. Hu, R. Binder, and S. W. Koch. $\chi^{(3)}$-formalism in optically-excited semiconductors and its applications in four-wave-mixing spectroscopy. *Phys. Rev. B*, **50**:18060, 1994.

[67] V. M. Axt and A. Stahl. A dynamics-controlled truncation scheme for the hierarchy of density-matrices in semiconductor optics. *Z. Phys. B*, **93**:195, 1994.

[68] T. Elsässer, J. Shah, L. Rota, and P. Lugli. Initial thermalization of photoexcited carriers in GaAs studied by femtosecond luminescence spectroscopy. *Phys. Rev. Lett.*, **66**:1757, 1991.

[69] P. Langot, R. Tommasi, and F. Vallée. Nonequilibrium hole relaxation dynamics in an intrinsic semiconductor. *Phys. Rev. B*, **54**:1775, 1996.

[70] V. M. Agranovich and O. A. Dubowskii. Effect of retarded interaction of exciton spectrum in 1-dimensional and 2-dimensional crystals. *JETP Lett.*, **3**:223, 1966.

[71] E. Hanamura. Rapid radiative decay and enhanced optical nonlinearity of excitons in a quantum well. *Phys. Rev. B*, **38**:1228, 1988.

[72] L. C. Andreani, F. Tassone, and F. Bassani. Radiative lifetime of free excitons in quantum wells. *Solid State Commun.*, **77**:641, 1991.

[73] D. S. Citrin. *Comments Condens. Matter Phys.*, **16**:263, 1993.

[74] D. F. Walls and G. J. Milburn. *Quantum Optics*. Springer-Verlag, New York, 1. edition, 1994.

[75] W. Hoyer, M. Kira, and S. W. Koch. Semiconductor Bloch equations for classical and quantum fields. In B. Deveaud and A. Quattropani, editors, *Electron and Photon Confinement in Semiconductor Nanostructures: Proceedings of the International School of Physics "Enrico Fermi", course CLI, Varenna on Lake Como, Villa Monastero, 25 June – 5 July 2002*. 2002. to be published.

[76] R. Zimmermann. *Many-Particle Theory of Highly Excited Semiconductors*. Teubner Verlagsgesellschaft., Leipzig, 1. edition, 1988.

[77] Q. T. Vu, H. Haug, and L. V. Keldysh. Dynamics of the electron-hole correlation in femtosecond pulse excited semiconductors. *Solid State Commun.*, **115**:63–65, 2000.

[78] D. S. Chemla. Ultrafast transient nonlinear optical processes in semiconductors. In R. K. Willardson and A. C. Beers, editors, *Nonlinear Optics in Semiconductors I*, volume **58**, pages 175–256. Academic, Chestnut Hill, 1998.

[79] J. Schilp, T. Kuhn, and G. Mahler. Quantum kinetics of the coupled carrier phonon system in photoexcited semiconductors. *Phys. stat. sol. (b)*, **188**:417, 1995.

[80] M. Herbst, V. M. Axt, and T. Kuhn. Temporally and spatially resolved electron-phonon quantum kinetics. *Phys. stat. sol. (b)*, **221**:419, 2000.

[81] M. Kira, W. Hoyer, T. Stroucken, and S. W. Koch. Exciton formation in semiconductors and the influence of a photonic environment. *Phys. Rev. Lett.*, **87**:176401, 2001.

[82] M. D. Girardeau. Formulation of the many-body problem for composite particles. *J. Math. Phys.*, **4**:1096, 1963.

[83] C. I. Ivanov, H. Barentzen, and M. D. Girardeau. On the theory of dense exciton systems. *Physica A*, **140**:612, 1987.

[84] J. N. Ginocchio and C. W. Johnson. Unified theory of fermion pair to Boson mappings in full and truncated spaces. *Phys. Rev. C*, **51**:1861, 1995.

[85] P. E. Selbmann, M. Gulia, F. Rossi, E. Molinari, and P. Lugli. Coupled free-carrier and exciton relaxation in optically excited semiconductors. *Phys. Rev. B*, **54**:4660, 1996.

[86] X. Marie, J. Barrau, P. Le Jeune, T. Amand, and M. Brosseau. Exciton formation in quantum wells. *Phys. stat. sol. (a)*, **164**:359, 1997.

[87] S. Glutsch, K. Hannewald, and F. Bechstedt. Green's function approach to photoluminescence in semiconductors. *Phys. stat. sol. (b)*, **221**:235, 2000.

[88] K. Hannewald, S. Glutsch, and F. Bechstedt. Theory of photoluminescence in semiconductors. *Phys. Rev. B*, **62**:4519, 2000.

[89] G. Khitrova, D. V. Wick, J. D. Berger, C. Ell, J. P. Prineas, T. R. Nelson Jr., O. Lyngnes, H. M. Gibbs, M. Kira, F. Jahnke, S. W. Koch, W. Rühle, and S. Hallstein. Excitonic effects, luminescence, and lasing in semiconductor microcavities. *Phys. stat. sol. (b)*, **206**:3, 1998.

[90] R. F. Schnabel, R. Zimmermann, D. Bimberg, H. Nickel, R. Lösch, and W. Schlapp. Influence of exciton localization on recombination line shapes: $In_xGa_{1-x}As$/GaAs quantum wells as a model. *Phys. Rev. B*, **46**:9873, 1992.

Publications

- W. Hoyer, M. Kira, and S. W. Koch, Pair-Correlation Functions in Incoherent Electron-Hole Plasmas, phys. stat. sol. (b) **234** (2002)
- M. Kira, W. Hoyer, and S. W. Koch, Excitons and Luminescence in Semiconductor Heterostructures, Journal of Nonlinear Optics, accepted (2002)
- W. Hoyer, M. Kira, and S. W. Koch, Semiconductor Bloch Equations for Classical and Quantum Fields, to be published in *Electron and Photon Confinement in Semiconductor Nanostructures: Proceedings of the International School of Physics "Enrico Fermi"* (2002)
- W. Hoyer, M. Kira, and S. W. Koch, Quantum-Optical Effects in Semiconductors, Advances in Solid-State Physics **24**, 55 (2002)
- S. W. Koch, T. Meier, W. Hoyer, and M. Kira, Theory of the Optical Properties of Semiconductor Nanostructures, Physica E **14**, 45 (2002)
- M. Kira, W. Hoyer, T. Stroucken, and S. W. Koch, Exciton Formation in Semiconductors and Influence of a Photonic Environment, Phys. Rev. Lett. **87**, 176401 (2001)
- M. Kira, W. Hoyer, F. Jahnke, and S. W. Koch, Exciton Population Effects in Semiconductor Luminescence, phys. stat. sol. (b) **221**, 301 (2000)
- F. Jahnke, M. Kira, W. Hoyer, and S. W. Koch, Influence of Correlation Effects on the Excitonic Semiconductor Photoluminescence, phys. stat. sol. (b) **221**, 189 (2000)
- M. Kira, F. Jahnke, W. Hoyer, and S. W. Koch, Coherent Effects in Semiconductor Light Emission, Proc. SPIE **3940**, 7 (2000)
- M. Kira, F. Jahnke, W. Hoyer, and S. W. Koch, Microscopic Theory of Semiconductor Light Emission, Proc. SPIE **3944**, 192 (2000)
- M. Kira, F. Jahnke, W. Hoyer, and S. W. Koch, Quantum Theory of Spontaneous Emission and Coherent Effects in Semiconductor Microstructures, Prog. in Quant. Electr. **23**, 189 (1999)
- M. Hübner, C. Ell, P. Brick, J. Prineas, G. Khitrova, H. M. Gibbs, W. Hoyer, M. Kira, and S. W. Koch, Emission from Radiatively Coupled Periodic Quantum Well Structures, Advances in Solid-State Physics **39** (1999)

Danksagung

Ein ganz besonderer Dank geht an meine Eltern, die mich von Anfang an in meinem Studium unterstützt und damit das Zustandekommen dieser Arbeit erst ermöglicht haben.

Danken möchte ich auch meinem Doktorvater Professor Stephan Koch für die Vergabe des interessanten Themas und noch mehr für seine stete Unterstützung und Förderung.

Außerdem danke ich Dr. Mackillo Kira für die enge und erfolgreiche Zusammenarbeit über all die Jahre hinweg, ohne die diese Arbeit in ihrer jetzigen Form sicherlich nicht zustande gekommen wäre.

Professor Peter Thomas sowie den anderen Mitgliedern der Arbeitsgruppe gilt mein Dank für häufige hilfreiche Diskussionen (nicht immer nur über die Physik), für die jährlichen Wanderungen und überhaupt für das nette Arbeitsklima.

Professor Florian Gebhard danke ich ganz herzlich für die Übernahme des Zweitgutachtens.

Besondere Unterstützung in wissenschaftlicher und finanzieller Hinsicht verdanke ich den Graduiertenkollegs „Optoelektronik mesoskopischer Halbleiter“ und „Electron-Electron Interactions in Solids“ .

Dann geht noch ein dickes Dankeschön an alle Freunde und Verwandte in Marburg und überall sonst auf dieser Welt, denen es gelingt, durch ausgedehnte Telefonate und regelmäßige Besuche den Kontakt nicht abreißen zu lassen. Bis zum nächsten Wiedersehen, Anna, André, Anke, Christian, Elisabeth, Florian, H. Christian, Holger, Jörg, Johannes, Kerstin, Marko, Sabine, Steffi, Stephanie, Thomas, Tom, Thorsten, Wenke…

Und Saskia möchte ich einfach danken für die gemeinsame Zeit. Sie hat mich meine Arbeit oft genug vergessen lassen und weiß immer, wie sie mir das Leben noch etwas schöner machen kann.